Seminars in Nuclear Medicine

VOL XXIX, NO 3 JULY 1999

The Coming Age of PET (Part 1)
Letter From the Editors

AS RECENTLY AS a few years ago, many nuclear medicine physicians would have taken the position that Cardiovascular Nuclear Medicine is now a static field. Similar perhaps in many ways to bone imaging, they would have suggested that all that is left to do is to make some detailed refinements of the techniques, but the big discoveries had been made. This issue and the second part of this issue of *Seminars in Nuclear Medicine* will certainly discredit that point of view. There are many, many new developments in this field. Many new technetium labeled agents for heart imaging are under investigation and these are reviewed in the article by Dr. Jain. Technetium-99m Sestamibi, which came to dominate the field of cardiac imaging much like thallium had earlier, now has a challenger in the form of technetium-99m tetrofosmin. Thallium also has retained a significant position in cardiac imaging. It remains to be seen whether the newer agents such as technetium-NOET also will achieve a significant clinical role.

In addition to these compounds, radioiodinated free fatty acid tracers have been under intensive investigation and are reviewed in a clearly detailed article by Dr. Corbett. They have many attractive features and a great potential for clinical application.

We have a beautifully detailed contribution from Drs. Galt, Cullom, and Garcia that discusses attenuation and scatter compensation in myocardial perfusion SPECT. This article nicely complements the review of nuclear cardiology in terms of quantitation of SPECT images as presented by Dr. Watson. Other important aspects of nuclear cardiology that are also included in the first part of this two-part *Seminars in Nuclear Medicine* are a review of gated SPECT, which provides additional functional information about routinely obtained perfusion images. We have included some material on myocardial infarct imaging and the continuing efforts to accurately detect patients with acute myocardial infarction.

Overall, this issue covers some of the most important aspects of cardiovascular nuclear medicine with great detail and clarity. There can be no question that this field is alive and well, and is an important part of nuclear medicine. It has been estimated that the number of cardiovascular nuclear medicine procedures in the United States has doubled from 2.9 million procedures in 1990 to 5.8 million procedures in 1997 (1997/1998 Nuclear Medicine Census Summary Report Analysis of Technology Marketing Group [DesPlains, IL]). Cardiovascular nuclear medicine studies account for a significant amount of all nuclear medicine imaging studies. The percentage of that contribution varies depending on the facility, but in our facility, approximately one third of all procedures at our institution fall under the classification of cardiology.

The editors would like to thank Drs. Travin and Wexler, who have kindly guest edited this issue and will guest edit the next issue as well. They have done an excellent job in bringing us up to date with the state of the field. Adding insult to injury, we have prevailed upon them to also contribute an article on pharmacologic stress testing in the next issue, which we look forward to along with the other contributions.

Leonard M. Freeman, MD
M. Donald Blaufox, MD, PhD

Letter From the Guest Editors

THE FIRST CARDIOVASCULAR nuclear medicine procedures were performed 70 years ago when circulation times were calculated after the injection of radon gas into humans. Forty years ago probe-derived time-activity curves were used to approximate cardiac output, and the first mathematical models of the transit of blood through the heart based on isotope time-activity curves were published. During the 1960s, multiprobe indicator dilution studies using time-activity curves in infants with complex congenital heart disease became a means of "visualizing" abnormal anatomy long before the availability of ultrasound. During the same time period, the Anger camera's development was used to capture images of a bolus of isotope as it traversed the heart. Count data from these images made it possible to calculate transit times, an approximation of flow per unit volume in the heart.

During the early 1970s, several new developments coapted to give birth to the field of cardiovascular nuclear medicine, including the availability of new radiopharmaceuticals for myocardial perfusion imaging, minicomputers dedicated to acquiring and processing nuclear medicine images, and techniques for labelling red blood cells with technetium. It was during this time that it was observed that a hydroxyapatite-like substance was deposited in the mitochondria of infarcted myocardial cells. This observation led to the use of Technetium-99m pyrophosphate to image acutely infarcted myocardium. Although this procedure subsequently fell out of favor, it remains an excellent example of hypothesis-driven research.

Relative regional myocardial perfusion at rest and after exercise imaged using first potassium 43 and then Thallium-201 permitted the noninvasive distinction between normal, ischemic, and what was then called infarcted myocardium. Computer controlled acquisition of rapid sequential images of bolus data, and then shortly thereafter methods of gating myocardial blood pool images yielded the determination of resting ejection fraction, and by 1977, ejection fraction changes induced by either supine or upright bicycle exercise. It was during this period that cardiovascular nuclear medicine became not only a diagnostic tool but also a means for noninvasive study of the physiology of the heart. Because these procedures were noninvasive it was possible to perform temporally sequential studies before, during, and after interventional therapy.

During the 1980s, several important advances took place including quantitation of perfusion imaging and the refinement of single photon emission computed tomography (SPECT) perfusion imaging. Pooling data from multiple centers using sophisticated alogorithms for quantitating planar perfusion images yielded normal data bases of regional myocardial perfusion in both men and women. These data provided the basis for objective evaluation of myocardial perfusion images. With reproducible SPECT imaging, it became possible to contrast enhanced perfusion images. Visual evaluation of SPECT images improved diagnostic accuracy compared to planar imaging and the initial quantitative algorithms for comparing SPECT images during rest and stress became widely available.

During the 1990s, an explosion of cardiovascular nuclear medicine achievement has occurred. New Technetium-99m labeled myocardial perfusion imaging agents, particularly Technetium-99m MIBI, were FDA approved as was the use of cardioactive pharmaceuticals such as dipyridamole, adenosine, and dobutamine as alternatives to physical exercise. These pharmaceuticals have expanded the ability of cardiovascular nuclear medicine procedures to be used to define the presence or absence of ischemic heart disease and also, importantly, to determine the severity of disease. Recently, increased understanding of the behavior of perfusion imaging agents has greatly improved our understanding of the concepts of hibernating and stunned myocardium at a cellular level.

During the early 1980s, cardiovascular nuclear medicine physicians acquired a huge amount of data that allowed comparisons with other standard techniques. For example, resting myocardial perfusion imaging was compared favorably to resting coronary arteriography. Indeed, perfusion imaging was frequently used to explain anatomic imaging. By the mid 1980s, cardiovascular nuclear medicine studies were so well accepted that their results became primary endpoints of many clinical trials sponsored by the National Institute of Health.

During the past decade, further developments and refinements of cardiovascular nuclear medicine procedures have taken place. Today, cardiovascular nuclear medicine procedures occupy a central deci-

Seminars in Nuclear Medicine, Vol XXIX, No 3 (July), 1999: pp 190-191

sion-making role in the management of patients with heart disease. Our understanding of the existing perfusion pharmaceuticals and the availability of new perfusion imaging agents are providing increased insight into the physiology of myocardial perfusion. Even infarct-avid imaging is being studied again.

New computer techniques using neural networks and artificial intelligence have improved our ability to quantitate myocardial perfusion and to understand the limitations of existing technology. Sophisticated analysis of SPECT image data and new camera developments are permitting image processing techniques including correction for attenuation that could only be dreamed of just a few years ago. Nonnuclear imaging modalities, particularly those based on a two dimensional echocardiogram, are providing information about myocardial function that correlates with nuclear imaging.

In this and the next issue of *Seminars in Nuclear Medicine* we have attempted to describe the current status of the ever-advancing field of cardiovascular nuclear medicine and perhaps provide just a small peek into the future.

Mark Travin, MD
John P. Wexler, MD, PhD
Guest Editors

Quantitative SPECT Techniques

Denny D. Watson

Quantitative imaging involves first, a set of measurements that characterize an image. There are several variations of technique, but the basic measurements that are used for single photon emission computed tomography (SPECT) perfusion images are reasonably standardized. Quantification currently provides only relative tracer activity within the myocardial regions defined by an individual SPECT acquisition. Absolute quantification is still a work in progress. Quantitative comparison of absolute changes in tracer uptake comparing a stress and rest study or preintervention and postintervention study would be useful and could be done, but most commercial systems do not maintain the data normalization that is necessary for this. Measurements of regional and global function are now possible with electrocardiography (ECG) gating, and this provides clinically useful adjunctive data. Techniques for measuring ventricular function are evolving and promise to provide clinically useful accuracy. The computer can classify images as normal or abnormal by comparison with a normal database. The criteria for this classification involve more than just checking the normal limits. The images should be analyzed to measure how far they deviate from normal, and this information can be used in conjunction with pretest likelihood to indicate the level of statistical certainty that an individual patient has a true positive or true negative test. The interface between the computer and the clinician interpreter is an important part of the process. Especially when both perfusion and function are being determined, the ability of the interpreter to correctly assimilate the data is essential to the use of the quantitative process. As we become more facile with performing and recording objective measurements, the significance of the measurements in terms of risk evaluation, viability assessment, and outcome should be continually enhanced.

THE CLINICAL UTILITY of adding quantification to single photon emission computed tomography (SPECT) imaging is easily debated but more difficult to evaluate. Quantification of images involves three different processes with different goals that need to be examined individually. The first goal is to define image characteristics that can be measured and to devise methods of **measurement.** The goal is to provide an objective measurement as contrasted with a subjective judgement of the images. Measurements made from images of a patient can next be compared with measurements made from a population that is known to be normal. The measurements then can be used to provide a **classification** of the images as normal or abnormal. The final goal is for **interpretation** of the study as indicating the presence or absence of significant disease. It is helpful to distinguish these goals and discuss them separately.

The quantification of an image is no different than measuring any other indicator of physiology, such as body temperature. An experienced clinician can subjectively determine whether a patient has a fever without a thermometer, but it is still useful to measure the patient's temperature. There are similar reasons for measuring the tracer uptake from a perfusion scan.[1] The measurements provide objective values that can be recorded, reproduced, objectively communicated, compared with normal standards, or compared with a patient's previous baseline.

The measurement, however, does not by itself provide a classification or an interpretation. To clarify this issue, consider a SPECT image with an inferior segment that measures 48% of the maximum myocardial tracer uptake. This image can be classified by comparing the measurements to a normal database. If 48% is outside the limits of normal, the image is classified as abnormal. The abnormal classification may or may not support an interpretation of coronary artery disease. The defect could indicate a myocardial perfusion defect, but it could also be motion artifact, subdiaphragmatic attenuation, interference from a high large bowel loop, the result of a misplaced left arm, a defective photomultiplier tube, bad correction tables, tumor invading the myocardium, attenuation from an extracardiac mass, faulty center of rotation correction, and so forth.

The example is meant to show that a computer can measure the relative tracer uptake using only the data contained within the image. To classify the

From the Heart Center, Department of Radiology and Cardiovascular Division, Department of Medicine, University of Virginia Health Sciences Center, Charlottesville, VA.

Address reprint requests to Denny D. Watson, PhD, Department of Radiology, Box 468-65, University of Virginia Health Sciences Center, Charlottesville, VA 22908.

0001-2998/99/2903-0001$10.00/0

image measurements as normal or abnormal, additional data providing a normal database and normal limits must be added to the data set. Finally, an interpretation requires additional knowledge not contained in either the images or the normal database. The additional information must be factored in using a logic more complex than the simple arithmetic of comparison with a normal standard.[2] The additional knowledge can be introduced by "expert systems." These are rule-based systems that attempt to have the computer reach the same conclusion as the "expert," whose knowledge was used to generate the rules.[3,4] Other strategies have been investigated, for example, the use of artificial intelligence.[5,6] This allows a computer to learn from measuring many studies and from using feedback regarding which studies were normal, which were abnormal, and which patients had coronary artery disease. Expert systems and artificial intelligence are being developed but are not mature or widely available at this time. Consequently, most of the knowledge required for interpretation must still come from an expert interpreter who uses the computer as an aid rather than as an expert. This does not reduce the value or the need for quantification.

The measurement is the foundation of quantitative imaging. If the measurements are not accurate and reproducible, then classification and interpretation cannot be reliably based on the measurements. If the measurements are reliable and reproducible, then it will be a relatively simple matter to determine normal values and associate abnormal values with the presence and severity of disease and with outcome. As this knowledge accumulates, the measurements become increasingly valuable to clinical imaging.

The remainder of this article will deal with the processes by which the goals of quantification, classification, and interpretation are approached. The following section will be an overview of common quantitative methods and some of the factors that affect measurement accuracy. In the next section on classification, I will examine some approaches and some statistical issues associated with classification by comparison with normal databases. In the final section on interpretation, I will examine some factors involved in translating the quantitative analysis into a clinical interpretation.

QUANTITATIVE METHODS

Quantification of Perfusion Images

Measurements of SPECT images conventionally start in the left ventricular cavity and search outward. The search pattern varies. Early versions used a cylindrical search pattern. This works well in the body of the ventricle but has problems near the apex. A spherical pattern also has been used, but this gives rays that traverse parts of the myocardium at oblique angles. Garcia et al[2,7] developed a hybrid search that is cylindrical in the body of the ventricle and switches to a spherical pattern to form a cap over the apex of the left ventricle. This is now a standard method.

The goal is to measure tracer activity in a specified region of the left ventricular myocardium, and the search pattern gives a set of rays extending outward across the myocardium. There are choices regarding what to measure. Intuitively, we might choose to integrate the myocardial activity in each voxel penetrated by each ray that passes through the myocardium from epicardial to endocardial borders. This approach has been developed and used with good results.[8,9] The problem with this approach is that the endocardial and epicardial borders must be known to define the integration limits. The accuracy of transmural integration of counts is limited by being dependent on the myocardial borders, which are poorly defined in the SPECT image. The alternative method is to simply find the maximum voxel count as the ray traverses the myocardium.

From the early days of quantitative planar imaging, experience taught investigators that recording the maximum count along a ray that traverses the myocardium was reproducible and robust in indicating myocardial perfusion defects. The apparent disadvantage of this method is that it would appear to miss subendocardial perfusion defects that have a well-perfused epicardial rim. This method worked well in practice, and we now understand that it works because of partial volume averaging.

Partial volume averaging has been described[10,11] and is shown in Figure 1. This shows a short-axis slice from a cardiac phantom of uniform tracer activity but varying wall thickness. The curve plot is of the peak activity obtained from a radial search across the myocardium plotted as a function of the myocardial wall thickness. The peak activity re-

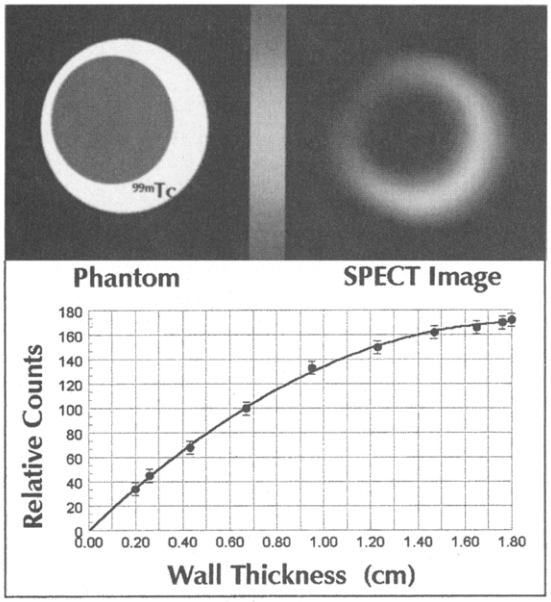

Fig 1. Phantom consisting of two nonconcentric cylinders with the void between filled with Technetium-99m. The thickness of the filled space between the cylinders ranges from 2 to 18 mm. The phantom was imaged, reconstructed, and reoriented. The SPECT short-axis image is shown to the right of a scale diagram of the source. The graph below shows the counts from a radial maximum-count search as used in quantitative SPECT. The maximum counts reflect the "myocardial" wall thickness. This is the result of the partial volume effect, which converts wall thickness into peak counts.

flects the wall thickness. This happens because the resolution of SPECT is less than the myocardial wall thickness for normal myocardium. Consequently, the peak activity of the voxels actually represents a transmural average rather than the actual activity at the point of the sample. If there were a scar or perfusion defect involving the endocardium and normal epicardial flow, the peak pixel counts will be reduced; reflecting a transmural average of tracer activity. Thus, the peak count method is actually a way of determining the transmural average of tracer activity without having to find the epicardial and endocardial edges.

The same partial volume effect can be used also to convert changes in wall thickness into changes in maximum pixel counts. In gated images, the partial volume effect can be used to determine regional wall thickening by comparing the transmural peak values determined from end-systolic and end-diastolic images. This method of quantification is identical for both perfusion and wall thickening. The only difference is that the end-systolic and end-diastolic images are substituted for stress and rest images.

Absolute Versus Relative Quantification

Myocardial activity is conventionally measured relative to the region of most intense uptake. This imposes some limitations. We cannot always be sure that there will be a normally perfused myocardial segment for a reference region. We cannot compare the amount of tracer uptake at rest with the amount of tracer uptake after stress, which would provide an estimate of coronary artery flow reserve capacity. We cannot perform quantitative longitudinal measurements that would show absolute changes in coronary reserve capacity resulting from therapeutic interventions. Clearly, absolute quantification would be a significant advance.

The absolute measurement of millicuries of tracer per gram of tissue has been an elusive goal. It is clear that attenuation correction is a prerequisite for this type of quantification. Much work has been done on attenuation correction, and much progress has been made.[12-17] However, it is not yet developed to the point that would be necessary to support absolute quantification. One issue seems to involve the role of scatter. Scatter correction is difficult, and may be necessary before accurate corrections for attenuation can be made.

Short of measuring millicuries per gram of tissue, for most clinical needs it would be useful to be able to use a patient as his own control and measure relative tracer activity under two different conditions (eg, stress and rest) or at different times (response to therapy). This could probably be done with acceptable accuracy if the reconstruction algorithms would maintain the count normalization during SPECT data processing. Unfortunately, most commercial systems at present do not. The reconstruction and filtering process usually results in all the data from the SPECT reconstruction being renormalized to an arbitrary value (for example, the peak myocardial activity is set to the value 256, regardless of the original raw projected image counts). This is expedient but eliminates a potentially powerful tool of SPECT imaging—the ability to compare two SPECT scans and quantitatively determine the fractional change in tracer uptake. Because this is a much easier problem to solve than that of measuring absolute millicuries per gram, we can hope that future modifications of SPECT

software will contain the ability to make these comparisons quantitatively.

Segmental Wall Motion

Gated SPECT can provide myocardial images at typically 8 or 16 samples through the cardiac cycle, and this can be used to determine regional and global left ventricular function.[18] The total counts of each frame, however, are limited to one eighth or one sixteenth of the counts of the ungated images. The statistical noise in these images is therefore very high, and only gross wall motion abnormalities will be consistently visualized. However, the gated images should be well suited for quantitative measurement of regional thickening fractions. The most straightforward approach would be to measure the epicardial and endocardial edges at end-systole and at end-diastole. This method has the disadvantage of depending on edge detection. The noise in gated images can make edge detection inaccurate. Moreover, in regions of severe perfusion defects, the myocardial edges may be undetectable. A second approach is to use the partial volume effect, which causes changes in wall thickness to appear as changes in peak myocardial counts. This approach has been investigated.[19-22] It has the advantage of requiring no edge detection. Smith et al[23] and Calnon et al[24] have used the partial volume effect to perform relative quantification of regional thickening fractions. The counts-based method depends only on relative changes between systole and diastole, and is therefore not affected by moderate perfusion defects. The thickening fraction cannot be measured in a myocardial segment that has no tracer uptake. In this case, the thickening fraction is arbitrarily set to zero, as a reasonable approximation. The counts-based method depends on the partial volume effect and will consequently fail if the myocardial wall thickness becomes thick enough to be comparable with the image resolution. This can happen in severe cases of left ventricular hypertrophy, causing underestimation of thickening fractions.

Measurement of Global Left Ventricular Function

The measurement of global left ventricular ejection fraction (LVEF) adds another dimension to quantitative SPECT. Again, there are several possible methods of measuring LVEF. The most straightforward approach is to find the endocardial edges at end-systole and at end-diastole and estimate the end-systolic and end-diastolic volumes. Several variations have been described.[25-27] The need for edge detection is a limitation. Everaert et al[28] described a statistical method based on the radial distribution of count densities to define myocardial borders. The method of Germano et al[29] estimates edges by fitting geometric shapes, and this alleviates many problems associated with less sophisticated edge detection methods. This method also facilitates automatic reorientation.[30] Smith et al[23] and Calnon et al[24] describe a purely counts-based approximation for estimation of global LVEF. LVEF is estimated from the regional thickening fractions, which are determined without need for any edge delineation. This requires some approximation, but appears to offer adequate accuracy and excellent reliability.

Representation of Quantitative Results

The visual representation of quantitative values obtained from SPECT images is an important part of the process. This is the user interface. The quantitative process generates several hundred numerical values, and there are typically several dozen image slices to examine. Garcia developed the idea of polar ("bull's eye") maps. These can represent all the data from the radial search pattern in a single two-dimensional image. The polar plots can also flag regions that differ significantly from a normal database and regions that have reversible defects. Figure 2 is an example from the Emory Cardiac Toolbox. The top row shows standard stress, rest, and reversibility polar plots. The middle row is plotted using a mapping that better represents the true extent of the defect. The lower row is a plot formed to highlight defect severity. Programs using the polar maps are commercially available and widely used. The polar map shown as well as Figures 3 and 4 are black-and-white reproductions from color computer monitor displays. They need to be viewed on a good color monitor to be fully appreciated.

Smith et al[23] and Calnon et al[24] use the same quantification methodology as developed by Garcia. However, the display of results was designed to achieve a direct visualization of the quantitative measurements for each myocardial segment. The segments are marked on myocardial images, and the values shown in a graphic just below the images. Figure 3A shows stress/rest perfusion data on a patient before coronary revascularization. For

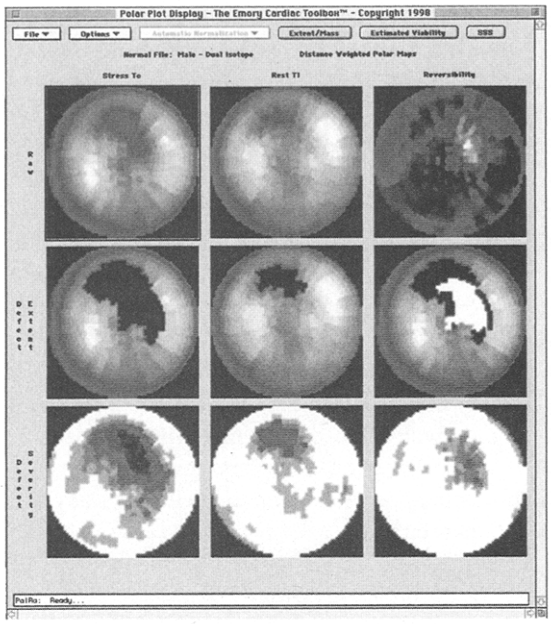

Fig 2. Polar map representations of SPECT images. The maps show stress and rest perfusion and reversibility, in a normal representation (A) and in representations that are designed to represent defect extent (B) and severity (C).

each segment, the stress and rest percentages are shown in the graphic above. If a segment is outside normal limits, the difference between stress and rest is entered in the lower graphic, and an asterisk shows if the difference constitutes statistically significant reversibility. The same segments are used to find thickening fractions from gated images. They are shown in Figure 3B.

Figure 4 shows the same patient after coronary revascularization. This study is within normal limits. For comparison, consider the midanterior segment. Preoperatively, at stress, there was only 55% of normal uptake, and the rest injection indicated partial but significant reversibility to a value of 61%. This segment was hypokinetic (as indicated by the asterisk in Fig 3B) with a thickening fraction of 23%. After revascularization, the same anterior segment had normal (and statistically equal) stress/rest uptake of 86% and 88% respectively, and a normal thickening fraction of 42%. There were similar changes shown in five other segments. The global LVEF increased from 48% to 59%.

This study shows regions of severe defect, partial reversibility, and hypokinesis preoperatively that normalized after revascularization, giving a quantitative record of preoperative hibernation and/or stunning. The sequence shows the value of displaying quantitative values for perfusion and function, which can be easily appreciated, recorded, and compared.

SPECT is intrinsically a three-dimensional modality, and there have been a number of efforts to construct visualization and quantification schemes in a three-dimensional mode as compared with conventional representations of multiple two-dimensional slices.[31,32] This can be done using modern computer displays. It certainly adds to the visual aesthetics, but has not yet reached the point of adding significantly to the clinical use of SPECT studies. It is also possible to achieve the fusion of multimodality imaging. For example, the cineangiographic images of the coronary artery tree can

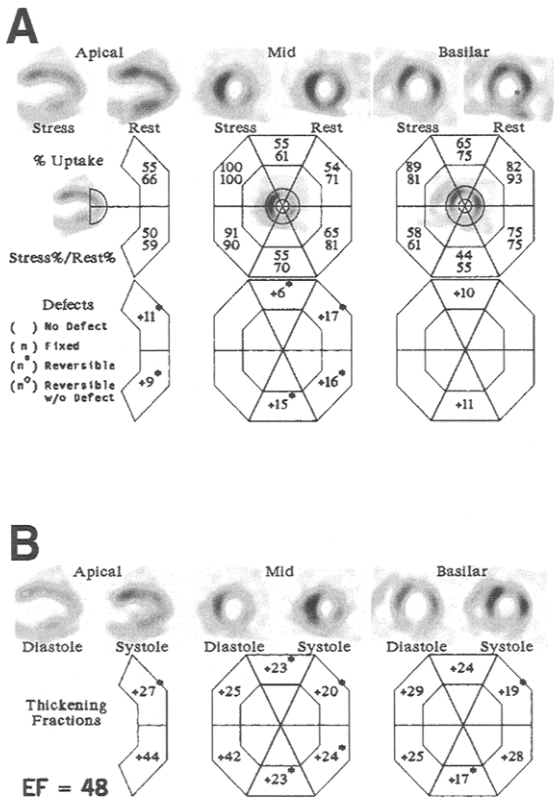

Fig 3. (A) Simplified visual presentation showing myocardial segments and the relative activity in each segment. In the segment graphic below, segments that are within normal limits are left blank. Numbered segments are those that have stress perfusion defects by comparison with the normal database. The numbers are the difference between stress and rest, and they are marked by an asterisk if the difference is statistically different, denoting reversibility. (B) Thickening fractions are shown for the same segments. An asterisk indicates the segment is hypokinetic by comparison with the normal database. Global LVEF is estimated from the thickening fractions. The measurements are all counts-based and do not require detection of the myocardial borders.

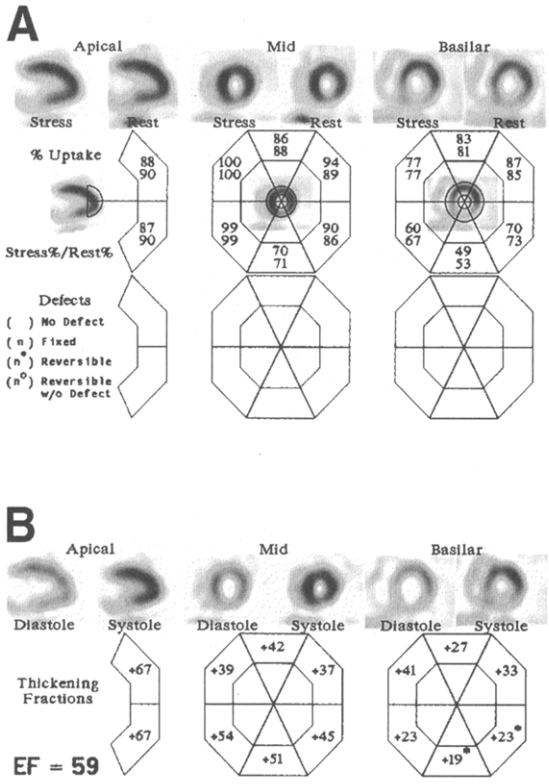

Fig 4. Study of the same patient as shown in Fig 3 after coronary artery revascularization. All segments are now within normal limits. Note that several segments in the postrevascularization study show greater uptake and better wall motion than the corresponding segments in the resting state in the prerevascularization study. The documentation of resting hypoperfusion and hypokinesis relative to the postrevascularization study would be consistent with myocardial hibernation. The display facilitates quantitative segmental comparisons.

be brought into registration with perfusion images to aid in the correlation of coronary anatomy and myocardial perfusion. These efforts could portend the future of imaging, but will not be included within the scope of this article.

CLASSIFICATION OF PERFUSION IMAGES

Detection of Perfusion Defects

A critical step in the quantitative process is to classify the image as normal or abnormal. This is done by comparing each segment with the normal limits. The normal limits are usually adjusted to lie about two standard deviations away from the normal average. This would imply false positive probability of 0.023 for each segment (this is the one-sided P value for a 2σ deviation). Because there are many segments, the overall false positive rate (that is, the probability that one or more segments will be positive) will be higher than the individual segment false positive rate. For an n-segment model, with each segment adjusted to have the same probability, $P(f+)$ of being a false positive, the expected specificity (probability of finding no abnormal segments in a normal image) would be $(1\text{-}P[f+])^n$. Thus for a 14-segment model with each segment threshold set at two standard deviations from the normal average, the statistically expected specificity would be 0.72. In a 20-segment model, the expected specificity would be 0.63. The specificity becomes lower with more segments because the statistical chance of finding at least one segment outside normal limits attributable only to statistical sampling error increases with the number of sampled segments. A large number of samples can be used with the additional requirement that two or more contiguous samples must be outside limits for the image to be classified as abnormal. This is essentially the same as using coarser sampling.

Another complication with the normal database comparison of images is that some segments characteristically are the regions of highest tracer activity and are normalized to exactly 100%. Standard deviations of these regions will be underestimated because of the inclusion of values arbitrarily set to exactly unity. Smith et al[23] and Calnon et al[24] use a hybrid scheme with limits for each segment set as the average minus two standard deviations or a constant, whichever is greater. This reduces false positive classifications from segments with underestimated standard deviations.

In the final analysis, the false positive and true positive rate of the quantitative scheme needs to be tested on a set of normal patients and a set of abnormal patients. The threshold for discriminating should be varied to produce a receiver operating curve (ROC) as shown in Figure 5. Ideally, the threshold should be adjustable so that the interpreter can adjust the computer to a known position on the ROC curve.

Detection of Reversibility

The likelihood of reversibility can be determined from the same normal database used above. In this case, however, we are testing for a significant difference between two measurements, and the statistical test must be appropriate. For a given abnormal segment measured at stress and during

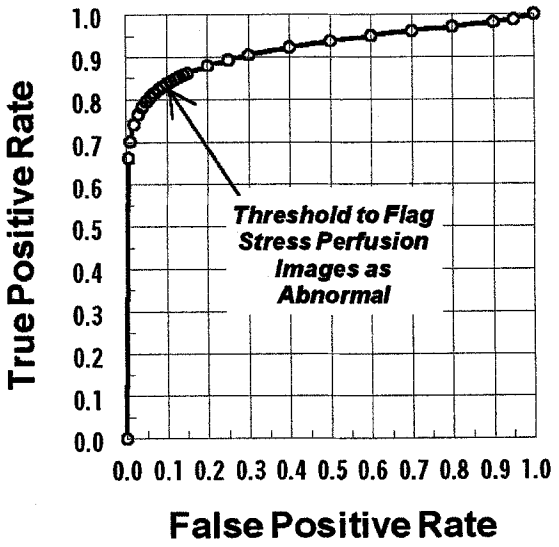

Fig 5. The ROC curve produced by a quantitative program. The set point adopted by this particular program is shown by the *arrow*. The computer threshold can be varied anywhere along the curve. For example, the computer threshold could be moved to obtain a 90% sensitivity, with a corresponding false positive rate of 30%. The set point chosen for this program provides approximately equal false-positive and false-negative rates.

rest, the question of reversibility is posed by testing the null hypothesis that "there is no difference between the two measurements." Reversibility is indicated if the null hypothesis is rejected at some predetermined level of confidence. The null hypotheses should not, however, be rejected at the usual $P = .05$ level. Using the $P = .05$ criteria would result in the identification of reversibility only if it were established with 95% likelihood. In practice, we interpret reversibility of a segment with reduced perfusion if it appears more likely to be reversible than to be fixed. Requiring a degree of certainty of 95% would mean that many reversible segments would be called fixed by the computer only because the statistical weight of evidence had not yet risen to the 95% level of certainty. To make the computer read more like an expert, we have it flag reversibility if the two measurements differ by more than one standard deviation. This amounts to using a confidence level to $P = .16$. In reality, the statistical certainty of an indicated reversible segment could be lower than the predicted value of .84. If there were two contingent abnormal segments, for example, the probability of one or the other being false positive for reversibility would be $(1-.84^2) = .29$. In this case, we would be right about 70% of the time if we indicated the segments to be reversible (or partly reversible), and most interpreters would read reversibility (or partial reversibility) at that level of certainty.

Reversibility, as defined above, should not be used to screen for an abnormal image. If 14 segments were scanned for reversibility using a one-sigma criteria, the false positive rate would be $(1-.84^{14})$, which is 91%. A 20-segment model would have a probability of 97% of having at least one segment more than one standard deviation greater on the rest images than on the stress images, purely as a result of sampling error.

The statistical gamesmanship may be described as follows: each myocardial segment from the stress image is examined and declared abnormal only if it is abnormal beyond a reasonable doubt (being at least 95% certain). Then the same segment is examined at rest and declared to be reversible by the preponderance of evidence. We must use the high threshold for finding an individual segment abnormal, for otherwise there would be an excessive probability of having at least one of the many sampled segments found falsely abnormal because of statistical sampling error. Once the segment is declared abnormal, we must drop to a lower standard of certainty, for otherwise there would be too many false negatives in the determination of reversibility.

The discussion above may reveal that comparing an image with a normal database is not as simple as comparing a single value with a normal limit. The complexity evolves first because there are many samples within a single image and the statistical complications of multiple samples must be accounted for. The second complication is that of testing for changes between two data sets representing a stress and rest image. There are many samples to be compared, and the two samples will not be identical because of statistical sampling error. The task is to determine if the change is caused by statistical variance or if it is caused by a true difference in myocardial perfusion. We cannot simply look for a difference in the values representing rest and stress uptake. We must perform a statistical test that shows if the difference is too great to be accounted for by chance. The mathematical operation is (or should be) the same as testing the null hypothesis that the two samples are drawn from identical perfusion images.

Detection of Regional Wall Motion Abnormalities

If the quantitative scheme being used provides some measure of regional wall thickening, then it is possible to obtain a normal database and identify segments with thickening fractions outside of normal limits. There is likely to be a large standard deviation for these measurements and, again, we must decide on the level of certainty before setting a threshold to flag segments as abnormal. We use the average minus two standard deviations for the limits of normal thickening. The probability of a sample being randomly below this value is .023. With a 14-segment model, this implies that 28% of normal subjects will have at least one false positive hypokinetic segment. With a 20-segment model, 37% of normal subjects will have a false positive hypokinetic segment when using 2σ limits. The sampling statistics must be kept in mind when interpreting segmental wall motion abnormalities and in the identification of poststress myocardial stunning.

INTERPRETATION OF QUANTITATIVE SPECT

Presence of a Significant Perfusion Defect

The most difficult step in image interpretation is to determine if the study indicates significant pathology and should be classified as clinically abnormal. The quantitative process will classify the study as technically normal or abnormal. Thus, the first job of the interpreter is to decide if the computer classification was clinically correct. A good computer program will correctly identify if the current study is outside the limits of normal variation. If so, the interpreter must decide if that is because of pathology or an unanticipated artifact. One of the most powerful tools for identifying artifacts is the raw projection images. The readability of raw images can be immensely improved by using temporal filtering of adjacent projections and also by careful masking so that the region of highest myocardial uptake sets the image color or gray scale. This must be done to avoid having the images scaled to a hot extracardiac organ such as the gall bladder or intestine. Projection images in the cine mode should be routinely reviewed to check for patient motion during acquisition. These features should be considered an indispensable part of the quantitative analysis. Projection images show more than just artifacts. Projection images show lung uptake, chamber sizes including atrial and right ventricular enlargement, extracardiac masses, pericardial fluid, and other clues that can make or lead to a clinical diagnosis. Careful attention to the quality of projection images and careful inspection can add greatly to clinical interpretation.

The computer may also falsely classify a study as normal. The most common reason for this is the presence of a small focal perfusion defect that is being averaged with surrounding normally perfused tissue. The computer necessarily uses fairly large samples, and small perfusion defects can be positioned so that the defect will be obvious to the eye but not flagged as quantitatively significant. There are occasional manifestations of diffuse multivessel disease that render the heart so uniformly hypoperfused that uptake will be quantitatively within normal limits. The quantitative measurements we use now are only relative and cannot indicate if the entire heart is hypoperfused.

Finally, the clinical interpretation of an ill-defined defect or one of only borderline statistical significance is best considered in the light of pretest probability of coronary artery disease. This brings us to venture quantitatively into the question of how pretest probability determines the predictive accuracy of a test interpretation. Every test interpreter learns at least intuitively the impact of Baye's theorem, which relates posttest likelihood of disease to pretest likelihood combined with test results. As an example, we have taken the ROC curve shown in Figure 5 and used Baye's analysis to calculate the predictive accuracy of a positive test result and the predictive accuracy of a negative test result as a function of where the computer (or interpreter) is positioned on the ROC curve. The analysis for a patient with low (10%) pretest likelihood is shown in Figure 6. This shows that if we keep the computer set to produce a 90% sensitivity, the predictive accuracy for a positive test result from this patient will be only about 30%. In other words, 70% of the positive test results for this population would be false positives. Examination of the curves of Figure 6 will show that by moving down on the ROC curve to a lower sensitivity threshold, the predictive accuracy of a positive test result could be improved to greater than 95%. Using the same altered threshold, the predictive accuracy of a negative test result could still be maintained at greater than 95%.

The example above shows the potential impor-

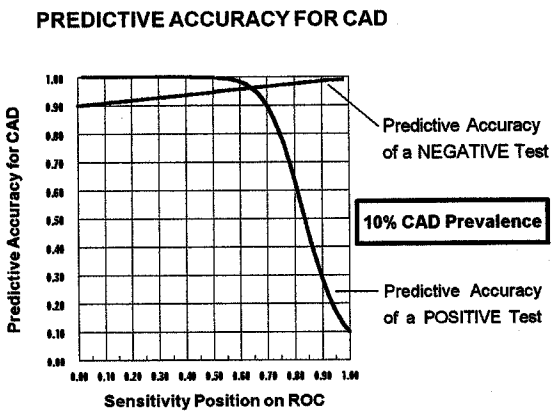

Fig 6. The result of a Bayes analysis showing predictive accuracy of a positive and negative test result for a population with pretest probability of 10%. The ROC curve of Fig 5 is used in the calculation. The predictive accuracy of a positive test result for this population is poor, but it can be dramatically improved by shifting the set point on the ROC curve.

tance of clinical pretest variables to the final test interpretation. These can be factored in quantitatively as shown above. Doing so could add an important element to quantitative analysis. The analysis above shows that the predictive accuracy of the test can still be very high even on patients with a low pretest probability. Simply stated, the analysis showed that for this population, a test result that is positive but only of borderline statistical significance does not indicate coronary artery disease (CAD); but if the test results were positive at a higher level of statistical certainty, then they would indicate CAD. The optimal interpretation needs to depend on how positive the test result is; that is by how far statistically outside normal limits the test result was. This important information is lost when the test results are bifurcated into normal and abnormal according to a fixed preset criteria. This potential of quantitative analysis seems to be largely unrecognized and is not presently being used.

Reversibility and Viability

Reversibility indicates myocardial ischemia. Ischemia implies viability. Myocardium may, however, be viable without being ischemic. Significant residual tracer uptake in a myocardial segment indicates significant residual viability, but not necessarily ischemia.

Clinically, the question of ischemia is important because ischemia can be efficaciously treated. The question of viability is also important, but the question is more complicated—the more clinically relevant question is whether myocardial function will be improved after revascularization. Significant residual viability, as indicated by significant tracer uptake in a myocardial region that has been severely ischemic, can indicate stunned or hibernated myocardium. It can also indicate a subendocardial scar. The distinction is important because if the segment is stunned or hibernating, reperfusion is more likely to result in recovery of myocardial contractile function.

There are two ways to show hibernating myocardium with perfusion tracers. One is to show resting redistribution of thallium-201, which indicates chronic resting hypoperfusion. The other is to show discordantly high (>50%) tracer uptake in a segment that is akinetic. Stunned myocardium also is expected to have discordantly high tracer uptake in the akinetic (stunned) segment. In either case, the mere observation of uptake is not adequate. The (quantitative) amount of tracer uptake in the segment is important. A segment with 20% uptake is not likely to show functional recovery. A segment with 60% uptake that is akinetic is likely to show improved contraction after reperfusion. A segment that is only mildly hypokinetic and with 60% uptake could be a subendocardial scar. An additional question here might be whether there is a high-grade residual stenosis; a stress test (to provide a stress/rest comparison) would be necessary to show that.

It seems clear that quantitative indicators of tracer uptake, reversibility, and regional function will be necessary to deal effectively with the questions of myocardial viability and especially when we are considering the more specific question of the likelihood of recovery of myocardial function after reperfusion.

Regional and Global Function

There are now some methods that appear to give clinically adequate estimation of global LVEF from gated SPECT. These methods need further validation and comparison before they can be recommended as an accurate substitute for established clinical measurements of LVEF. However, they have become a useful adjunctive measurement[33-35] as a routine part of SPECT perfusion imaging. In our hands, the SPECT measurements of LVEF have been more robust than radionuclide ventriculography.

A significant problem that remains at present is that the computer programs developed to date do not provide credible quality control features. Errors related to arrhythmia, improper electrocardiograph (ECG) gate signals, and improper selection of end-diastolic and end-systolic frames, for example, cannot be discovered after the SPECT images are processed and sent to the reading room. There are no quality control indicators such as R-R histogram, indications of beats or total counts recorded, or cross-checks on the ECG trigger point or the selection of end-systolic frame. Until such devices can be developed and added to the program, the interpreters must be wary and have good communication with and great confidence in the technologist performing the study.

Determination of regional function using gated SPECT is possible but less well established. The counts-based method, described earlier, has provided reliable relative measurements in our hands but has not been widely tested. Methods that rely on detection of endocardial edges can be difficult because of the poor resolution and high image noise in gated SPECT images that have only one eighth or one sixteenth of the counts of nongated images.

Another problem inherent to the use of SPECT perfusion images for determining segmental wall thickening is the presence of segmental perfusion defects. On same-day study protocols, the high dose is usually used for the stress study. This provides the best definition of stress-induced perfusion defects, but with the Technetium-99m agents that do not redistribute, the stress-induced defect will remain in the poststress resting study even though stress-induced ischemia has resolved and wall motion has returned to normal. By visual interpretation, such a segment is likely to be graded as having abnormal contraction simply because it is poorly visualized and the lack of tracer activity in the region provides a strong interpreter bias to read the segment as abnormal. In this situation, quantification should provide the more reliable estimate of wall motion, but methods that depend on thresholding to detect edges may be in error because the perfusion defect will distort the edge isocount contours.

There are a number of challenging problems associated with the measurement of SPECT images. Methods are now in place that deal effectively with most of these problems. Reliable measurements can be made. One could argue that some engineering is still needed to bring these measurements into a more simple and usable format for clinicians who interpret SPECT studies. Some additional standardization is needed to facilitate the storage of meaningful quantitative results in large databases that can be used to produce more meaningful normal standards and for data mining operations, such as for longitudinal outcomes studies.

Classification of studies as normal or abnormal can be done effectively by computer programs using existing normal database comparisons. However, the statistical methods of defining when a study is abnormal by comparison with a normal database are complex and may be poorly understood by users. At the least, the user should be aware of the ROC curve his or her computer program is operating on and be able to understand where the computer is set to operate on that ROC curve. Most existing programs do not address this issue, and the clinician must learn this by experience in the sense of "getting a feel" for the false positive and false negative propensity of the computer program. This reduces the value of quantification because the clinician is forced to develop the skill and artistry of interpretation in spite of having measurements at hand. Most computer programs do use some level of expert logic, but it may be obscure to the interpreter. A clear definition of the logic used in the classification scheme would be helpful. Systems that impose expert rules or some form of artificial intelligence that is obscure to the interpreter should be approached with caution. Integration of pretest clinical variables with the specific perfusion test analysis could be performed to yield higher predictive accuracy for the quantitative classification.

Interpretation of SPECT studies is aided both by quantification of the perfusion portion and by having functional information such as regional wall motion and global left ventricular function. Prognosis and viability assessment are both related to the extent and severity of perfusion defect and also the extent and severity of abnormal ventricular function. Having these parameters available from the SPECT study on a continuous scale rather than a categorical (normal/abnormal) scale is essential for the evaluation of risk and viability. The measured values are equally essential in follow-up studies to evaluate response to therapy. The goal of having the computer render a complete analysis and inter-

pretation of the study has not yet been achieved in routine clinical practice. It is not out of the question to do this, but it is not yet in the realm of realistic expectations. There are many developing tools that could have a major impact on quantitative SPECT imaging.

REFERENCES

1. Wackers FJ: Science, art, and artifacts: how important is quantification for the practicing physician interpreting myocardial perfusion studies? J Nucl Cardiol 5:S109-S117, 1994
2. Garcia EV: Quantitative myocardial perfusion single-photon emission computed tomographic imaging: quo vadis? (Where do we go from here?) J Nucl Cardiol 1:83-93, 1994
3. Garcia EV, Krawczynska EG, Folds RD, et al: Expert system interpretation of myocardial perfusion tomograms: validation using 288 prospective patients. J Nucl Med 37:48P, 1966
4. Ezquerra NF, Garcia EV: Artificial intelligence in nuclear medicine imaging. Am J Card Imaging 3:130-141, 1989
5. Fujita H, Katafuchi T, Uehara T, et al: Application of artificial neural network to computer-aided diagnosis of coronary artery disease in myocardial SPECT bull's-eye images. J Nucl Med 33:272-276, 1992
6. Hamilton D, Riley PJ, Miola UJ, et al: A feed forward neural network for classification of bull's-eye myocardial perfusion images. Eur J Nucl Med 22:108-115, 1995
7. Garcia EV, Cooke CD, Van Train K, et al: Technical aspects of myocardial SPECT imaging with Tc-99m sestamibi. Am J Nucl Cardiol 66:23E-31E, 1990
8. Liu H, Sinusas AJ, Shi CQ, et al: Quantification of technetium 99m–labled sestamibi single-photon emission computed tomography base on mean counts improves accuracy for assessment of relative regional myocardial blood flow: experimental validation in a canine model. J Nucl Cardiol 3:312-320, 1996
9. Mortelmans LA, Wackers FJ, Nuyts JL, et al: Tomographic and planar quantitation of perfusion defects on technetium 99m-labeled sestamibi scans: evaluation in patients treated with thrombolytic therapy for acute myocardial infarction. J Nucl Cardiol 2:133-43, 1995
10. Hoffman EJ, Huang SC, Phelps ME: Quantitation in positron emission computed tomography: 1. Effect of object size. J Comput Assist Tomogr 3:299-308, 1979
11. Galt JR, Garcia EV, Robbins WL: Effects of myocardial thickness on SPECT quantification. IEEE Trans Med Imaging 9:144-150, 1990
12. Gullberg GT: Innovative design concepts for transmission CT in attenuation corrected SPECT imaging. J Nucl Med 39:1344-1347, 1998
13. King MA, Xia W, deVries DH, et al: A Monte Carlo investigation of artifacts caused by liver uptake in single-photon emission computed tomography perfusion imaging with technetium 99m–labeled agents. J Nucl Cardiol 3:18-29, 1996
14. King MA, Tsui BM, Pan TS, et al: Attenuation compensation for cardiac single-photon emission computed tomographic imaging: Part 2. Attenuation compensation algorithms. J Nucl Cardiol 3:55-64, 1996
15. Ficaro EP, Fessler JA, Shreve PD, et al: Simultaneous transmission/emission myocardial perfusion tomography. Circulation 93:463-473, 1996
16. King MA, Tsui BMW, Pan T-S: Attenuation compensation for cardiac SPECT imaging: part 1. Impact of attenuation and methods of estimating attenuating maps. J Nucl Cardiol 2:513-524, 1995
17. King MA, Tsui BMW, Pan T-S, et al: Attenuation compensation for cardiac single-photon emission computed tomographic imaging: part 2. Attenuation compensation algorithms. J Nucl Cardiol 3:55-64, 1996
18. Cullom J, Case JA, Bateman TM: Electrocardiographically gated myocardial perfusion SPECT: technical principles and quality control considerations. J Nucl Cardiol 4:418-425, 1998
19. Mochizuki T, Murase K, Fujiware Y, et al: Assessment of systolic thickening with thallium-201 ECG-gated single-photon emission computed tomography: a parameter for local left ventricular function. J Nucl Med 32:1496-1500, 1991
20. Marcassa C, Marzullo P, Gianmaro S, et al: Prediction of reversible perfusion defects by quantitative analysis of post-exercise ecg-gated acquisition of Tc-99m MIBI myocardial perfusion scintigraphy. Eur J Nucl Med 19:796-799, 1992
21. Cooke DC, Garcia EV, Cullom J, et al: Determining the accuracy of calculating systolic wall thickening using a fast fourier transform approximation: a simulation study based on canine and patient data. J Nucl Med 35:1185-1192, 1994
22. Kumata S, Kumazaki T: Assessment of left ventricular function with 99mTc-MIBI gated myocardial SPECT using 3 head rotating gamma camera. Kaku Igaku 31:43-52, 1994
23. Smith WH, Kastner RJ, Calnon DA, et al: Quantitative gated SPECT imaging: a counts-based method for display and measurement of regional and global ventricular systolic function. J Nucl Cardiol 5:451-463, 1997
24. Calnon DA, Kastner RJ, Smith WH, et al: Validation of a new counts-based gated SPECT method for quantifying left ventricular systolic function: comparison to equilibrium radionuclide angiography. J Nucl Cardiol 5:464-471, 1997
25. DePuey EG, Nichols K, Dobrinsky C: Left ventricular ejection fraction assessed from gated technetium-99m-sestamibi SPECT. J Nucl Med 34:1871-1876, 1993
26. Yang KTA, Chen HD: A semi-automated method for edge detection in the evaluation of left ventricular function using ECG-gated single-photon emission tomography. Eur J Nucl Med 21:1206-1211, 1994
27. Boonyaprapa S, Ekmahachai M, Thanachaikun N, et al: Measurement of left ventricular ejection fraction from gated technetium-99m sestamibi myocardial images. Eur J Nucl Med 22:528-531, 1995
28. Everaert H, Franken PR, Flamen P, et al: Left ventricular ejection fraction from gated SPECT myocardial perfusion studies: a method based on the radial distribution of count rate density across the myocardial wall. Eur J Nucl Med 23:1628-1633, 1996
29. Germano G, Kiat H, Kavanagh PB, et al: Automatic quantification of ejection fraction from gated myocardial perfusion SPECT. J Nucl Med 36:2138-2147, 1995
30. Germano G, Kavanagh PB, Chen J, et al: Operator-less processing of myocardial perfusion SPECT studies. J Nucl Med 36:2127-2132, 1995

31. Faber TL, Akers MS, Peshock RM, et al: Three-dimensional motion and perfusion quantification in gated single-photon emission computed tomograms. J Nucl Med 32:2311-2317, 1991

32. Faber TL, Cooke CD, Peifer JW, et al: Three-dimensional displays of left ventricular epicardial surface from standard cardiac SPECT perfusion quantification techniques. J Nucl Med 36:697-703, 1995

33. Palmas W, Friedman JD, Diamond GA, et al: Incremental value of simultaneous assessment of myocardial function and perfusion with technetium-99m sestamibi for prediction of extent of coronary artery disease. J Am Coll Cardiol 25:1024-1031, 1995

34. Elkayam U, Weinstein M, Berman D, et al: Stress thallium-201 myocardial scintigraphy and exercise technetium ventriculography in the detection and location of chronic coronary artery disease: comparison of sensitivity and specificity of these noninvasive tests alone and in combination. Am Heart J 101:657-666, 1981

35. Smanio PE, Watson DD, Segalla DL, et al: The value of gating of technetium-99m-sestamibi single-photon emission tomographic (SPECT) imaging. J Am Coll Cardiol 30:1687-1692, 1997

Attenuation and Scatter Compensation in Myocardial Perfusion SPECT

James R. Galt, S. James Cullom, and Ernest V. Garcia

Nonuniform attenuation, Compton scatter, and limited, spatially varying resolution degrade both the qualitative and quantitative nature of myocardial perfusion SPECT. Physicians must recognize and understand the effects of these factors on myocardial perfusion SPECT for optimal interpretation and use of this important imaging technique. Recent developments in the design and implementation of compensation algorithms and transmission-based imaging promise to provide clinically realistic solutions to these effects and provide the framework for truly quantitative imaging. This achievement should improve the diagnostic accuracy and cost-effectiveness of myocardial perfusion SPECT.

SINGLE PHOTON EMISSION computed tomography (SPECT) is widely established as a noninvasive method for the diagnosis and management of patients with coronary disease.[1] More recently, it has emerged as an effective tool to assess left ventricular myocardial function and prognostication.[2,3] These attributes exist despite the limited ability to obtain images that reliably represent the true tracer distribution as a result of image noise, limited spatial resolution that varies within the image, Compton scatter, and photon attenuation. These combined factors preclude a linear relationship between the counts (intensity) in the image and the true tracer distribution. Of these, artifacts resulting from photon attenuation in the variable media of the thorax are the most significant factors limiting interpretative accuracy in myocardial SPECT.[2,4,5]

Attenuation reduces the specificity of cardiac SPECT by causing variations in normal tracer patterns that may resemble patterns in the presence of disease. Quantification of the tracer distribution in studies affected by attenuation has been limited because conventional reconstruction algorithms do not provide the mathematical framework to correct for attenuation, Compton scatter, and spatially varying resolution. New hardware and reconstruction techniques directed toward solving these problems have become available commercially and are being introduced clinically. Although initial clinical reports are promising, much work remains before we fully understand the benefits and limitations of these new technologies and techniques.

From the Department of Radiology and the Center for Positron Emission Tomography, Emory University School of Medicine, Atlanta, GA; and Cardiovascular Consultants, Mid-America Heart Institute, Kansas City, MO.

Disclosure: The authors receive royalties from the sale of software for SPECT attenuation correction, scatter compensation, and resolution recovery.

Address reprint requests to James R. Galt, PhD, Division of Nuclear Medicine, Department of Radiology, Emory University School of Medicine, Atlanta, GA 30322.

0001-2998/99/2903-0002$10.00/0

CLINICAL IMPLICATIONS OF ATTENUATION AND SCATTER

Attenuation affects cardiac SPECT images in both easily identifiable and subtle ways. The most commonly cited effects are artifacts associated with breast attenuation in women and diaphragmatic attenuation in men.[2,5] However, the association with gender is not exclusive and the position and extent may vary greatly. Exaggerated diaphragmatic attenuation can occur in women and significant pectoral musculature or gynecomastia in men can yield artifacts similar to breast attenuation expected more in women.

Breast attenuation artifacts are commonly identified as a region of decreased count density over the anterior myocardial wall resembling hypoperfusion. Significant amounts of breast tissue overlying the heart for an extended number of views in the acquisition can preclude clearly identifiable artifacts associated with more dense and localized breast tissue. For these patients, global count density may be significantly reduced, leading to increased image noise and reduced image quality, particularly for the low-count perfusion studies. The severity and extent of the attenuation pattern depend on the thickness, density, shape, and position of the breast relative to the myocardium.[2,6,7] Changes in breast position during rest and stress imaging may also change the attenuation pattern, thereby resembling changes in perfusion. If the breast position is the same between scans, the appearance of a fixed perfusion defect may result and may be interpreted as partial reversibility (ischemia) or scar, depending on how fixed the

defect appears. Similar changes in apparent perfusion patterns can result from diaphragmatic attenuation in the inferior wall (Fig 1). Both situations are problematic for mild or moderate fixed defects, which often cannot be sufficiently discriminated from soft-tissue attenuation patterns.

Quantification by normal data base analysis can lead to false-positive interpretation when exaggerated attenuation (unrecognized by the clinician) reduces the normalized counts beyond the threshold criteria for abnormality.[8] Without proper attenuation compensation, the normal files reflect external factors, including anatomical variation in the normal population, gender differences, and imaging system resolution limitations.[8,9] People of both sexes vary greatly in shape and size (Fig 2). Consequently, abnormality criteria are required to be broad, leading to increased uncertainty in the quantitative identification of perfusion patterns.

MINIMIZING THE CLINICAL IMPACT OF ATTENATION AND SCATTER

Reviewing the projection images in a cine format before the interpretation of the tomograms is an effective tool in the identification of attenuation artifacts.[2,4,5] When viewed in this manner, attenuation that may cause artifacts will appear as a decrease in relative count density and resemble a shadow moving across the myocardium and surrounding regions. This finding should correlate with the known location of anatomical structures such as the breast and should help to differentiate true hypoperfusion from artifact. Unfortunately, the combined effects of hypoperfusion and attenuation are often difficult to differentiate objectively, leading to reduced test sensitivity.

With Technetium-99m sestamibi, sufficient counts exist to temporally gate the SPECT acquisitions with the electrocardiogram (ECG) yielding dynamic tomographic images of the myocardium for functional assessment.[3] This technique provides an effective way to characterize fixed defects as scar or attenuation artifact through assessment of thickening and regional wall motion.[10] Myocardial regions with positive thickening and normal wall motion are an indicator of viability.[3] Therefore, a single gated-SPECT acquisition performed at stress may provide the same diagnostic information as conventional separate injection rest/stress protocols in patients without prior myocardial infarction.[3] This is because the stress perfusion study is acquired with the patient at rest, thus simultaneously providing stress perfusion but resting functional information. One complication is that if a patient shows reduced counts in the stress perfusion study because of attenuation, it could appear to normally thicken and thus be interpreted as an ischemic wall. This situation would require a separate resting perfusion study to confirm a fixed defect due to attenuation. Thus, accurate attenuation correction of a stress study would have eliminated the need for the resting study. This approach

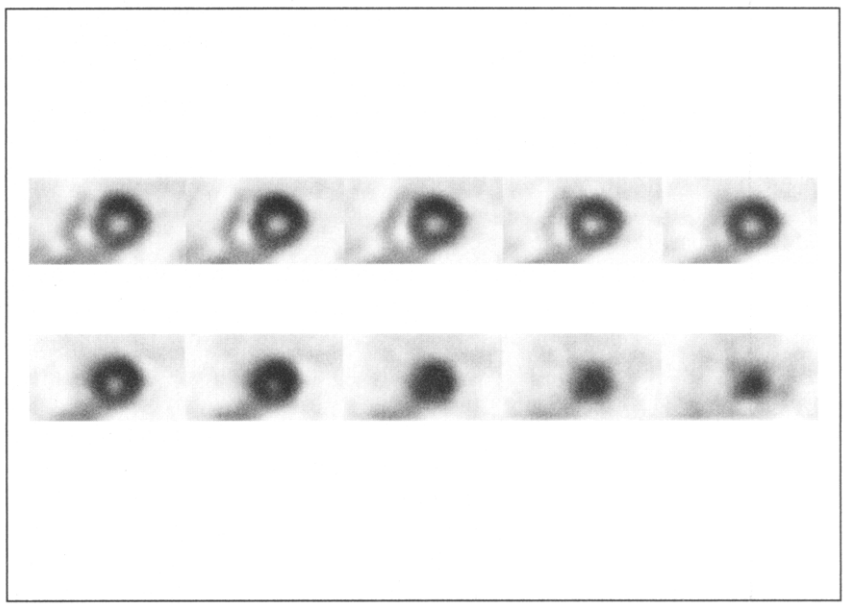

Fig 1. Example of diaphragmatic attenuation artifact in a Tc-99m sestamibi study of a male patient with low likelihood for coronary artery disease showing suppressed count density in the inferior and septal walls. Base (upper left) to apex (lower right).

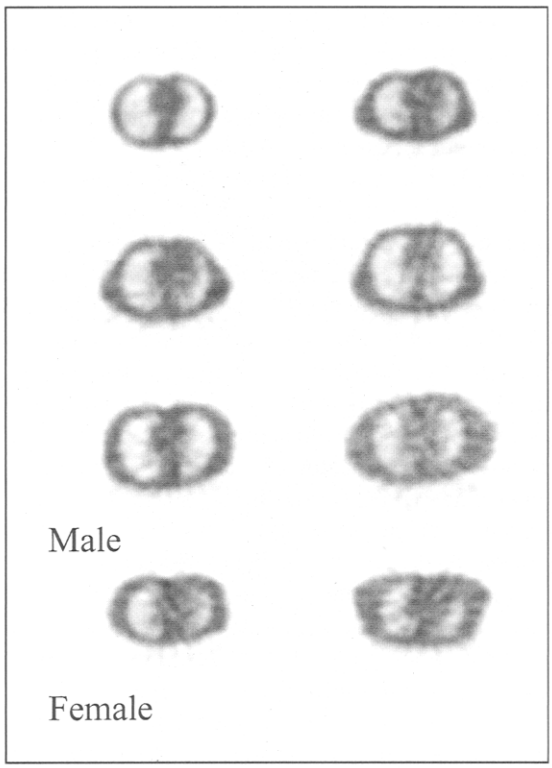

Fig 2. Transmission tomograms of eight patients (six men and two women) at the level of the heart. There is a great deal of diversity in the size and shape of patients' chests.

would provide significant cost-effectiveness in diagnosing coronary disease.

SPECT imaging in the prone position has also been reported as a method of minimizing attenuation artifacts.[11] When positioned this way, the heart and diaphragm as well as subphrenic structures shift to reduce inferior wall attenuation while potentially increasing anterior wall attenuation. For assessing suspected inferior wall attenuation, a planar static left lateral decubitus view can be acquired with the patient on his/her right side and used for comparison with the corresponding lateral projection of the SPECT acquisition. The shifting position of the organs relative to the myocardium in this view often reveals an increase in inferior wall counts relative to the anterior regions correlating with diaphragmatic attenuation artifacts in the SPECT supine study.

A method that minimizes the effects of attenuation artifacts by using a select range of projection angles determined to be minimally affected by attenuation has been described.[12] In this approach, a sinogram representation of the projection data is examined to identify the angular views that are most affected by attenuation. A 180° angular range is defined that excludes these projections as much as possible. Although this technique lessens the effects of attenuation, it cannot provide complete compensation.

Although clinicians may become very adept at recognizing breast and diaphragmatic attenuation, in general attenuation artifacts may be subtle. They may contribute to erroneous count ratios between the left ventricular walls[13] that may mask the severity of perfusion defects.[6,7] Patients with unique anatomy such as vertically or horizontally positioned hearts may present unique attenuation patterns that are not easily identified. As a result of these variations, the specificity of SPECT is limited, and additionally the frequency of false-negative interpretations can be increased when physicians attempt to read around artifacts and incorrectly attribute a decrease in counts to attenuation instead of hypoperfusion.

The need for reliable and efficient attenuation compensation methods for cardiac perfusion SPECT with thallium-201 and Tc-99m labeled imaging agents has long been recognized.[2,4,5] Cardiac positron emission tomography (PET) has clinically efficient attenuation compensation, which contributes to its quantitative superiority over SPECT.[14,15] Although the attenuation compensation techniques emerging for SPECT were inspired by methods used in PET,[16,17] the problem of attenuation compensation for SPECT is significantly more complex because of differences in the emission process and associated measured quantities.

PHYSICAL FACTORS THAT COMPROMISE MYOCARDIAL PERFUSION SPECT

Artifacts in SPECT images arise from the combined effects of photon absorption, Compton scatter, and the degradation in resolution with distance from the collimator. Each of these interrelated factors produces inconsistent information in the planar projections in violation of the assumptions behind filtered back-projection (FBP), the most widely used tomographic reconstruction algorithm. The effect of these factors on myocardial SPECT is quite complex, as illustrated in Figure 3. Photons emitted from the heart and picked up by the detector in an anterior view have traversed a relatively small amount of tissue (soft tissue and bone). In a lateral view, photons must traverse a

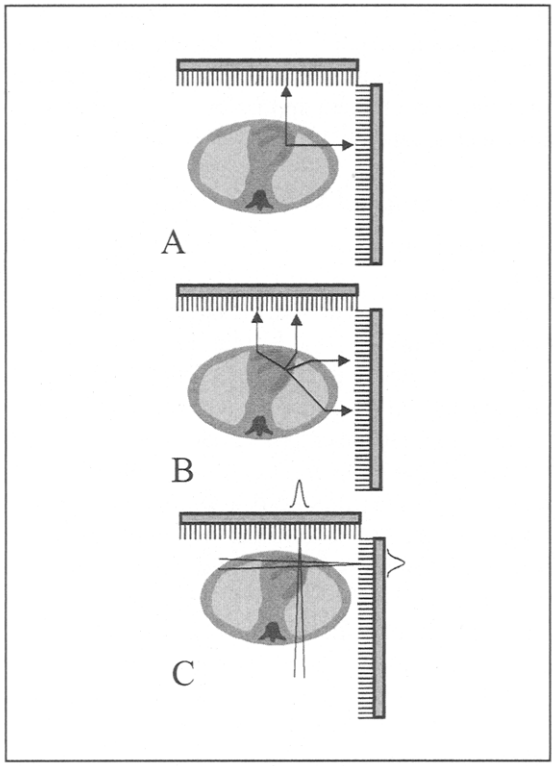

Fig 3. Physical factors that compromise myocardial perfusion SPECT include (A) Nonuniform attenuation (photons emitted from a single point in the heart pass through different materials in different planar projections); (B) Compton scatter (photons emitted from that point no longer appear to originate there); and (C) Nonstationary resolution (the further the distance from the point to the camera in each projection, the poorer the resolution).

greater distance but through different materials (including lung) to reach the detector. As the detector moves about the patient, the projection profile varies with the attenuation along the projection ray and the distance to the collimator.

Attenuation is described quantitatively by the linear attenuation coefficient (commonly depicted by the Greek letter mu [μ]).[18] The process of attenuation is described by Equation 1, where A_x is the activity measured after attenuation through a thickness of tissue x and A_0 is the true activity at a point in the body.

$$A_x = A_0 e^{-\mu x} \quad (1)$$

The term $e^{-\mu x}$ represents the fraction of photons that are attenuated over a distance x and includes the effects of photons lost to Compton scatter and absorption. For the ideal case when no scatter is detected in the photopeak energy window, the μ value for a given energy is referred to as narrow beam and is unique depending on the composition of tissue. When scattered photons are detected in the photopeak energy window, the μ values are referred to as broad beam or effective and are no longer unique. The narrow and broad beam values of μ for Tc-99m in soft tissue are approximately equal to those of water and are 0.154 cm^{-1} and 0.12 cm^{-1}, respectively.[19] The probability of absorption decreases as photon energy increases, and this is the reason why attenuation artifacts are reported to be less severe (but still significant) with Tc-99m agents than with T1-201.[4,5] Narrow beam attenuation coefficients[20] and corresponding half-value layers for selected materials in the body are given in Table 1. The half-value layer is defined as the distance needed for attenuation to remove half of the photons.

When a photon undergoes Compton scattering though interactions with an electron, it changes direction and loses energy. If detected in the photopeak energy window, Compton-scattered photons are likely to be mispositioned in the transverse image, leading to reduced image contrast and reduced lesion detection. A Tc-99m photon at 140 keV scattering through 45° will lose 7.4% of its energy (about 10 keV), which is well within the 20% (±10%) energy window commonly used for SPECT acquisitions. T1-201 photons originate as characteristic x-rays spanning a range from 69 to 83 keV. A 73-keV photon from T1-201 that scatters through 45° only loses 4% (about 3 keV) of its energy. Just as with attenuation, scatter can be a more severe problem with T1-201 than Tc-99m. When the hypoperfused regions are detected with T1-201 or Tc-99m tracers, scatter affects the apparent extent and severity of the abnormality. In some patients the scatter from high concentrations of activity in abdominal organs (primarily liver and bowel) may artifactually increase the counts in the inferior wall of the myocardium.[21-23]

Table 1. Narrow-Beam Attenuation Coefficients (μ) and Half-Value Layers (HVL) for Selected Materials

	Tl-201 (73 keV)		Tc-99m (140 keV)	
Material	μ (l/cm)	HVL (cm)	μ (l/cm)	HVL (cm)
Bone	0.429	1.62	0.286	2.42
Muscle	0.191	3.63	0.153	4.53
Lung	0.063	11.00	0.051	13.59
Air	0.0002	3465	0.0002	3465

The most important factors in the spatial resolution of images made with a conventional scintillation camera are the geometry of the collimator and the distance from the camera face. The resolution of both fan beam and parallel hole collimators degrades with distance. As the camera orbits the patient for a circular acquisition, the only point in the patient that maintains the same distance from the collimator in all the views is the center of rotation. The spatial resolution at any given point in a SPECT image is a result of the resolution in each of the planar projections. Thus, the center of rotation is the only point in the image with symmetric resolution. This spatially varying resolution can lead to significant distortion in the reconstructed images, particularly for 180° acquisitions.[24,25] Although combining the two opposing views of a 360° acquisition degrades spatial resolution, it also minimizes its variation across the transverse plane.[26] If body contour or elliptical orbits are used, the variations in resolution may result in even more severe artifacts.[27]

ATTENUATION COMPENSATION

Conventional Methods

Although many methods have been proposed for attenuation compensation in cardiac SPECT, the most common methods used in commercial systems until recently have been a prereconstruction method based on work by Sorenson[28] and a postreconstruction method developed by Chang.[29] Both of these methods assume that the attenuation within the body is homogeneous and have been used effectively for SPECT applications where the attenuation is approximately homogeneous, such as liver imaging.

For the Sorenson and Chang methods, it is required that the outside body contour be defined. In practice, commercial methods often fit the body with an ellipse, defined either by the operator or a count threshold of the emission data. Some manufacturers allow each transverse image to be fitted by a separate ellipse, but some assume that a single ellipse will adequately fit the body for all transverse images. With these methods, empirically derived or effective attenuation coefficients have been measured under different anatomical conditions to compensate for variations in tissue density as well as the effects of Compton scatter. By using a broad-beam value for μ (lower than the narrow-beam value), the effective attenuation coefficients allow scattered photons to be included in the reconstructed image.[28,29] The attenuating material in a patient's thorax is too varied for a constant attenuation coefficient approximation to be used to any great advantage.[30]

Transmission-Based Methods

Accurate attenuation correction in areas of nonhomogenous attenuation requires that an accurate estimate of the patient-specific attenuation distribution be known. Methods that use transmission imaging to achieve this for SPECT were first investigated in the 1980s and proposed much earlier.[26] In 1986, an external flood source was used for attenuation compensation in liver SPECT.[31] A transmission scan produced a tomographic image similar to that of a CT scan but with reduced, poorer resolution and increased image noise. A similar approach was used for attenuation compensation of cardiac images by Bailey et al.[32] This method also used a flood source mounted on the scintillation camera gantry opposite the camera and parallel hole collimation. The compensation algorithm was based on Chang's method but with the use of the measured attenuation map instead of a homogeneous one. Other researchers investigated the use of point sources of radioactivity and converging collimation for improved imaging sensitivity.[33,34]

In the past few years a wide range of equipment has been designed for transmission imaging with SPECT scanners (Fig 4). The first system to be commercialized was based on the work of Tung et al[34] using a triple-detector SPECT.[35] This approach uses a line source coupled with a long-focal-length (60-cm) fan beam collimator to acquire a transmission scan separately or simultaneously with the standard emission scan (Fig 4A). Fan beam collimated detectors also collect the emission projection. Similar approaches using triple-detector systems have been proposed by others combining parallel hole collimation to collect the emission projections and fan beam geometry to collect the transmission data.[36] These systems yield simultaneous or sequential emission-transmission images with high counting efficiency. One criticism of this configuration is that portions of the body may be truncated in the transmission projections by the fan beam collimation. Image artifacts can result from severely truncated transmission images without proper compensation.[37] Suboptimal images and

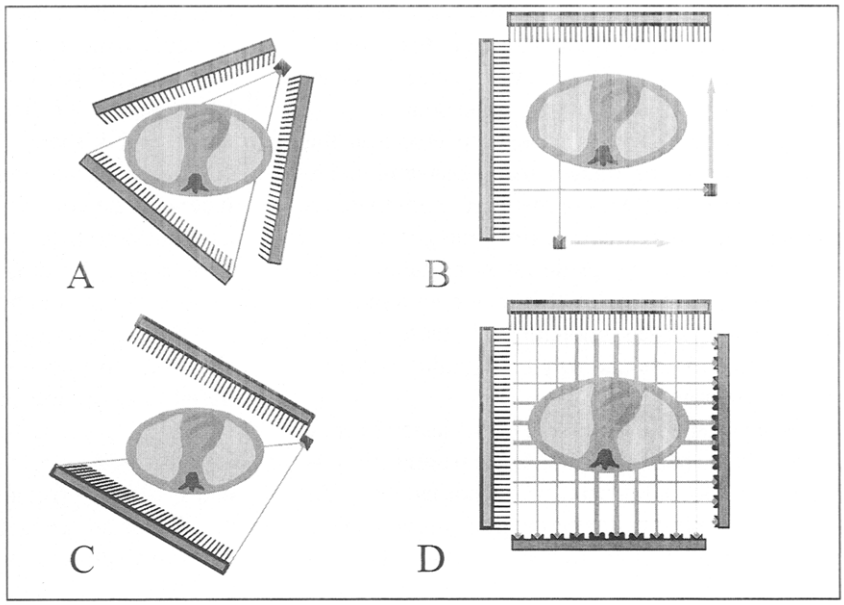

Fig 4. Selected SPECT-based transmission imaging configurations: (A) line-source and fan-beam collimation for triple-detector systems, (B) scanning collimated line sources for dual 90° detector systems, (C) asymmetric fan-beam geometry for dual 180° opposed systems that can also be implemented on triple-detector systems, and (D) arrays of line sources mounted opposite both cameras of a dual 90° detector system.

artifacts can result from severely truncated images without proper compensation. The use of new reconstruction techniques that use information about the patient contour and complex detector orbits can minimize the effect of truncation in the reconstructed image.

Most manufacturers of dual 90° detector SPECT systems have developed attenuation compensation hardware based on a scanning line source approach first described by Tan et al.[38] This method uses conventional parallel hole collimators and collimated line sources that scan across the field of view of the camera simultaneously with the emission acquisition or in a separate acquisition (Fig 4B). Only the portion of the detector directly across from the line source receives photons from the transmission source. This is accomplished through the use of an electronic window or masking that moves in unison across from each of the line sources. The remainder of the detector surface acquires the emission scan in the usual manner. The scanning electronic mask coupled with energy discrimination circuitry minimizes energy cross-over between the transmission and emission photons, and the geometry provides good approximation to the narrow beam values.[38] A limitation is the complexity of moving parts and the start-up and maintenance costs of the line sources.

A third method for obtaining transmission images has been shown for dual 180° opposed or triple-detector systems[39,40] (Fig 4C). A line source is placed next to one of the detectors opposite an asymmetric fan-beam collimator on the transmission detector that is focused on the line source. The line source is out of the field of view of the other detector(s) that are used for emission imaging. With this approach, only half of the emission field of view is sampled by the transmission scan at any given planar projection, and a 360° camera orbit is required to complete the scan.

A fourth approach uses an array of line sources positioned close enough together that they appear as a continuous distribution to the scintillation cameras acquiring the transmission scan (Fig 4D). The sources can be configured with different strengths such that the flux is greater in the center of detector (shown in the figure as rays of differing widths).[41] This approach maximizes the counts received through the more attenuating central regions of the patient and minimizes the flux at the directly exposed regions of the detector. The latter can contribute to high count rates that can impair detector performance causing dead-time errors and errors in the accuracy of the attenuation coefficient values.

A fifth approach uses a "sheet line source" constructed from a narrow long fluoroplastic tube embedding in a rectangular acrylic board mounted in front of one detector on a dual 180° detector system.[42] The opposite detector acquires the transmission scan. This design allows the use of a fillable transmission source that covers the full face

of the camera (to avoid truncation) but without the problems that occur when standard sheet sources are rotated on a SPECT camera gantry (such a bubbles at the top and bulging at the bottom).

Experimental systems have been proposed that obtain transmission images using conventional x-ray imaging. These systems may minimize the problems of patient imaging time, image noise, and spectral crossover by using an x-ray tube to produce much higher photon flux than does a radionuclide source. When implemented, these systems may be able to produce very high quality transmission tomograms.[43,44]

An important consideration in the design of these systems is the absorbed dose to the patient from the external radionuclide source. Absorbed dose depends on the photon flux of the transmission source and time of exposure. Absorbed dose values obtained with the current systems do not appear to be a limitation to the transmission-based attenuation compensation.[38]

Radionuclide Sources for Transmission Scanning

Most early studies of attenuation correction used sources filled with Tc-99m for the transmission scan because of Tc-99m's cost and availability.[45] Although Tc-99m may still be considered for some systems, its use is limited to T1-201[42,46] or sequential scanning with Tc-99m agents. Tc-99m's 6-hour half-life would also require that the source be filled on daily basis (if not more frequently).

An ideal transmission source for cardiac perfusion SPECT requires that the source (1) is relatively inexpensive and commercially available, (2) has a long half-life for practical clinical use, and (3) has favorable spectral properties for gamma camera imaging and sufficient separation from the T1-201 and Tc-99m photo peaks. Proposed sources for transmission imaging and their physical properties are listed in Table 2.

Gadolinium-153 (Gd-153) has emerged as a popular choice for transmission imaging largely because of its relatively long half-life (242 days) and approximately 100 keV (actually two peaks at 97 and 103 keV) photon emissions, which lie between the T1-201 and Tc-99m photo peaks. Additional k-shell x-rays at 40 to 50 keV may contribute an additional dose to the patient and increase detector count rate without contributing to transmission image formation. Therefore, filtering with copper or other materials may be used to remove this lower-energy component.[36]

Americium-241 (Am-241) with its 59-keV emissions has also been used successfully for SPECT-based transmission scanning and attenuation compensation.[47] It has the advantage of a very long half-life (432 years) and falls below the photo peak energies of Tc-99m and T1-201. The photo peak of Am-241 is adjacent to the T1-201 energy window, which may present challenges for scatter compensation techniques based on measured scatter models and T1-201 imaging.

The dual nature of emission-transmission imaging requires that crossover of photons from one radionuclide into the energy window of the other be minimized by the imaging hardware and protocol or by applying compensation algorithms.[47,49] Rapid sequential imaging protocols (emission study followed by transmission study) and interlaced protocols (emission and transmission images acquired sequentially at each projection) have been proposed to minimize the crossover of the emission and transmission images.[50,51]

The spectral crossover characteristics depend on the particular combination of transmission and emission sources. For example, emission photons from Tc-99m (140 keV) can scatter and be detected in the Gd-153 energy window at 100 keV (Fig 5). Without compensation, the measured attenuation values can be underestimated because scattered photons artificially increase the measured transmission count density, corresponding to less attenuation along the measured ray and yielding reduced attenuation coefficient values.[47,48] Similarly, with

Table 2. Radionuclides Proposed for SPECT-Based Transmission Imaging

Nuclide	Decay Mode	Photon Emissions (keV and yield [%])	K-Shell X-Ray Emissions (keV and yield [%])	Half-Life
Technetium-99m	IT	140 (89)	18-21 (6)	6 h
Thallium-201	EC	135 (3), 167 (10)	69-82 (94)	73 h
Gadolinium-153	EC	97 (28), 103 (20)	41-48 (119)	242 d
Cobalt-57	EC	122 (86), 137 (10)	N/A	271 d
Americium-241	Alpha	59 (36)	N/A	432 y

Abbreviations: EC, electron capture; IT, isomeric transition; alpha,alpha decay.

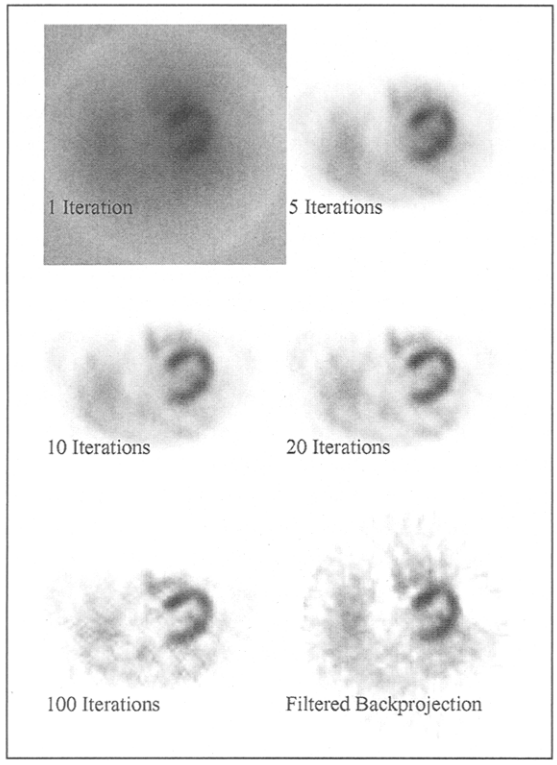

Fig 5. Iterative reconstruction of a Tc-99m sestamibi patient study (transaxial slices). The quality of images reconstructed with the maximum likelihood algorithm (beginning with a uniform image) and attenuation correction improves with successive iterations. After a point, however, image noise begins to degrade the image, as can be seen in an image produced by 100 iterations. Starting the process with an image reconstructed by filtered back-projection may reduce the number of iterations.

Gd-153 as the transmission source, photons can down-scatter and be detected in the 69- to 80-keV energy window of T1-201. As a result, count distributions may be artificially (and nonuniformly) increased in the T1-201 image, leading to reduced image quality. Similar situations may exist for other source combinations.

Because the transmission image is usually obtained using different photon energy compared with the emission image in simultaneous acquisition, the attenuation map must correspond to the photo peak emission energy.[52] A linear scaling has been implemented but may not be sufficient for bone, particularly for the lower-emission energy of T1-201.[48] This step requires an assumption about the photo peak scatter components of the emission and transmission images because attenuation coefficient values depend on the proportion of scatter in these images, as described earlier. Further improvements in attenuation compensation methods will likely result from the use of Compton scatter correction techniques.

Acquisition of Transmission Scans

The transmission-based approach to attenuation compensation requires that the emission and transmission images be spatially aligned (registered) in three dimensions. Alignment errors caused by shifting of the patient between transmission and emission scans of a sequential acquisition protocol, for example, can cause significant errors in the corrected images. The importance of this requirement has been recognized for PET[53] and applies equally to SPECT.[54-56] Alignment is especially important for the lateral wall of the left ventricle where myocardium and lung abut.[13] A misalignment between the attenuation map and emission image in this region would cause improper attenuation compensation of the heart's lateral wall, depending on the nature of the misalignment.

Most commercial systems are being developed for simultaneous acquisition. However, sequential scanning protocols can minimize the effect of spectral crossover between the emission and transmission sources but limit the timing of injection and imaging options. They also require the patient to remain motionless between the emission and transmission scans to preserve registration of the emission and transmission data.

Image noise is present in both the emission and transmission projections. Noise in the transmission scan is driven by the lowest-count projections in the acquisitions. As the transmission sources decay and are used with heavier patients, the noise will increase because fewer photons will pass through the patient. The transmission scan must, however, be of sufficient statistical certainty that errors introduced into the attenuation map do not significantly affect the attenuation compensated emission image. These errors can be propagated from the attenuation map into the emission images by the attenuation compensation algorithm. It has been shown in simulation with a converging geometry approach to transmission imaging that with transmission imaging methods for SPECT, noise in the emission images is the limiting factor when compared with noise in the transmission images.[57] In PET, the problem is somewhat reversed in that the transmission statistics are the limiting factor.[58]

One solution to the problem of noise in the

transmission scan with PET has been to segment an attenuation map into regions of similar tissue composition to which previously determined attenuation coefficients are assigned, generating a "noise-free" estimate of the attenuation map.[58] A compensation for attenuation is calculated from these data and applied to the emission data. Similar methods have been shown for cardiac SPECT.[59,60] This approach requires further investigation for SPECT, where it may also offer a solution to the problem of down-scatter into the transmission image by assigning known coefficients to affected regions. A rapid-acquisition transmission image with lower counts could then potentially be used for attenuation compensation. A potential limitation to the segmented approach is that the "perfect" resolution images that result may lead to a resolution mismatch between the emission and transmission images. This effect is most critical at borders between significantly different attenuating tissues such as the lateral wall–right lung interface, where artifacts may result from misregistration.[53,54] Therefore, the spatial resolution of the two images must be similar and objective methods for determining the segmented boundaries must be established to make this approach optimal for clinical SPECT.

Attenuation Maps Without Transmission Imaging

Techniques for obtaining patient-specific attenuation maps without transmission imaging have also been reported.[61-63] These techniques seek to segment the body by defining the boundaries of the lungs and the body surface. Tc-99m macroaggregated albumin (MAA) is used to define the lung boundaries. The body surface is determined either by use of a scatter window[62] or use of a flexible body wrap containing Tc-99m.[63] Once attenuation coefficients are assigned to the segmented map, it is used in the same manner as transmission-based attenuation maps. These methods have shown successful attenuation compensation in experimental studies and a small number of patients, but remain to be demonstrated as a clinically practical approach.

Iterative Reconstruction

To date, no analytical solution exists for the reconstruction of the tracer distribution with attenuation compensation in a nonhomogeneous medium. A mathematical approach to solving this problem is the use of iterative reconstruction algorithms. Iterative algorithms were first proposed for image reconstruction as algebraic solutions to large systems of discrete equations describing the process of SPECT.[26] It was recognized that the physical factors affecting the formation of projection images could be included in the terms of the equations. More recently, two broad classes of iterative reconstruction algorithms have emerged for application to attenuation correction in cardiac SPECT: iterative filtered back-projection algorithms[64-66] and statistical reconstruction algorithms.[30,34] Iterative algorithms model the SPECT acquisition using a mathematical representation of the projection image formation process (reprojector), a back-projector algorithm, an initial estimate of the transverse tracer distribution, and the attenuation coefficient map. These algorithms differ from the analytic filtered back-projection algorithm in that they attempt to improve the accuracy of the tracer distribution through successive image approximation that includes the physics of the imaging process.

Iterative Filtered Back-projection

The Chang method described earlier forms a basis for the class of reconstruction algorithms referred to as iterative filtered back-projection (IFBP) algorithms. These algorithms use the FBP algorithm as the back-projector component. With these algorithms, an initial uncorrected FBP reconstruction is typically used as the initial tracer estimate. Several hybrid approaches that combine preprocessing techniques with IFBP for attenuation correction have also been described.[65-69] An important characteristic of the IFBP and hybrid algorithms is that they very rapidly approach an image beyond which no significant change in the image data occurs with successive iteration. The rapid convergence can be accounted for largely by the facts that these algorithms use (1) a difference calculation between the measured and reprojected data, (2) the ramp filter of the FBP algorithm as the basis for back-projection, and (3) a multiplicative operation with the attenuation compensation matrix where values can be significantly greater than 1.0. However, the combined effects of these properties leads to an increase in image noise and artifacts for higher iteration numbers that can degrade image quality and quantitative accuracy.[30] Noise filtering or other mathematical techniques must be used to constraint the pixel values to resemble their neigh-

bors and prevent image artifacts.[64,65,70] When the reprojected estimates approximate the measured images with a predetermined accuracy, the process is said to have converged. In the strict sense, convergence of any iterative algorithm represents an ideal result that can only be achieved with some bias.[70]

The point to which IFBP algorithms converge and their mathematical properties are not as well defined mathematically as other proposed algorithms.[71] They can be modified to incorporate Compton scatter and spatial resolution information in addition to the attenuation map in the reprojection steps of the algorithm.[64] However, even without the strong theoretical basis of other iterative algorithms, IFBP algorithms have shown significant potential to improve the diagnostic accuracy of cardiac SPECT with attenuation correction.[71]

Statistical Reconstruction Algorithms

Statistical reconstruction algorithms are based on the probability of photon interaction and detection given attenuation and other physical factors affecting photon transport. They attempt to reconstruct the images based on the quantitative criteria they are optimizing.[30,34,48] These algorithms also require an imaging model for reprojection that can incorporate physical factors affecting the accuracy of the projections such as attenuation, Compton scattering, the statistics of radioactive decay, and variable spatial resolution.[72-74]

One of the important developments was the demonstration that the maximum-likelihood criteria commonly used in statistical analysis could be used to accurately reconstruct nuclear medicine images.[75] The maximum-likelihood expectation maximization (MLEM) implementation of this algorithm was later investigated for attenuation compensation in cardiac SPECT.[30] The MLEM algorithm attempts to determine the tracer distribution that would most likely yield the measured projections given the imaging model and attenuation map. The MLEM algorithm converges slowly, requiring many more iterations than the IFBP algorithms. The slowly converging characteristics of this algorithm yield greater control over image noise.[30,76] An example of the reconstruction of the myocardium with the MLEM algorithm is shown in Figure 6. The point of convergence of this algorithm and related number of iterations for clinical use is a source of debate.[70] To date, there is no common rule for stopping the algorithms after an optimal number of iterations on clinical data, and protocols describing the optimal number of iterations will largely be empirically based.

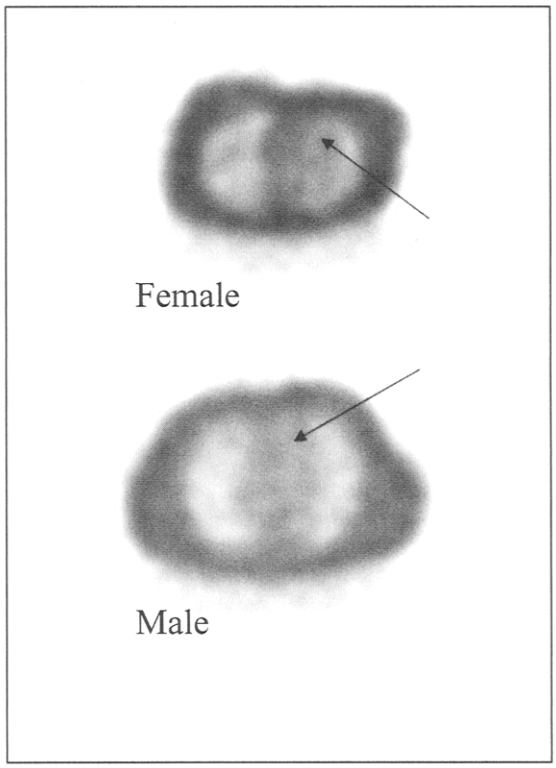

Fig 6. Down-scatter from the emission radiopharmaceutical can degrade the quality of a transmission scan. This figure shows transmission transaxials from a Tc-99m sestamibi scan made with Gd-153 scanning line sources. The density of the body in the area of the heart (shown by the arrows) is underestimated because of down-scatter of Tc-99m photons (140 keV) into the Gd window (centered on 140 keV).

Recently, the MLEM algorithm has been implemented for iterative reconstruction of images by the Ordered-Subsets Expectation Maximization (OSEM) approach.[77] This approach performs an ordering of the projection data into subsets. The subsets are used in the iterative steps of the reconstruction to greatly speed up the reconstruction. The advantage of the OSEM is that an order of magnitude increase in computational speed can be obtained.

Statistical-based reconstruction algorithms can also be used to reconstruct the attenuation maps from transmission scanning.[48] These algorithms have shown advantages over the FBP algorithm approach for estimating attenuation maps in the presence of transmission projection truncation that

can occur with converging imaging geometry.[37] However, in the absence of truncation, both methods yield accurate attenuation coefficient values and accurate attenuation compensation, providing that adequate statistics are available.

SCATTER COMPENSATION

Scatter compensation methods for SPECT require estimation of the number of scattered photons in each pixel of the image. This is a complex matter because the scatter component of the image depends on the energy of the photon, the energy window used, and the composition and location of the source and the scattering medium.[78,79] These methods can be divided into three broad categories: energy-window–based methods, deconvolution methods, and reconstruction-based methods.

One of the earliest and most widely used energy-window–based methods is the dual-window scatter subtraction method suggested by Jaszczak et al for Tc-99m.[80] This method requires a second energy window at a lower energy (127 to 153 keV) than the photo peak window (127 to 153 keV). A fraction of this window is subtracted from the photo peak window. The dual-window technique makes the assumption that the scattered photons in the scatter window are linearly proportional to the scattered photons in the photo peak window. The triple-energy–window technique (TEW) uses scatter windows on either side of the photo peak window. The contribution of scattered photons to the photo peak window is estimated as the average counts in the two scatter windows normalized to the photo peak windows.[81] Scatter compensation techniques using many energy windows have also been suggested.[82,83] At best, energy-window–based methods can provide only approximate scatter compensation and may result in an increase in image noise.[84]

Deconvolution techniques for scatter compensation assume that the scattered photons within the image can be modeled by a function independent of the scattering medium distribution. Scatter is removed or deconvolved from the image by restorative filtering methods.[85,86] Although these methods only require that a single energy window be acquired, they can also only provide approximate scatter compensation.

Reconstruction-based methods incorporate compensation for Compton scatter directly into the iterative reconstruction.[87-89] The physics of photon interactions provides a relationship between image scatter and the attenuation distribution in patients, suggesting that a measured attenuation map (from a transmission scan) can be used in conjunction with the source distribution provided by the emission scan to provide a study-specific correction.[90] Reconstruction-based techniques using this information incorporate a physical model of the scattering process in the iterative reconstruction algorithm information.[91-94] Preliminary results suggest that these methods, although complex, hold a great deal of promise.

RESOLUTION RECOVERY

Several approaches have been proposed to compensate for the loss of resolution with distance from the collimator and the resulting distortions produced in the SPECT images. Analytical approaches to the problem of distance varying the resolution model the shape of the collimator response to remove the effects from the image.[95,96] Another approach is to use the Frequency Distance principle,[97,98] which states that points at a specific source-to-detector distance correspond to specific regions in frequency space of the sinograms Fourier transform. Applying a spatially variant inverse filter to the sinograms performs the resolution recovery. This inverse filtering is relatively fast, but care must be taken not to amplify noise in the image.

Resolution recovery can also be included in iterative reconstruction methods. It is possible to include resolution recovery in both iterative filtered back-projection[64,99] and maximum likelihood reconstruction techniques.[72,73] These methods take considerably more computations to implement than the FDP but have potential to more accurately compensate for the resolution response.[74]

COMBINING ATTENUATION COMPENSATION, SCATTER COMPENSATION, AND RESOLUTION RECOVERY

Preliminary results with attenuation compensation suggest that both 180° and 360° scans can be significantly improved.[100,101] It has been shown that when there is significant hepatic or abdominal tracer uptake lying adjacent to the inferior wall of the heart, photons can scatter into this region, affecting interpretation of perfusion.[21-23] The region of the abdomen just inferior to the heart normally consists of homogeneous soft tissue. Attenuation in

this homogeneous region can be several times greater than for the nonhomogeneous thorax. After attenuation compensation, the brightness of abdominal activity normally suppressed by the homogeneous attenuation below the heart may be significantly increased relative to the myocardial walls[102] (Fig 7). It has also been shown that attenuation compensation without scatter compensation can result in an artificial increase in inferior wall counts.[23,56] Other reports show that photo peak scatter compensation further improves image accuracy when combined with attenuation compensation. It has become evident in recent reports that photo peak scatter compensation is essential for accurate attenuation compensation.[59,103]

As described in the literature, optimal accuracy of SPECT image reconstruction will require compensation for Compton scatter, the distance-dependent spatial resolution of collimated SPECT systems, and image noise together with the attenuation compensation.[68,74,103,104] Iterative reconstruction algorithms provide the opportunity to investigate complete compensation of cardiac SPECT images for the effects of the patient's anatomy as described by the attenuation map and the limited, spatially varying resolution of SPECT. It is anticipated that further improvements in the accuracy of cardiac SPECT reconstruction and diagnostic accuracy will result as these methods evolve.

When quantification is used, compensated normal files have been shown to provide statistically significant reductions in variability with some methods improving the certainty of interpretation.[7,100] The wide variety of techniques being implemented will require that normal files be specific for a given compensation technique, or it must be shown that the abnormality criteria are independent of the method. Ideally, proper compensation would yield images with counts related linearly to the true tracer concentration and therefore independent of technique.

ATTENUATION COMPENSATION AND DUAL ISOTOPE PROTOCOLS

The difference in the emission energy of T1-201 and Tc-99m yield different attenuation patterns and must be interpreted appropriately.[2,4] Generally, attenuation effects are greater in magnitude with T1-201 compared with the lower emission energy. For the sequential resting T1-201/stress Tc-99m sestamibi SPECT protocols,[105] the differences in attenuation can be a source of diagnostic error, particularly for the nonexpert. Increased attenuation of T1-201 from breast tissue can yield the appearance of a "reverse redistribution" because the same pattern may appear less severe in the stress sestamibi image and may be attributed to artifact.[106] T1-201 images also have reduced contrast relative to Tc-99m agents because of the increased proportion of photo peak scatter. This tends to make the left ventricular chamber appear smaller in the resting T1-201 image compared with

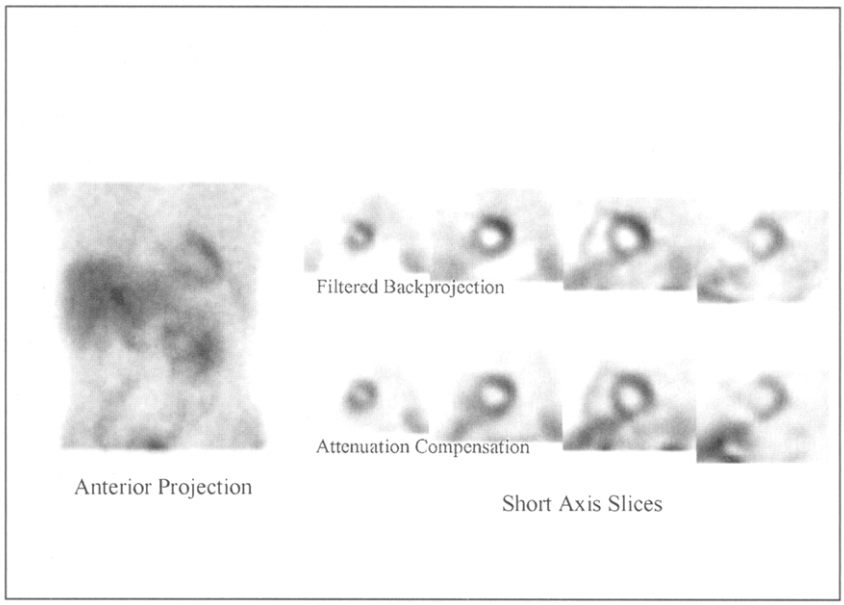

Fig 7. Attenuation correction will alter the appearance of extracardiac activity as well as the appearance of the myocardium. The short-axis slices in this Tc-99m sestamibi stress study with mild to moderate diaphragmatic attenuation (apex to base shown left to right) show that activity below the septal wall of the heart can become much more pronounced when attenuation correction is applied (even with the use of window-based scatter correction). In some cases this may complicate diagnoses.

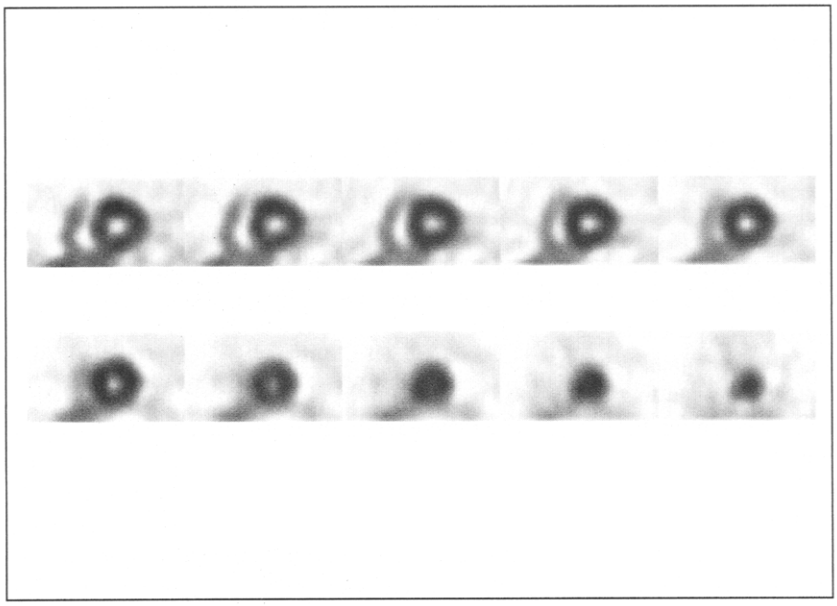

Fig 8. Iterative reconstruction including attenuation, Compton scatter, and nonstationary resolution compensation performed on the same Tc-99m sestamibi study of a male patient with low likelihood for coronary artery disease shown in Fig 2. The corrections improve the appearance of the uniform tracer distribution associated with normal perfusion. Additional improvement in image contrast is provided by scatter and resolution compensation. Base (upper left) to apex (lower right).

the stress Tc-99m image. In fixed defects resulting from scar, the contrast difference for the two energies may yield the appearance of partial redistribution suggestive of ischemia, requiring different thresholds for abnormality when interpreting. Proper attenuation compensation (with scatter compensation) should minimize these differences, yielding images of similar accuracy.

Proposed simultaneous T1-201/Tc-99m sestamibi SPECT protocols would require compensation for down-scatter of Tc-99m photons into the T1-201 energy window to become clinically feasible.[107-108] These scans could benefit from attenuation correction, but the scenario becomes more complicated because three different energies must be imaged and separated (two emission and one transmission). Other dual-isotope applications, such as sequential or simultaneous Tc-99m sestamibi and $F^{18}DG$ SPECT for perfusion and viability, should also benefit from proper attenuation compensation.[109,110]

CONCLUSIONS

Myocardial perfusion imaging with SPECT continues to be an important diagnostic tool, but as other technologies advance, SPECT techniques must also advance to remain viable. Compensation for attenuation, Compton scatter, and spatially varying resolution are integral parts of this continued development (Fig 8). Interest in the emerging compensation algorithms and instrumentation has prompted several recent review articles.[17,20,45,103,111] Transmission-based attenuation compensation techniques for myocardial perfusion SPECT are now a commercial reality, and are entering a phase of clinical evolution to define their benefits and limits.[7,42,56,69,100,112-117] Initial clinical results are very promising, however, data from ongoing prospective evaluation of these methods using angiographic correlation or PET imaging as a gold standard is just beginning to emerge.[118] These results are essential to define objectively the methods as accurate and cost-effective techniques. Standardization through quantification and further investigation to define the characteristics of the different methods will be important for their optimal use. Effective compensation methods will represent a significant advance toward truly quantitative SPECT. Most importantly, the management of cardiac patients should improve as a result of more accurate diagnosis and expanded use of myocardial perfusion SPECT.

ACKNOWLEDGMENTS

The authors would like to express their appreciation to Michel Blais, CNMT, and John Vansant, MD, for their assistance with the figures.

REFERENCES

1. Maddahi J, Berman DS, Kiat H: State of the art perfusion imaging. Clin Cardiol 12:199-222, 1994

2. DePuey EG, Garcia EV: Optimal specificity of thallium-201 SPECT through recognition of imaging artifacts. J Nucl Med 30:441-449, 1989

3. Chua T, Kiat H, Germano G, et al: Gated technetium-99m sestamibi for simultaneous assessment of stress myocardial

perfusion, post-exercise regional ventricular function and myocardial viability. Correlation with echocardiography and rest thallium-201 scintigraphy. J Am Coll Cardiol 23:1107-1114, 1995

4. Garcia EV, Cooke CD, Van Train KF, et al: Technical aspects of myocardial SPECT imaging with technetium-99m sestamibi. Am J Cardiol 66:23E-31E, 1990

5. DePuey EG: How to detect and avoid myocardial perfusion SPECT artifacts. J Nucl Med 35:699-702, 1994

6. Manglos SH, Jaszczak RJ, Floyd CE, et al: Non-isotropic attenuation in SPECT: quantitative tests of effects and compensation techniques. J Nucl Med 28:1584-1591, 1987

7. Manglos SH, Thomas FD, Gagne GM, et al: Phantom study of breast attenuation in myocardial imaging. J Nucl Med 34:992-996, 1993

8. Garcia EV, Van Train K, Maddahi J, et al: Quantification of rotational thallium-201 myocardial tomography. J Nucl Med 26:17-26, 1985

9. Eisner RL, Tamas MJ, Cloninger K, et al: Normal SPECT thallium-201 bull's eye display: gender differences. J Nucl Med 29:1901-1909, 1988

10. DePuey EG, Rozanski AR: Using gated technetium-99m-sestamibi SPECT to characterize fixed defects as infarct or artifact. J Nucl Med 36:952-955, 1995

11. Esquerre JP, Coca FJ, Martinez SJ, et al: Prone decubitus: a solution to inferior wall attenuation in thallium-201 myocardial tomography. J Nucl Med 30:398-401, 1989

12. Bateman TM, Kolobrodov VV, Vasin AP, et al: Extended acquisition for minimizing attenuation artifacts in SPECT cardiac perfusion imaging. J Nucl Med 35:625-627, 1994

13. DiBella EVR, Eisner RL, Barclay AB, et al: Attenuation artifacts in SPECT: effect of wrap-around lung in 180° cardiac studies. J Nucl Med 37:1891-1896, 1996

14. Schwaiger M: Myocardial perfusion imaging with PET. J Nucl Med 35:693-698, 1994

15. Marwick TH, Go RT, MacIntyre WJ, et al: Myocardial perfusion imaging with positron emission tomography and single photon emission computed tomography: frequency and causes of disparate results. Eur Heart J 12:1064-1069, 1991

16. Garcia EV, Cullom SJ, Galt JR: Symbiotic developments in PET and SPECT to quantify and display myocardial tomography. J Nucl Med 32:166-168, 1991

17. Bacharach SI, Buvat I: Attenuation correction in cardiac positron emission tomography and single-photon emission computed tomography. J Nucl Cardiol 2:246-255, 1995

18. Sorenson SA, Phelps ME: Physics in Nuclear Medicine (ed 3). Philadelphia, PA, Saunders, 1987

19. Hubbell JH: Photon cross sections, attenuation coefficients and energy absorption coefficients from 10 keV to 100 GeV. National Bureau of Standards. U.S. Department of Commerce NSRDS-NBS 29, 1969

20. King MA, Tsui BMW, Pan TS: Attenuation compensation for cardiac single-photon emission computed tomographic imaging: part 1. Impact of attenuation and methods of estimating attenuation maps. J Nucl Cardiol 2:513-524, 1995

21. Germano G, Chua T, Kiat H, et al: A quantitative phantom analysis of artifacts due to hepatic activity in technetium-99m myocardial perfusion SPECT studies. J Nucl Med 35:356-359, 1994

22. Nuyts J, DuPont P, Van den Maegdenbergh V, et al: A study of the liver-heart artifact in emission tomography. J Nucl Med 36:133-139, 1995

23. King MA, Xia W, DeVries DJ, et al: A monte carlo investigation of artifacts caused by liver uptake in single-photon emission computed tomography perfusion imaging with Tc-99m-labeled agents. J Nucl Cardiol 3:18-29, 1996

24. Eisner RL, Nowak DJ, Pettigrew R, et al: Fundamentals of 180° reconstruction in SPECT imaging. J Nucl Med 27:1717-1728, 1986

25. Knesaurek K, King MA, Glick SJ, et al: Investigation of causes of geometric distortion in 180° and 360° angular sampling in SPECT. J Nucl Med 30:1666-1675, 1989

26. Budinger TF, Gullberg GT: Three-dimensional reconstruction in nuclear medicine emission imaging. IEEE Trans Nucl Sci NS-21:2-20, 1974

27. Maniawski PJ, Morgan HT, Wackers FJT: Orbit-related variations in spatial resolution as a source of artifactual defects in thallium-201 SPECT. J Nucl Med 32:871-875, 1991

28. Sorenson JA: Quantitative measurement of radioactivity in vivo by whole body counting, in Hine JH, Sorenson JA (eds): Instrumentation in Nuclear Medicine, 2. New York, NY, Academic Press, 1974, pp 311-348

29. Chang LT: A method for attenuation correction in radionuclide computed tomography. IEEE Trans Nucl Sci 1:638-643, 1978

30. Tsui BMW, Gullberg GT, Edgerton ER, et al: Correction of nonuniform attenuation in cardiac SPECT imaging. J Nucl Med 30:497-507, 1989

31. Malko JA, Van Heertum RL, Gullberg GT, et al: SPECT liver imaging using an iterative attenuation correction algorithm and an external flood source. J Nucl Med 27:701-705, 1986

32. Bailey DL, Hutton BF, Walker PJ: Improved SPECT using simultaneous emission and transmission tomography. J Nucl Med 28:844-851, 1987

33. Manglos SH, Bassano DA, Duxbury CE, et al: Attenuation maps for SPECT determined using cone beam transmission computed tomography. IEEE Trans Nucl Sci 37:600-608, 1990

34. Tung CH, Gullberg GT, Zeng GL, et al: Non-uniform attenuation correction using simultaneous transmission and emission converging tomography. IEEE Trans Nucl Sci 39:1134-1143, 1992

35. Morgan HT, Thornton BG, Shand DC, et al: A simultaneous transmission-emission imaging system: description and performance. J Nucl Med 35:193P, 1994

36. Jaszczak RJ, Gilland DR, Hanson MW, et al: Fast transmission CT for determining attenuation maps using a collimated line source and rotatable air-copper-lead attenuators and fan-beam collimation. J Nucl Med 34:1577-1586, 1993

37. Maniawski PJ, Morgan HT, Gullberg GT, et al: Performance evaluation of a transmission reconstruction algorithm with simultaneous transmission-emission SPECT system in a presence of data truncation. Proceedings of the IEEE Nuclear Science Symposium and Medical Imaging Conference 4:1578-1581, 1994

38. Tan P, Bailey DL, Meikle SR, et al: A scanning line source for simultaneous emission and transmission measurements in SPECT. J Nucl Med 34:1752-1760, 1993

39. Hawman EG, Ficaro EP, Hamill JJ, et al: Fan beam collimation with off center focus for simultaneous emission/transmission SPECT in multi-camera SPECT systems. J Nucl Med 35:92P, 1994

40. Chang W, Loncaric S, Huang NB, et al: Asymmetrical-fan transmission CT on SPECT to derive μ-maps for attenuation correction. Phys Med Biol 40:913-928, 1995

41. Cellar A, Sitek A, Stoub E, et al: Multiple line source array for SPECT transmission scans: simulation, phantom, and patient studies. J Nucl Med 39:2183-2189, 1998

42. Hashimoto J, Ogawa K, Kubo A, et al: Application of transmission scan-based attenuation compensation to scatter-corrected thallium-201 myocardial single-photon emission tomographic images. Eur J Nucl Med 25:120-127, 1998

43. Lang TF, Hasegawa BH, Liew SC, et al: Description of a prototype emission-transmission computed tomography imaging system. J Nucl Med 33:1881-1887, 1992

44. Kalki K, Blankespoor SC, Brown JK, et al: Myocardial perfusion imaging with a combined x-ray CT and SPECT system. J Nucl Med 38:1535-1540, 1997

45. Bailey DL: Transmission scanning in emission tomography. Eur J Nucl Med 25:774-787, 1998

46. Welch A, Gullberg GT, Christian PE, et al: A comparison of Gd/Tc versus Tc/T1 simultaneous transmission and emission imaging using both single and triple detector fan-beam SPECT systems. IEEE Trans Nucl Sci 41:2779-2786, 1994

47. Ficaro EP, Rogers WL, Schwaiger M: Comparison of Am-241 and Tc-99m as transmission sources for the attenuation correction of T1-201 SPECT imaging of the heart. J Nucl Med 35:652-663, 1994

48. Ficaro EP, Fessler JA, Ackermann RJ, et al: Simultaneous transmission-emission thallium-201 cardiac SPECT: effect of attenuation correction on myocardial tracer distribution. J Nucl Med 36:921-931, 1995

49. Frey EC, Tsui BMW, Perry JR: Simultaneous acquisition of emission and transmission data for improved thallium-201 cardiac SPECT imaging using a technetium-99m transmission source. J Nucl Med 33:2238-2245, 1992

50. Wang H, Jaszczak RJ, Coleman RE: Attenuation-map determination based on Gd-153 for fast sequential TCT/ECT. J Nucl Med 36:50P, 1995

51. Tsui BMW, Frey EC, Lalush DS, et al: A fast sequential SPECT/TCT data acquisition method for accurate attenuation compensation in cardiac SPECT. J Nucl Med 36:41P, 1995

52. Fleming J: A technique for using CT images in attenuation correction and quantification in SPECT. Nucl Med Commun 10:83-97, 1989

53. McCord ME, Bacharach SL, Bonow RO, et al: Misalignment between PET transmission and emission scans: its effect on myocardial imaging. J Nucl Med 33:1209-1214, 1992

54. McCormick JW, Gilland DR, Jaszczak RJ, et al: The effect of registration errors between transmission and emission scans on a SPECT system designed for fast sequential scanning. J Nucl Med 36:174P, 1995

55. Stone CD, McCormick JW, Gilland DR, et al: Effect of registration errors between transmission and emission scans on a SPECT system using sequential scanning. J Nucl Med 39:365-373, 1998

56. Matsunari I, Boning G, Ziegler SI, et al: Effects of misalignment between transmission and emission scans on attenuation-corrected cardiac SPECT. J Nucl Med 39:411-416, 1998

57. Tung CH, Gullberg GT: A simulation of emission and transmission noise propagation in cardiac SPECT imaging with non-uniform attenuation correction. Med Phys 21:1565-1576, 1994

58. Xu EZ, Mullani NA, Gould KL, et al: A segmented attenuation correction for PET. J Nucl Med 32:161-165, 1990

59. Galt JR, Cullom SJ, Garcia EV: SPECT quantification: a simplified method of scatter and attenuation correction for cardiac imaging. J Nucl Med 33:2232-2237, 1992

60. Pan TS, King MA, Der-Shan L, et al: Estimation of attenuation maps from scatter and photopeak window single photon emission computed tomographic images of technetium 99m-labeled sestamibi. J Nucl Cardiol 4:42-51, 1997

61. Madsen MT, Kirchner PT, Edlin JP, et al: An emission-based method for obtaining attenuation correction data for myocardial SPECT studies. Nucl Med Commun 14:689-695, 1993

62. Wallis JW, Miller TR, Koppel P: Attenuation correction in cardiac SPECT without a transmission measurement. J Nucl Med 36:506-512, 1995

63. Madsen MT, Kirchner PT, Grover-McKay M, et al: Emission-based attenuation correction of myocardial perfusion studies. J Nucl Cardiol 4:477-486, 1997

64. Liang Z: Compensation for attenuation, scatter and detector response in SPECT reconstruction via iterative FBP methods. Med Phys 20:1097-1106, 1993

65. Wallis JW, Miller TR: Rapidly converging iterative reconstruction algorithms in single-photon emission computed tomography. J Nucl Med 34:1793-1800, 1993

66. Maze A, Le Cloirec J, Collorec R, et al: Iterative reconstruction methods for nonuniform attenuation distribution in SPECT. J Nucl Med 34:1204-1209, 1993

67. Faber TL, Lewis MH, Corbett JR, et al: Attenuation correction for SPECT: an evaluation of hybrid approaches. IEEE Trans Med Imaging MI-3:101-107, 1984

68. Ye J, Liang Z, Harrington DP: Quantitative reconstruction for myocardial perfusion SPECT: an efficient approach by depth-dependent deconvolution and matrix rotation. Phys Med Biol 39:1263-1279, 1994

69. Rigo P, Van Boxem PH, Safi JF, et al: Quantitative evaluation of a comprehensive motion, resolution, and attenuation correction program: initial experience. J Nucl Cardiol 5:458-468, 1998

70. Snyder DL, Miller MI, Thomas LJ Jr, et al: Noise and edge artifacts in maximum-likelihood reconstructions for emission tomography. IEEE Trans Med Imaging MI-6:228-238, 1987

71. Cullom SJ, Hendel RC, Liu L, et al: Diagnostic accuracy and image quality of a scatter, attenuation and resolution compensation method Tc-99m-sestamibi cardiac SPECT. J Nucl Med 37:81P, 1996

72. Tsui BMW, Hu GB, Gilland DR: Implementation of simultaneous attenuation and detector response correction in SPECT. IEEE Trans Nucl Sci 35:778-783, 1988

73. Zeng GL, Gullberg GT, Tsui BMW, et al: Three-dimensional iterative reconstruction with attenuation and geometric point response correction. IEEE Trans Nucl Sci 38:693-702, 1991

74. Tsui BMW, Frey EC, Zhao X, et al: The importance and implementation of accurate 3D methods for quantitative SPECT. Phys Med Biol 39:509-530, 1994

75. Shepp LA, Vardi Y: Maximum likelihood reconstruction for emission tomography. IEEE Trans Med Imag 1:113-121, 1982

76. Lalush DS, Tsui BMW: Improving the convergence of iterative filtered backprojection algorithms. Med Phys 21:1283-1285, 1994

77. Hudson HM, Larkin RS: Accelerated image reconstruction using ordered sunsets of projection data. IEEE Trans Med Imaging MI-13:601-609, 1994

78. Floyd CE, Jaszczak RJ, Coleman RE: Scatter detection in SPECT imaging: dependence on source depth, energy, and energy window. Phys Med Biol 33:1075-1081, 1988

79. Frey EC, Tsui BMW: Modeling the scatter response function in inhomogenous scattering media for SPECT. IEEE Trans Nucl Sci 41:1585-1593, 1994

80. Jaszczak RJ, Greer KL, Floyd CE Jr, et al: Improved SPECT quantification using compensation for scattered photons. J Nucl Med 25:893-900, 1984

81. Ichihara T, Ogawa K, Motomura N, et al: Compton scatter compensation using the triple-energy window method for single- and dual-isotope SPECT. J Nucl Med 34:2216-2221, 1993

82. Gagnon D, Todd-Pokropek A, Laperiere L: Analysis of scatter, quantum noise, and camera nonuniformity in nuclear medicine studies using holospectric imaging. J Nucl Med 30:807, 1989 (abstr)

83. Koral KF, Wang X, Rogers WL, et al: SPECT Compton scattering correction by analysis of energy spectra. J Nucl Med 29:195-202, 1988

84. Buvat I, Rodriguez-Villafuerte M, Todd-Pokropek A, et al: Comparative assessment of nine scatter correction methods based on spectral analysis using Monte Carlo simulations. J Nucl Med 36:1476-1488, 1995

85. Floyd CE, Jaszczak RJ, Greer KL, et al: Deconvolution of Compton scatter in SPECT. J Nucl Med 26:403-408, 1985

86. King MA, Coleman M, Penney BC, et al: Activity quantitation in SPECT: a study of prereconstruction Metz filtering and the use of a scatter degradation factor. Med Phys 18:184-189, 1991

87. Frey EC, Tsui BMW: A practical method for incorporating scatter in a projector backprojector for accurate scatter compensation in SPECT. IEEE Trans Nucl Sci NS-40:1007-1016, 1993

88. Frey EC, Ju ZW, Tsui BMW: A fast projector/backprojector pair modeling the asymmetric, spatially varying scatter response function in SPECT imaging. IEEE Trans Nucl Sci NS-40:1192-1197, 1993

89. Beekman F, Eijkman E, Viergever M, et al: Object shape dependent PSF model for SPECT imaging. IEEE Trans Nucl Sci NS-40:31-39, 1993

90. Mukai T, Links JM, Douglass KH, et al: Scatter correction in SPECT using non-uniform attenuation data. Phys Med Biol 33:1129-1140, 1988

91. Meikle SR, Hutton BF, Bailey DL: A transmission-dependent method for scatter correction in SPECT. J Nucl Med 35:360-367, 1994

92. Welch A, Gullberg GT, Christian PE, et al: A transmission-map-based scatter correction technique for SPECT in inhomogeneous media. Med Phys 22:1627-1635, 1995

93. Beekman FJ, den Harder JM, Viergever MA, et al: SPECT modeling in non-uniform attenuating objects. Phys Med Biol 42:1133-1142, 1997

94. Kadrmas DJ, Frey EC, Karimi SS, et al: Fast implementations of reconstruction-based scatter compensation in fully 3D SPECT image reconstruction. Phys Med Biol 43:857-873, 1998

95. Soares EJ, Byrne CL, Glick SJ, et al: Implementation and evaluation of an analytical solution to the photon attenuation and nonstationary resolution reconstruction problem in SPECT. IEEE Trans Nucl Sci NS-40:1231-1237, 1993

96. Pan X, Metz CE, Chen CT: Non-iterative methods and their noise characteristics in 2D SPECT image reconstruction. IEEE Trans Nucl Sci 44:1388-1397, 1997

97. Lewitt RM, Edholm PR, Xia W: Fourier method for correction of depth-dependent collimator blurring. SPIE 1092: 232-243, 1989

98. Glick SJ, Penney BC, King MA, et al: Noniterative compensation for the distance-dependent detector response and photon attenuation in SPECT imaging. IEEE Trans Med Imaging 7:135-148, 1988

99. Younes RB, Mas J, Pousse A, et al: Introducing simultaneous spatial resolution and attenuation correction after scatter removal in SPECT imaging. Nucl Med Commun 12:1031-1043, 1991

100. Ficaro EP, Fessler JA, Shreve PD, et al: Simultaneous transmission/emission myocardial perfusion tomography. Diagnostic accuracy of attenuation-corrected ^{99m}Tc-sestamibi single-photon emission computed tomography. Circulation 93:463-473, 1996

101. LaCroix KJ, Tsui BMW, Hasegawa BH: A comparison of 180° and 360° acquisition for attenuation-compensated thallium-201 SPECT images. J Nucl Med 39:562-574, 1998

102. Heller EN, DeMan P, Liu YH, et al: Extracardiac activity complicates quantitative cardiac SPECT imaging using a simultaneous transmission-emission approach. J Nucl Med 38:1882-1890, 1997

103. Tsui BMW, Frey EC, LaCroix KJ, et al: Quantitative myocardial perfusion SPECT. J Nucl Cardiol 5:507-522, 1998

104. Liu L, Cullom SJ, White ML: A modified wiener filter method for nonstationary resolution recovery with scatter and iterative attenuation correction for cardiac SPECT. J Nucl Med 37:210P, 1996

105. Berman D, Kiat H, Friedman JD, et al: Separate acquisition rest thallium-201/stress technetium-99m sestamibi dual-isotope myocardial perfusion single-photon emission computed tomography: a clinical validation study. J Am Coll Cardiol 22:1455-1464, 1993

106. Maddahi J, Berman DS: Reverse redistribution of T1-201. J Nucl Med 36:1019-1021, 1995

107. Kiat H, Friedman J, Van Train K, et al: Simultaneous rest T1-201/stress Tc-99m sestamibi dual isotope myocardial perfusion SPECT: a pilot study. J Nucl Med 32:1006, 1991

108. Weinstein H, King MA, Reinhardt CP, et al: A method of simultaneous dual-radionuclide cardiac imaging with technetium 99m and thallium 201. 1: analysis of interradionuclide crossover and validation in phantoms. J Nucl Cardiol 1:39-51, 1994

109. Martin W, Delbeke D, Patton JA, et al: ^{18}FDG-SPECT: correlation with ^{18}FDG-PET. J Nucl Med 36:988-995, 1995

110. Sandler MP, Videlefsky S, Delbeke D, et al: Evaluation of myocardial ischemia using a rest metabolism/stress perfusion protocol with ^{18}FDG/^{99m}Tc-MIBI and dual isotope simultaneous acquisition SPECT. J Am Coll Cardiol 26:870-878, 1995

111. King MA, Tsui BMW, Pan TS, et al: Attenuation compensation for cardiac single-photon emission computer tomographic imaging: part 2. Attenuation compensation algorithms. J Nucl Cardiol 3:55-63, 1996

112. Prvulovich EM, Lonn AHR, Bomanji JB, et al: Effect of attenuation correction on myocardial thallium-201 distribution

inpatients with a low-likelihood of coronary artery disease. Eur J Nucl Med 24:266-275, 1997

113. Kluge R, Sattler B, Seese A, et al: Attenuation correction by simultaneous emission-transmission myocardial single-photon emission tomography using a technetium-99m-labelled radiotracer: impact on diagnostic accuracy. Eur J Nucl Med 24:1107-1114, 1997

114. Chouraqui P, Livschitz S, Sharir T, et al: Evaluation of an attenuation correction method for thallium-201 myocardial perfusion tomographic imaging of patients with low-likelihood of coronary artery disease. J Nucl Cardiol 5:369-377, 1998

115. Gallowitsch HJ, Syokora J, Mikosch P, et al: Attenuation corrected thallium-201 single-photon emission tomography using a gadolinium-153 moving line source: clinical value and the impact of attenuation correction on the extent and severity of perfusion abnormalities. Eur J Nucl Med 25:220-228, 1998

116. Matsunari I, Boning G, Ziegler SI, et al: Attenuation corrected thallium-201/stress technetium 99m sestamibi myocardial SPECT in normals. J Nucl Cardiol 5:48-55, 1998

117. Hendel RC, Berman DS, Cullom SJ, et al: A Multicenter trial to evaluate the efficacy of correction for photon attenuation and scatter in SPECT myocardial perfusion imaging. Circulation (in press)

118. Matsunari I, Boning G, Ziegler SI, et al: Attenuation-corrected 99mTc-tetrofosmin single-photon emission computer tomography in the detection of viable myocardium: comparison with positron emission tomography using 18F-fluorodeoxyglucose. J Am Coll Cardiol 32:927-935, 1998

Technetium-99m Labeled Myocardial Perfusion Imaging Agents

Diwakar Jain

^{99m}Tc labeled myocardial perfusion tracers have significantly advanced the field of noninvasive diagnostic evaluation and risk stratification of patients with known or suspected coronary artery disease by providing comprehensive information about myocardial perfusion and function from a single study. Of various currently available invasive and noninvasive test modalities, myocardial perfusion imaging provides the most powerful prognostic information that is incremental to the information obtained from invasive evaluation. Future research should focus on the development of perfusion tracers that linearly track myocardial blood flow over a wide range and have minimal splanchnic uptake. Availability of an effective attenuation and scatter correction program would further eliminate some of the current limitations of this technique.

MYOCARDIAL PERFUSION imaging with radionuclides is an integral component of the clinical evaluation of patients with known or suspected coronary artery disease in current clinical practice.[1] Initial attempts at myocardial perfusion imaging with potassium-43 (^{43}K) in the early 1970s were met with a number of technical limitations, but nevertheless provided a conceptual framework for future developments in this field.[2,3] The introduction of thallium-201 (^{201}Tl) in the mid 1970s was a turning point in the widespread clinical use of myocardial perfusion imaging.[4,5] Myocardial perfusion imaging with ^{201}Tl had a profound impact on the diagnostic evaluation, risk stratification, and therapeutic decision making in patients with coronary artery disease over the next 2 decades. However, ^{201}Tl has several important limitations, and the search for better myocardial perfusion imaging agents started soon after its clinical introduction.[6,7] The vulnerability of ^{201}Tl to attenuation artifacts caused by the relatively lower energy of emitted photons and lower count rates caused by the dose constraints may result in poor or suboptimal images in a significant proportion of studies. Because of the dynamic nature of its kinetics, ie, redistribution, image acquisition should start soon after injection of ^{201}Tl. Therefore, ^{201}Tl is not suitable for situations in which immediate imaging may not be possible, such as in patients with acute myocardial infarction or in the setting of chest pain centers. Compared with ^{201}Tl, technetium-99m (^{99m}Tc) yields relatively higher energy photons and can be used in much higher doses. ^{99m}Tc can be incorporated into a wide range of organic as well as inorganic molecules, which can be used to study various anatomic, physiological, and biochemical phenomena in the body. Therefore, ^{99m}Tc was the radioisotope of choice for the development of the next generation of myocardial perfusion imaging agents. Another major advantage of ^{99m}Tc labeled agents over ^{201}Tl is that simultaneous assessment of myocardial perfusion and function can be obtained from a single study.[8] ^{99m}Tc sestamibi has been in clinical use for over 8 years and ^{99m}Tc tetrofosmin for nearly 3 years in the United States. A number of newer ^{99m}Tc labeled agents that are under development may be available clinically in the future.

HISTORICAL DEVELOPMENT OF ^{99m}Tc PERFUSION TRACERS

The observation of Deutsch et al[6,7,9-11] of cardiac uptake of lipophilic ^{99m}Tc cations (^{99m}Tc[III] compounds with $^{+}1$ charge) stimulated interest in the development of ^{99m}Tc myocardial perfusion imaging agents. As a class, these agents can be schematically represented as $(^{99m}\text{Tc[ligand]}_2 \times {}_2)^{+}$. $(^{99m}\text{Tc[DMPE]}_2\text{Cl}_2)^{+}$ (DMPE = 1,2 bis-dimethyl phosphinoethane) was used initially in human studies.[10] Although these early agents yielded images of acceptable quality in animal models, the image quality was very poor in humans because of excessive liver and lung uptake and poor myocardial uptake. Furthermore, there was rapid washout of the myocardial activity. It was subsequently realized that significant differences exist among ^{99m}Tc cationic agents depending on their lipophilicity, vulnerability to in vivo reduction to neutral compounds, and affinity for binding to various circulating proteins.[11] These factors are responsible

From the Section of Cardiovascular Medicine, Yale University School of Medicine, New Haven, CT.

Address reprint requests to Diwakar Jain, MD, 3 FMP Section of Cardiovascular Medicine, Yale University School of Medicine, 333 Cedar Street, New Haven, CT 06520.

0001-2998/99/2903-0003$10.00/0

for marked qualitative differences among different ^{99m}Tc cationic perfusion agents. Furthermore, there can be significant interspecies differences in the in vivo binding of various agents to plasma proteins. It is now known that poor quality of (^{99m}Tc $[DMPE]_2Cl_2)^+$ for myocardial perfusion imaging in human studies is attributable to the fact that this is not a stable in vivo cationic compound. In humans, this is rapidly reduced to a neutral Tc(II) compound ($[^{99m}Tc\ (DMPE)_2Cl_2]^+ + e^- = [^{99m}Tc\ (DMPE)_2Cl_2]^0$).[11] This neutral species washes out of the myocardium and accumulates in the liver and several other organs. A wide range of ^{99m}Tc core agents, isonitriles, bis-arenes, and hexakis-phosphites, were tested for their potential for myocardial perfusion imaging. Although many of these agents showed good myocardial uptake in animal models, they failed to achieve adequate clearance from nontarget tissues, particularly blood and liver and sometimes lungs, resulting in poor image quality in humans. Among the initial compounds tested, only hexakis-isonitrile compounds showed promise for use in myocardial perfusion imaging in humans.[12,13] ^{99m}Tc sestamibi belongs to this group of agents and is currently in extensive clinical use.[8,14-17]

Research on diphosphine ligands yielded compounds with heteroatomic function instead of simple alkyl or aryl groups. This overcame some of the problems encountered with earlier diphosphine ligands. Several new ^{99m}Tc diphosphine compounds were developed with characteristics suitable for myocardial perfusion imaging in humans.[18-24] Among these agents, tetrofosmin was found to be the most suitable. Another series of mixed ligands called Q complexes was developed. Q3 and Q12 have characteristics suitable for myocardial perfusion imaging but are not approved for clinical use.[25-31]

Apart from the cationic agents mentioned earlier some neutral agents also have been found to have potential for myocardial perfusion imaging.[32-38] ^{99m}Tc labeled myocardial perfusion imaging agents can be divided into two broad categories: lipophilic cationic agents, consisting of (1) isonitriles (sestamibi), (2) diphosphines (tetrofosmin), and (3) Q complexes; and lipophilic neutral agents, consisting of (1) teboroxime and (2) N-NOET.

SESTAMIBI

The isonitrile complexes have a general formula of $(Tc[CNR6])^+$. Of the various isonitrile derivatives tested, methoxyisobutyl isonitrile (sestamibi, Du Pont Pharmaceuticals, North Billerica, MA) has the most favorable characteristics for myocardial perfusion imaging.[12-14] After intravenous injection, ^{99m}Tc sestamibi rapidly clears from the blood pool.[14] The peak activity is seen at 1 minute after injection, and <5% activity is seen 5 minutes postinjection. Myocardial uptake is 1% of the injected dose after rest injection and 1.4% after exercise injection at 1 hour postinjection.[14] Sestamibi is formulated in a kit preparation, and radiolabeling is performed by boiling with ^{99m}Tc pertechnetate. ^{99m}Tc sestamibi is mainly excreted by the hepatobiliary system, with a small renal excretion.[14] The upper large intestine, small intestine, and gall bladder get the highest radiation dose. With a 30-mCi injection, upper large intestines receive 4.6 and 4.7 rads respectively with exercise and rest injection. With a dose of 30 mCi, the whole-body radiation dose is 0.49 rads in exercise studies and 0.46 rad for rest studies.[14]

TETROFOSMIN

Tetrofosmin (1,2-bis[bis(2-ethoxyethyl)phosphino]ethane), (Nycomed Amersham, Princeton, NJ) is formulated in a freeze-dried kit that can be labeled with ^{99m}Tc at room temperature to give a lipophilic dioxomonocation complex ($[^{99m}Tc(tetrofosmin)_2O_2]^+$).[20] The labeled preparation is stable for more than 8 hours.[20] ^{99m}Tc tetrofosmin has rapid blood clearance with less than 5% blood pool activity at 10 minutes postinjection. Figure 1 shows blood clearance curves of ^{99m}Tc tetrofosmin after injection at rest and during exercise. The heart is well visualized in 5-minute images with good retention. Clearance from the liver is rapid. Approximately 1.2% of the administered dose is taken up by the myocardium in resting as well as in exercise studies. The liver uptake decreases rapidly from 7.5% ± 1.7% at 5 minutes to 2.1% ± 1.0% at 1 hour after rest injection. Gall bladder activity increases rapidly in the first 2 hours, indicating rapid hepatic clearance. ^{99m}Tc tetrofosmin has a relatively low hepatic, gastrointestinal, splenic, and lung uptake after stress and rest injections. Moreover, the clearance from these organs is rapid.[23] This allows images to be acquired soon after radiotracer injection. Stress images can be acquired 5 to 10 minutes after the tracer injection, whereas rest images can be obtained 30 minutes after injection. A convenient 1-day stress-rest ^{99m}Tc

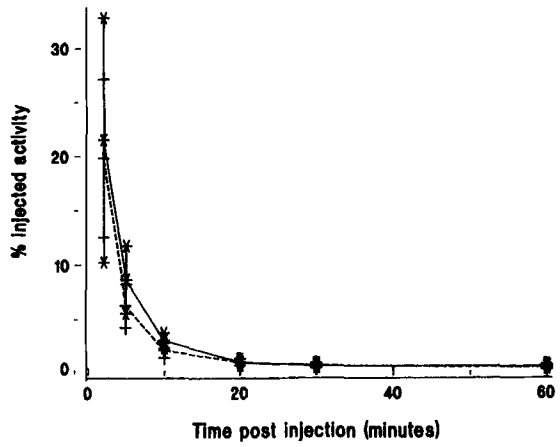

Fig 1. Clearance of ^{99m}Tc tetrofosmin from blood at rest (×—×) and exercise (+-----+) in 12 healthy subjects (mean ± SD). Data presented as percent injected activity in estimated total blood volume. Blood activity at 5 and 10 minutes postinjection was lower in the exercise study. ($P < .01$) (Reprinted with permission.[21])

tetrofosmin imaging protocol similar or even shorter in duration compared with conventional ^{201}Tl imaging is feasible.

^{99m}Tc tetrofosmin shows approximate equal clearance by both renal and fecal routes.[21] After rest injection, 72% ± 6% of the administered activity is excreted from the body by 48 hours, and after exercise injection, 67% ± 6% of administered activity is excreted by 48 hours. Excretory organs (gall bladder, small and large intestines, urinary bladder, and kidneys) receive the highest radiation dose.[21] The estimated whole-body dose after 30-mCi ^{99m}Tc tetrofosmin administration (with bladder voiding at 3.5 hours) is 1.0 rads in the rest studies and 0.8 rads after exercise. The gall bladder receives the highest individual organ dose (3.7 to 5.4 rads).

Q COMPOUNDS

Q complexes are a series of mixed cationic ligands.[25-31] These complexes contain monophosphine ligands complexed to a distinct Schiff base ligand. Two of these agents, Q3 and Q12 (Mallinckrodt Medical, St Louis, MO), have undergone clinical evaluation for myocardial perfusion imaging.[25,28-31] The monophosphine ligands of Q3 and Q12 are similar (tris[3-methoxy-1-propyl]phosphine), but the Schiff base ligands are different: N,N′-ethylenebis(acetylacetoneimine) for Q3 and 1,2-bis(dihydro-2,2,5,5-tetramethyl-3[2H]furanoato-4-methyleneimino)ethane for Q12.[29] Q12 has been formulated into a kit formulation, but no kit formulation has been developed for Q3. Each Q12 vial contains an admixture of the Schiff-based and the monophosphine ligands. Radiolabeling requires boiling in a water bath for 15 minutes with sodium pertechnetate. Q12 is more suitable for myocardial perfusion imaging because of lower liver activity and faster liver clearance and has been used for further clinical evaluation. Recently, some newer Q compounds (Q63 and Q64) have been developed that have more suitable characteristics for myocardial perfusion imaging (personal communication, Myron C. Gerson, MD, November, 1998). However, this new generation of Q compounds is still in an early stage of development. Q12 has rapid blood clearance with an initial half life of 1.8 ± 0.1 minutes.[26] Less than 5% activity is present in blood 20 minutes after its injection at rest. Q12 is cleared from the body by renal as well as hepatobiliary routes. After initial uptake, myocardial activity of Q12 remains stable with no evidence of redistribution over a period of the next 4 to 5 hours. The maximum first-pass extraction (E_{max}) of Q12 is 0.29 ± 0.01.[26]

Exercise-rest ^{99m}Tc Q12 imaging compares favorably with exercise-redistribution ^{201}Tl imaging with high concordance for the presence or absence of abnormalities and for the diagnostic categories of normal, ischemia, scar, or scar and ischemia.[30] The FDA has asked for additional clinical data before ^{99m}Tc Q12 can be granted approval for clinical use. At this point it is not clear whether the manufacturer of ^{99m}Tc Q12 is planning to submit these required data.

^{99m}Tc-TEBOROXIME

^{99m}Tc teboroxime is a neutral lipophilic agent.[32-36] The exact mechanism of its myocardial uptake is not known. This may be because of nonspecific loose binding to the cell membrane caused by its lipophilicity. This agent has the highest first-pass myocardial extraction of all myocardial perfusion tracers and has a linear relationship between myocardial uptake and myocardial blood flow over a very wide range (0 to 4.5 mL/min/g).[36] Despite this, the overall clinical experience has been rather disappointing because of its very short myocardial residence time. Two thirds of myocardial activity washes out within 3.6 ± 0.6 min.[36] Myocardial imaging should be finished within 5 to 6 minutes of its injection, which is difficult in most clinical

studies. This agent shows differential washout from the normal and ischemic myocardium.[33] Rapid dynamic imaging has been proposed to differentiate normal from ischemic myocardium from a single stress study.[33] Teboroxime also binds to red blood cells, which may partly account for rapid washout from the myocardium.[34] This agent is currently not in clinical use.

^{99m}Tc-N-NOET

^{99m}Tc N-Noet (CISBio International, France) is a member of a class of neutral myocardial perfusion imaging agents, ^{99m}Tc nitrido dithiocarbamates, which are characterized by the presence of the ^{99m}Tc N triple-bond group (Tc N)2+.[37] Chemically, this agent is called bis(N-ethoxy, N-ethyl dithiocarbamato) nitrido ^{99m}Tc(V). This lipophilic compound is prepared through a two-step reaction; the first step involves boiling ^{99m}Tc pertechnetate with an acidic solution containing an admixture of trisodium tri(m-sulfophenyl) phosphine and S-methyl N-methyl dithiocarbazoate for 20 minutes.[38] This intermediate compound bearing the $(Tc \equiv N)^{2+}$ core is then mixed with dithiocarbamate ligand to obtain neutral ^{99m}Tc N-Noet. The radiochemical purity is checked by thin-layer chromatography. After the initial injection of ^{99m}Tc N-Noet, its clearance from the blood pool is significantly slower compared with the cationic agents (Fig 2). At 30 minutes after injection, blood activity decreased to 20% of the peak activity at 2 minutes, but thereafter it decreased very slowly with 19% activity at 90% and 14% at 240 minutes.[38] These levels are much higher that those observed with ^{201}Tl and cationic ^{99m}Tc labeled myocardial perfusion imaging agents. ^{99m}Tc N-Noet also showed a rapid washout. Relative to the myocardial uptake at 5 minutes postinjection, cardiac uptake decreased by 44% after 60 minutes in myocardial segments with normal perfusion.[38] In segments with decreased myocardial perfusion and decreased uptake initially, there is an increase in activity over time. However, in the presence of continued low flow, this process is much slower, whereas if flow is normalized after the initial uptake, redistribution is almost complete within 90 minutes.[38,39]

Despite very interesting data from the animal studies, only limited human studies have evaluated the role of ^{99m}Tc N-Noet imaging for the detection of coronary artery disease.[40] This agent is not yet approved for routine clinical use. Clearly, there is a need for more human studies.

Table 1 summarizes the important characteristics of the major myocardial imaging agents. However, none of these radiotracers meet the requirements of an ideal perfusion tracer. An ideal perfusion tracer should have a high first-pass extraction with stable myocardial retention, which linearly tracks myocardial blood flow over a wide range. Hepatic and gastrointestinal uptake should be minimal with exercise as well as with pharmacological stress and rest studies. Tracers that redistribute, but in a predictable and reliable manner, and allow a clinically viable imaging protocol also potentially are useful. Future research should focus on the development of perfusion tracers to meet these requirements.

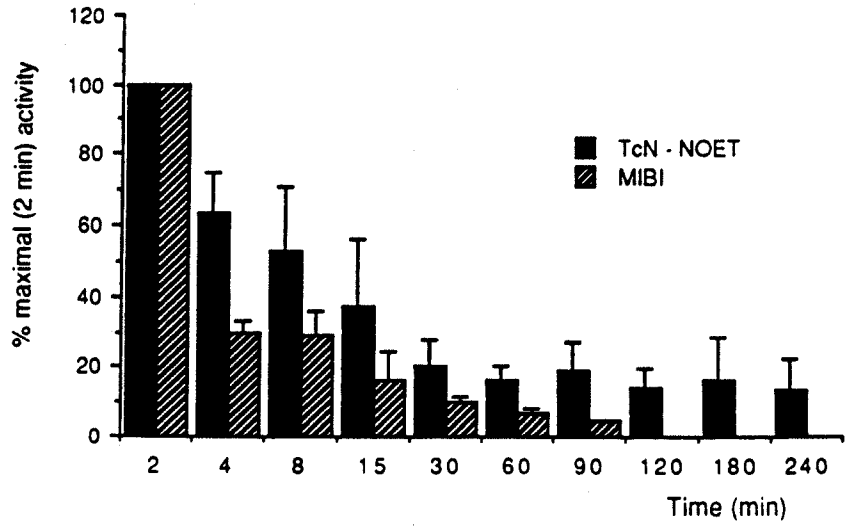

Fig 2. Blood activity of ^{99m}Tc N-Noet and ^{99m}Tc sestamibi from blood expressed as percent (mean ± SD) of the activity at 2 minutes postinjection in an experimental canine preparation. (Reprinted with permission.[38])

Table 1. Properties of Different ^{99m}Tc Labeled Myocardial Perfusion Imaging Agents

	Sestamibi	Tetrofosmin	Q12	Teboroxime	N-Noet
Chemical structure	Cationic	Cationic	Cationic	Neutral	Neutral
Kit formulation	Available	Available	Available	Available	Two-step kit
Labeling	Boiling	Room temperature	Boiling	Boiling	Boiling
Redistribution	Minimal	None	None	Significant	Significant
FP extraction (%)	0.39 ± 0.09	0.24	0.26 ± 0.01	0.88	0.76 ± 0.04
Myocardial uptake with injection at rest (%)	1.0	1.2	1.2-2.2	3-4*	4
Excretion	Mainly hepatobiliary	Renal and hepatobiliary	Hepatobiliary and renal	Hepatobiliary	Hepatobiliary
Liver uptake	+++	++	++	++++	Unknown
Heart-to-liver ratios 15 to 20 min postinjection (exercise studies)	0.65	1.2 ± 0.3	0.95 ± 0.15	Negligible	Unknown
Heart-to-liver ratios 15 to 20 min postinjection (rest studies)	0.5 ± 0.1	0.78 ± 0.14	0.75	Negligible	Unknown

Abbreviation: FP, first pass.

*Soon after the tracer injection, washes out within minutes.

MECHANISM OF MYOCARDIAL UPTAKE OF ^{99m}Tc PERFUSION IMAGING AGENTS

Myocardial ^{201}Tl uptake occurs through ATPase dependent Na^+/K^+ channels. The myocardial uptake mechanism of ^{99m}Tc labeled agents is quite different and differs for cationic and neutral agents. The cellular uptake of all cationic ^{99m}Tc perfusion agents is similar and is independent of Na^+/K^+ channels. This is mediated by a nonspecific charge-dependent transfer of lipophilic cations across the sarcolemma. Unlike ^{201}Tl, cellular uptake of these cationic agents is not affected by cation channel inhibitors such as ouabain, amiloride, bumetanide, nifedipine, or by acidosis.[41-45] However, the uptake of these agents is inhibited by the metabolic inhibitors, iodoacetic acid and 2,4-dinitrophenol, which interfere with potential across the sarcolemma.[41-44] The uptake of cationic agents is dependent on their lipophilicity. However, the requirement of cellular metabolic activity rules out lipophilicity alone as the mechanism for cellular uptake of these tracers.

In isolated adult rat ventricular myocyte preparations, uptake of ^{99m}Tc cationic agents is found to be a metabolism-dependent process that does not involve cation channel transport and is caused by electrochemical potential-driven diffusion of the lipophilic cations across the sarcolemmal and mitochondrial membranes.[42,43,45] Thus, cationic technetium agents differ from ^{201}Tl in that they do not act as potassium analogs, but do require metabolic integrity for uptake by the myocytes.

Inside the myocytes, the mitochondria are the predominant site of localization of these cationic agents, although there is a small difference in the mitochondria-associated fraction of various ^{99m}Tc cationic perfusion tracers.[42,43,46] Studies using isolated mitochondrial preparations show rapid mitochondrial uptake of ^{99m}Tc cationic agents in the presence of oxidative substrate.[44] Addition of the mitochondrial uncoupler 2,4-dinitrophenol causes release of most of the activity. Figure 3 shows the kinetic effects of oxidative mitochondrial coupling (by addition of succinate) and oxidative uncoupling (by addition of 2,4 dinitrophenol) on ^{99m}Tc tetrofosmin uptake by the isolated mitochondria. Mitochondrial localization of ^{99m}Tc cationic agents appears to be related to a high negative charge (−165 mV) across the mitochondrial membrane compared with other intracellular organelles. Mitochondrial uptake of ^{99m}Tc cationic agents requires integrity of their oxidative metabolism. These data support a theoretical role for ^{99m}Tc cationic agents as a means of assessing myocardial viability, as described in a later section of this article.

Washout of activity from myocytes loaded with ^{99m}Tc cationic agents has been studied by transferring these cells to a ^{99m}Tc free medium. Washout is found to be much slower than uptake and is biexponential with two compartments (approximately 20% and 80%). The half lives of these compartments are 8.5 and 246 minutes for ^{99m}Tc tetrofosmin and 6 and 90 minutes for ^{99m}Tc sestamibi.[41,43] This explains the apparent lack of or minimal redistribution with ^{99m}Tc cationic agents in human studies.

^{99m}Tc labeled cationic perfusion tracers are also taken up by various tumors in in-vivo or in in-vitro cell cultures.[47-49] The mechanism and kinetics of myocellular uptake and tumor cell uptake are quite

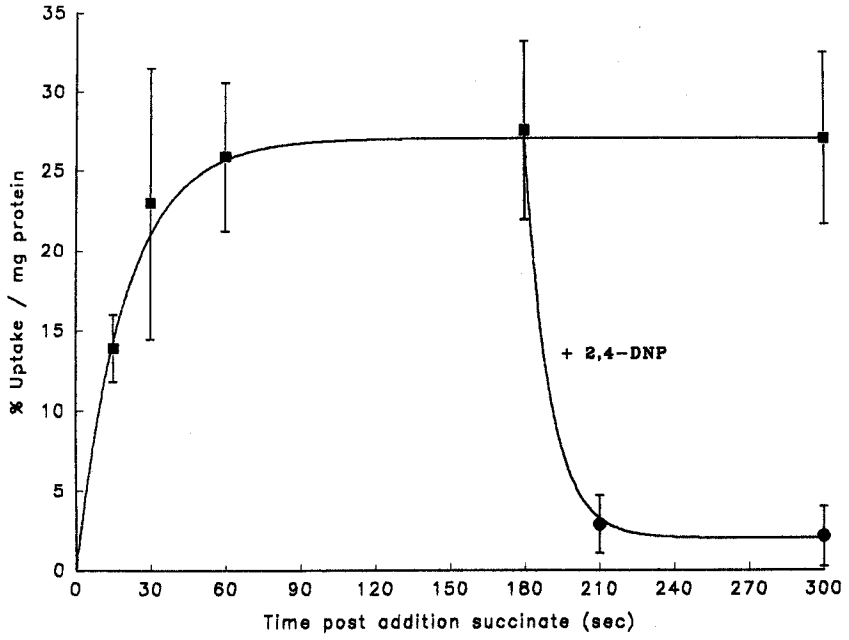

Fig 3. Kinetics of ^{99m}Tc tetrofosmin uptake by isolated mitochondria from rat heart suspended in a medium containing ^{99m}Tc tetrofosmin. Mitochondrial binding of ^{99m}Tc tetrofosmin was assessed from aliquots of mitochondrial suspension, drawn at various time points. The addition of succinate, an energy source for the mitochondria, resulted in immediate uptake of ^{99m}Tc tetrofosmin by the mitochondria, and the addition of dinitrophenol, an uncoupler of mitochondrial oxidative phosphorylation, resulted in immediate release of ^{99m}Tc tetrofosmin from the mitochondria. (Reprinted with permission.[43])

similar, and this fact has been used for studying the myocardial uptake mechanism using tumor cell culture preparations.[47-49] These tracers are also finding application for tumor imaging, and have been successfully used for breast tumor imaging.[50]

The myocardial uptake of neutral compounds is attributable to their lipophilicity, and the myocyte membrane is the predominant site of their localization with no specific localization in the cytosolic and mitochondrial components.[51,52]

RELATIONSHIP BETWEEN MYOCARDIAL BLOOD FLOW AND RADIOTRACER UPTAKE

The first-pass myocardial extraction fraction and the myocardial blood flow–tracer extraction relationship over a wide range of myocardial perfusion are the two important characteristics of myocardial perfusion tracers. An ideal tracer should have a high (close to 1.0) first-pass extraction with a linear relationship between myocardial tracer accumulation and myocardial perfusion over the physiological range of myocardial blood flows. First-pass extraction is studied in experimental animal models by simultaneous injection of known activities of the myocardial perfusion tracer and a nonextractable radiotracer, such as ^{131}I or ^{111}In labeled albumin, in the left atrium with continuous coronary sinus blood sampling. The ratio of the two agents in coronary sinus blood provides an index of first-pass extraction. None of the perfusion tracers has a first-pass extraction fraction of 1.0. ^{201}Tl has a first-pass extraction of 0.73, whereas all ^{99m}Tc cationic agents have significantly lower first-pass extraction fraction (0.24 to 0.39) (Table 1). In contrast, the lipophilic neutral ^{99m}Tc labeled agents have significantly higher first-pass extraction (0.76 for ^{99m}Tc N-Noet).

The relationship between myocardial flow and radiotracer accumulation has been studied in a canine model of coronary artery occlusion and pharmacological hyperemia and by simultaneous left atrial injection of the radiotracer and radiolabeled microspheres, which are completely trapped in the capillaries.[46,53-55] With all cationic ^{99m}Tc labeled agents and ^{201}Tl, a linear correlation between microsphere-determined regional blood flow and radiotracer uptake is seen only over a relatively narrow blood flow range. Overestimation of the myocardial blood flow occurs in segments with very low flows, whereas underestimation of the flow occurs in segments with very high flow rates (roll-off). The threshold at which roll-off occurs varies among different tracers. ^{99m}Tc labeled neutral agents show a linear relationship over a relatively wide range. ^{201}Tl shows a linear relation over a range of 0.3 to 2.5 mL/min/g. As a class, ^{99m}Tc cationic agents have the narrowest range over which this liner relationship is observed (0.3 to 2.0 mL/min/g). Among different cationic agents, there are only minor differences for threshold at which

roll off occurs.[53,54] Preliminary studies indicate that the second generation of Q compounds (Q63, Q64) may have a linear relationship between flow and tracer uptake over a wider range (personal communication, Myron Gerson, MD, November, 1998).

Unlike the cationic agents, ^{99m}Tc N-Noet and ^{99m}Tc teboroxime do not show a roll-off even at high flow rates (>3.0 mL/min/g).[33,38] This is a potentially attractive feature of ^{99m}Tc Noet. However, in studies involving a segmental comparison between the activities of the perfusion tracer and simultaneously injected microspheres, differential washout in the interval between the radiotracer injection and the time when animals are killed may result in an apparent but small underestimation of myocardial flow in segments with high flow rates.[38]

Early roll-off in hyperemic segments can potentially result in a significant underestimation of myocardial perfusion abnormalities with lower grade of coronary obstruction, particularly in conjunction with the use of pharmacological stress imaging. Figure 4 gives a schematic representation of the relationship between myocardial flow and uptake of various perfusion tracers and the mechanism of potential underestimation of flow heterogeneity at high flow rates because of early roll-off. Comparing the intensity and extent of perfusion abnormalities with simultaneously administered ^{201}Tl and ^{99m}Tc tetrofosmin or ^{99m}Tc sestamibi, with the microsphere-determined myocardial blood flow in a canine model of varying degrees of coronary artery occlusion and adenosine induced hyperemia, both ^{201}Tl and ^{99m}Tc agents underestimated the flow heterogeneity compared with the microspheres.[46,55] However, the extent of underestimation was significantly more with ^{99m}Tc agents compared with ^{201}Tl. This difference was seen with critical as well as mild stenosis. On ex vivo imaging of the heart slices, ^{99m}Tc defects were significantly smaller compared with ^{201}Tl defects. When single photon emission computed tomography (SPECT) images with ^{201}Tl and ^{99m}Tc tetrofosmin during pharmacological stress in patients with coronary artery disease were compared, the differences between the extent and intensity of reversible perfusion abnormalities were less impressive.[56] It is likely, that the contribution of attenuation and scatter observed in clinical studies decreases the potential differences because of the different first-pass extraction characteristics of ^{201}Tl and ^{99m}Tc cationic agents.

REDISTRIBUTION OF ^{99m}Tc-LABELED AGENTS

The mechanisms of redistribution or differential washout of ^{201}Tl and ^{99m}Tc labeled cationic agents and ^{99m}Tc neutral agents are quite different because of the different sites of intracellular localization and mechanism of release and uptake from the myocytes. ^{99m}Tc sestamibi shows some redistribution in animal studies, which at best is minimal and clinically unimportant in human studies.[57,58] No redistribution has been observed with ^{99m}Tc tetrofosmin and ^{99m}Tc Q12.[59] Myocardial washout with

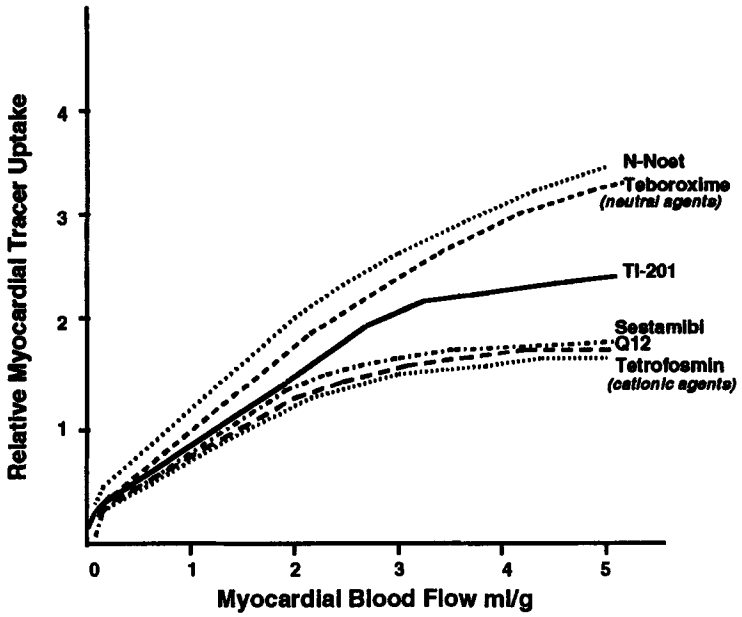

Fig 4. A diagrammatic representation of relationship between myocardial blood flow and uptake of various perfusion tracers.

earlier ^{99m}Tc cationic agents (DMPE) agents resulted from a loss of their $^{+}1$ charge because of in vivo reduction, resulting in generation of neutral compounds that wash out of the myocardium.[10] The currently used ^{99m}Tc cationic agents are nonreducible in vivo, which explains their stable intracellular retention and a lack of redistribution.

In contrast, the neutral lipophilic agents show considerable redistribution and differential washout. This is partly caused by their relatively loose binding to the cell membrane and partly by their interaction with the blood components. ^{99m}Tc N-Noet also binds to red blood cells and albumin.[60] In an experimental rat heart preparation, after a bolus injection of ^{99m}Tc N-Noet, a significant cardiac radiotracer washout was observed when perfused with red blood cells, but practically no washout was observed when perfused with red cell free buffer solution. The addition of albumin to perfusate containing red cells further enhanced the clearance of ^{99m}Tc N-Noet. Red blood cells incubated with a solution containing ^{99m}Tc N-Noet extracted significant amounts of the radiotracer. Addition of these red blood cells to the perfusate resulted in the extraction of the radiotracer from the red blood cells to the myocardium. Thus, ^{99m}Tc N-Noet has high binding affinity to blood elements and there is a bidirectional transfer between myocardium and blood components. This interaction between ^{99m}Tc N-Noet and blood components may represent a potential mechanism of ^{99m}Tc N-Noet redistribution.[60] ^{99m}Tc teboroxime also shows significant binding to red blood cells, but it appears there is no bidirectionality between the myocardium and red blood cells,[34] which may at least partly explain a much slower washout of the ^{99m}Tc N-Noet compared with ^{99m}Tc teboroxime from the myocardium.

COMPARISON BETWEEN ^{99m}Tc-LABELED PERFUSION TRACERS AND ^{201}Tl

^{99m}Tc sestamibi and ^{99m}Tc tetrofosmin have been compared with standard ^{201}Tl imaging in separate studies. Both ^{99m}Tc tracers have similar sensitivity, specificity, and overall diagnostic accuracy for the detection of perfusion abnormalities compared with ^{201}Tl.[22,61-65] However, these studies were not designed to evaluate the superiority of these ^{99m}Tc agents over ^{201}Tl. Only patients with interpretable studies with both agents were included in the analysis. Despite similar overall sensitivity, specificity, and overall diagnostic accuracy observed in these studies, ^{99m}Tc sestamibi and ^{99m}Tc tetrofosmin provide superior-quality images with higher counts. This difference is particularly important for SPECT imaging. Higher count density also allows gated SPECT imaging with ^{99m}Tc labeled agents. Regional myocardial wall motion and thickening and left ventricular ejection fraction can be derived from gated SPECT images.[8,66] Therefore, left ventricular perfusion and function can be evaluated from a single study. Gated SPECT is also helpful in differentiating true defects from attenuation artifacts, which is particularly useful in women.

In a study comparing interobserver agreement and variability in the interpretation of ^{99m}Tc tetrofosmin and ^{201}Tl images from a multicenter phase III study, where ^{201}Tl and ^{99m}Tc tetrofosmin images were read independently by multiple readers, a higher degree of interobserver agreement was observed for ^{99m}Tc tetrofosmin images compared with ^{201}Tl images. This was attributed to the better image quality with ^{99m}Tc perfusion tracers.[67]

EXTRACARDIAC ACTIVITY WITH ^{99m}Tc PERFUSION TRACERS

A significant difference between ^{201}Tl and ^{99m}Tc labeled agents is the difference in the pattern of extracardiac activity. Both ^{99m}Tc tetrofosmin and ^{99m}Tc sestamibi have higher hepatic, gall bladder, and gut activity compared with ^{201}Tl, which can cause artifacts and difficulties in image interpretation. Subdiaphragmatic activity is particularly prominent in rest and pharmacological stress studies. Intense hepatic activity can interfere with the image interpretation in several ways: (1) underestimation of inferior wall perfusion abnormalities because of scattered counts from the liver, (2) false anterior perfusion abnormality caused by artifactually higher counts in the inferior wall, (3) false defects in the inferior wall caused by oversubtraction of counts from the inferior wall adjacent to hot liver during image processing. Figure 5 is an example of a pharmacological stress study in which intense hepatic tracer uptake interferes with image interpretation. Sometimes bowel loops with tracer activity may be close to or even overlapping the heart. This can substantially degrade the image quality and can render the images uninterpretable. Great caution is required in interpreting images in the presence of marked subdiaphragmatic activity. Attempts should be made to reduce the extracardiac

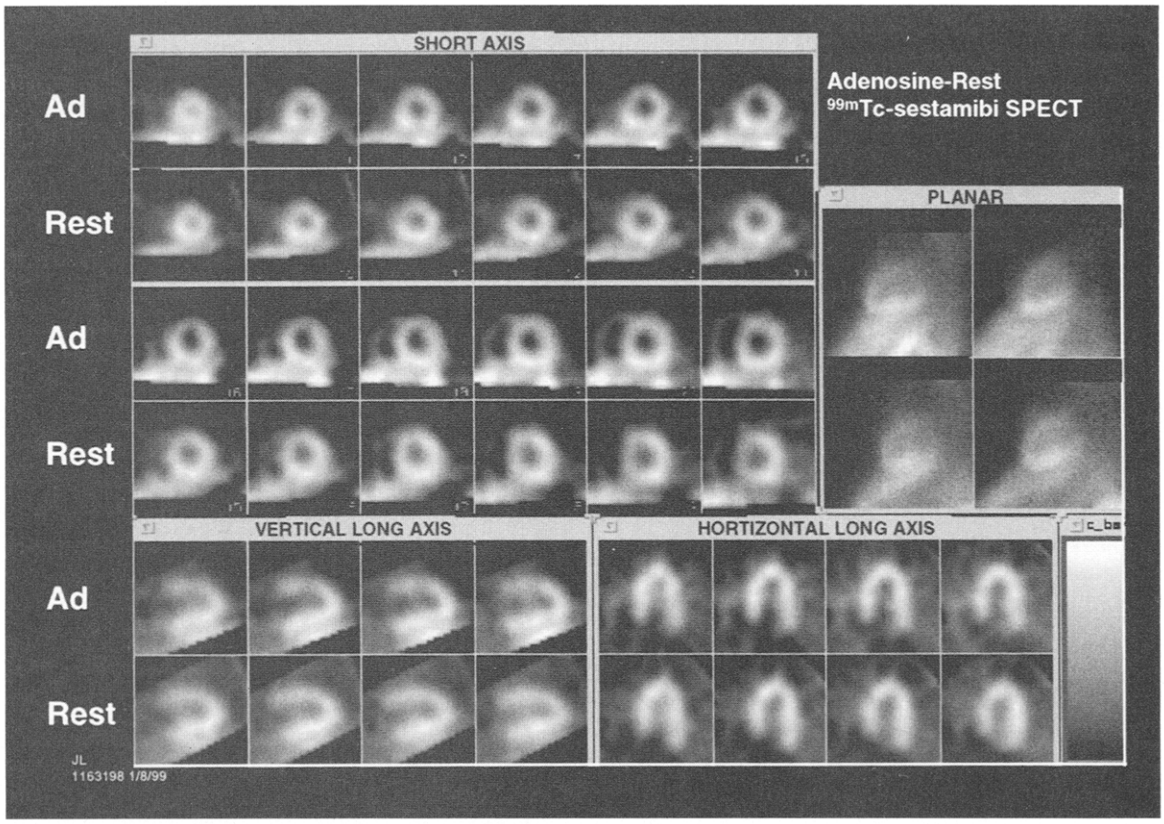

Fig 5. Adenosine stress and rest ^{99m}Tc sestamibi SPECT images of a 38-year-old obese woman with Cushing's disease, hypertension, and chest pain. The patient was unable to perform even low-level exercise. Note marked hepatic tracer uptake with artifactually high counts in the inferior wall, making it difficult to interpret the images. In addition there is some breast attenuation of the anterior wall. There is relatively less uptake in the anterior wall, which may be an artifact caused by high liver activity and breast attenuation. Gated SPECT imaging showed normal wall motion and thickening and normal left ventricular ejection fraction.

activity by increasing the interval between the tracer injection and imaging and by keeping the patient fasting before tracer injection. Combining low-level exercise with dipyridamole or adenosine also reduces hepatic activity with resultant improvement in image quality and reduction in artifacts caused by hepatic activity.[68,69] If intense bowel activity overlapping the heart is observed during the image acquisition, the image acquisition should be discontinued and should be repeated a few minutes after repositioning the patient. ^{99m}Tc tetrofosmin has lower subdiaphragmatic activity with faster clearance compared with ^{99m}Tc sestamibi. In a recent study, ^{99m}Tc tetrofosmin was found to have a higher sensitivity compared with ^{99m}Tc sestamibi for the detection of right coronary artery and left circumflex coronary artery lesions in patients with multivessel coronary artery disease, whereas there was no difference in sensitivity for detecting lesions of left anterior descending coronary artery. This difference was attributed to the lower hepatic uptake observed with ^{99m}Tc tetrofosmin compared with ^{99m}Tc sestamibi.[70] Ingestion of milk or fatty food after the injection of radiotracer does not enhance hepatic clearance. In fact, this may result in more artifacts because of gall bladder activity in the gut.

CLINICAL IMAGING PROTOCOLS WITH ^{99m}Tc PERFUSION TRACERS

Because ^{99m}Tc sestamibi and ^{99m}Tc tetrofosmin require two separate injections for stress and rest imaging, there is no single standard protocol for the performance of these studies. Ideally, the two studies should be performed on 2 separate days to allow for the decay and clearance of activity from the first injection. However, this is inconvenient and impractical in most clinical instances, particularly in outpatient settings. To accommodate stress and rest imaging in 1 day, a number of issues must

be addressed: order of the two studies (stress imaging first versus rest imaging first); minimum delay between the two injections; and optimal dose ratio between the first and second injections (lower dose for the first injection and higher dose for the second injection). Stress-rest sequence is preferable because with a normal stress study, rest imaging is not required. However, with the use of ^{99m}Tc sestamibi, the stress-rest imaging sequence was observed to slightly underestimate the defect reversibility compared with the rest-stress sequence.[15] Therefore rest-stress imaging sequence is preferred over the stress-rest imaging sequence with ^{99m}Tc sestamibi. A dose of 10 to 12 mCi of ^{99m}Tc sestamibi for rest injection and 20 to 25 mCi for the stress injection 2 to 3 hours later seems to be adequate for most patients. A ^{99m}Tc tetrofosmin stress-rest imaging sequence at an interval of 4 hours has been observed to provide information similar to 2-day imaging, and this protocol was used for a phase III clinical study.[62] A dose of 10 to 12 mCi of ^{99m}Tc tetrofosmin for stress injection and 20 to 25 mCi for rest injection is adequate for most patients.

To reduce the time required for completing the entire rest-stress imaging and to eliminate the effect of residual activity from the first injection, the combined use of ^{201}Tl (for rest imaging) and ^{99m}Tc sestamibi or ^{99m}Tc tetrofosmin (for stress imaging) has been advocated.[71,72] In a recent study, a short same-day stress-rest ^{99m}Tc tetrofosmin imaging protocol within 2 hours was observed to provide information concordant with that obtained with a standard 2-day imaging protocol.[73] Relatively less splanchnic uptake seen with ^{99m}Tc tetrofosmin allows a short stress-rest imaging protocol. This approach has distinct advantages over the conventional short imaging protocols using rest-stress imaging with dual isotopes or with the same ^{99m}Tc labeled radiotracers by providing an option of omitting rest imaging if stress images are normal. This has a potential for cost savings and improving the patient throughput, as well as reducing the radiation exposure to patients. Furthermore, any confounding effects of comparing stress and rest images acquired with isotopes with different attenuation and scatter characteristics also is eliminated.[74] However, this short stress-rest imaging sequence may not be optimal with pharmacological stress imaging because of the greater subdiaphragmatic uptake seen with pharmacological stress imaging. For pharmacological stress imaging, one should continue to use rest-stress sequence with both ^{99m}Tc sestamibi and ^{99m}Tc tetrofosmin for same-day imaging. In very obese patients, 1-day stress-rest imaging may result in suboptimal images because of low counts. In such patients stress and rest imaging should be performed on 2 separate days so that a full radiotracer dose can be given on each occasion.

INCREASED LUNG TRACER UPTAKE AND ^{99m}Tc-LABELED PERFUSION AGENTS

An abnormally increased lung ^{201}Tl uptake on stress images provides additional diagnostic and prognostic information with ^{201}Tl imaging.[75-77] Abnormal lung ^{201}Tl uptake is associated with greater segmental myocardial perfusion abnormality, increased severity and extent of coronary artery disease, impaired left ventricular function, and worse prognosis. There has been a concern about the potential loss of this important information with the use of ^{99m}Tc labeled perfusion agents.[78,79] Comparison of lung with heart ratios on exercise ^{201}Tl and exercise ^{99m}Tc tetrofosmin images from the phase III multicenter study showed a fair correlation between the two imaging agents.[80] Patients with abnormal lung-to-heart ratio on ^{201}Tl images had significantly higher lung-to-heart ratio on ^{99m}Tc tetrofosmin imaging. A lung-to-heart ratio of 0.44 on ^{99m}Tc tetrofosmin imaging was predictive of abnormal lung-to-heart ratio (0.50) with ^{201}Tl. Lung-to-heart ratio with ^{99m}Tc tetrofosmin may continue to provide diagnostic and prognostic information similar to that with ^{201}Tl. This may be related to the fact that ^{99m}Tc tetrofosmin imaging was performed relatively early after completion of the exercise.

COMPARATIVE STUDIES BETWEEN DIFFERENT ^{99m}Tc LABELED AGENTS

Although, the currently available ^{99m}Tc labeled agents (sestamibi and tetrofosmin) have been compared with ^{201}Tl and coronary angiography in separate studies, the direct comparative studies are relatively few and small.[81,82] Potential differences for the detection of myocardial ischemia and overall diagnostic accuracy may exist based on the differences in their first-pass extraction and confounding effect of extracardiac activity, particularly

while used in conjunction with pharmacological stress. Limited studies carried out so far have not shown significant and clinically relevant differences. In a recent study, where the diagnostic accuracy of ^{99m}Tc sestamibi and ^{99m}Tc tetrofosmin were compared with coronary angiography in separate patients, the overall sensitivity, specificity, and diagnostic accuracy were similar; however, ^{99m}Tc tetrofosmin had higher sensitivity for the detection of right coronary artery and left circumflex coronary artery disease in patients with multivessel coronary artery disease, which was attributed to lower hepatic uptake with ^{99m}Tc tetrofosmin.[70] Clearly, a larger prospective study is required to delineate any potential differences between these two tracers.

QUALITATIVE AND QUANTITATIVE INTERPRETATION OF PERFUSION IMAGES

The use of computer-based quantitative analysis programs that compare the myocardial radiotracer distribution with that of a normal reference file obtained from a group of normal individuals has been shown to significantly enhance the image interpretation and reduce the interobserver as well as intraobserver variability.[83] This technique also allows a quantitative estimation of the size and intensity of scar and ischemia and any change in them on follow-up studies. The normal reference files differ with the use of different tracers, and thus separate tracer-specific reference files are required.[84] With the likely availability of more ^{99m}Tc labeled radiotracers in future, the issue of a separate reference file for each tracer may come up. However, it appears that although there is a significant difference in the normal reference files between ^{201}Tl and ^{99m}Tc labeled agents, the differences between ^{99m}Tc sestamibi and ^{99m}Tc tetrofosmin are relatively small and practically inconsequential. Furthermore, the difference is more obvious in reference files for planar images and relatively less marked for SPECT images.[84] This may primarily result from significant differences in the background patterns between ^{201}Tl and ^{99m}Tc labeled perfusion imaging agents and the use of background subtraction algorithms used for quantitative analysis. Therefore, it is conceivable that a single reference file may be adequate for use with currently available ^{99m}Tc labeled perfusion tracers.[85]

RISK STRATIFICATION IN PATIENTS WITH CORONARY ARTERY DISEASE

A larger number of studies have shown the prognostic value of stress ^{201}Tl imaging in all groups of patients with coronary artery disease including chronic stable coronary artery disease, post–myocardial infarction, patients with unstable angina, and patients with suspected coronary artery disease. Patients with normal myocardial perfusion have an excellent prognosis, even in the presence of angiographic coronary artery disease, with $<1\%$ annual event rate for myocardial infarction and death. In patients with abnormal study results, the size and extent of perfusion abnormalities correlate with the risk of infarction and death. Patients with multiple reversible defects, a single large defect, or a reversible defect with increased lung ^{201}Tl uptake and/or transient left ventricular dilatation are at highest risk for adverse cardiac events. Similar prognostic data have been acquired with ^{99m}Tc sestamibi SPECT imaging.[86-89] Patients with normal ^{99m}Tc sestamibi study results had an annual adverse cardiac event rate of 0.6%, whereas those with abnormal study results had a nearly 12 times higher cardiac event rate in a pooled analysis of several studies.[89] There was a high correlation between the size of the reversible defects and the incidence of cardiac events, with threefold to fourfold higher cardiac events in those with quantitatively large defects compared with those with small defects. The results of myocardial perfusion imaging also had a direct influence on the decision to perform coronary angiography. Only 3% of the patients with normal results, 17% with mild abnormalities, and 27% to 42% with severe perfusion abnormalities underwent coronary angiography. Because ^{99m}Tc tetrofosmin has been in clinical use for only 3 years, no long-term prognostic data are yet available for this tracer.

PREOPERATIVE RISK STRATIFICATION BEFORE NONCARDIAC SURGERY

^{201}Tl stress perfusion imaging with pharmacological stress is very effective in predicting the risk of perioperative cardiac events in patients undergoing vascular surgery. Recent studies have shown a similar predictive value with the use of ^{99m}Tc sestamibi imaging.[89] Apart from predicting the perioperative risk of cardiac events, ^{99m}Tc ses-

tamibi imaging is also predictive of risk of adverse cardiac events in the postoperative period.

MYOCARDIAL VIABILITY AND ^{99m}Tc PERFUSION TRACERS

^{201}Tl rest-redistribution imaging is an important imaging modality for the detection of viable myocardium and for selecting appropriate patients for revascularization. Presence of rest-redistribution and/or 50% uptake in abnormal myocardial segments on quantitative analysis are indicators of viable myocardium. Because of a lack of redistribution, ^{99m}Tc sestamibi and ^{99m}Tc tetrofosmin were initially questioned for their ability to detect myocardial viability. However, myocellular uptake and retention of these tracers is dependent on the integrity of cellular metabolism. Subsequent studies have shown that similar to ^{201}Tl, 50% ^{99m}Tc sestamibi uptake in abnormal myocardial segments is associated with improvement in regional function after revascularization.[90-92] Another interesting approach is the use of nitrate-augmented ^{99m}Tc sestamibi imaging for the detection of myocardial viability. The administration of intravenous, oral, or sublingual nitrates before the injection of ^{99m}Tc sestamibi results in augmented tracer uptake in viable myocardial segments supplied by critically narrowed coronary arteries. This is a promising technique for the detection of myocardial viability.[90,91] Administration of trimetazidine, an agent that improves mitochondrial metabolism, before injecting ^{99m}Tc sestamibi also has been shown to enhance radiotracer uptake in the dysfunctional but viable myocardium.[93] Imaging with ^{99m}Tc perfusion tracers also can be used for ruling out coronary artery disease in patients who present with congestive heart failure of uncertain etiology and with no other evidence of coronary artery disease.

GENDER RELATED ISSUES IN MYOCARDIAL PERFUSION IMAGING

Breast attenuation artifacts lower the sensitivity as well as specificity of myocardial perfusion imaging in women. Because of the lower energy of photons, this is a major problem with ^{201}Tl in women. ^{99m}Tc has relatively less attenuation compared with ^{201}Tl. Figure 6 shows an example in which marked breast attenuation seen on ^{201}Tl imaging was not present on imaging with a ^{99m}Tc perfusion tracer. SPECT imaging allows a better appreciation of attenuation artifacts compared with planar imaging. Simultaneous assessment of wall motion and thickening with gated SPECT or with dynamic first-pass imaging further helps in the differentiation of attenuation artifacts from the true perfusion abnormalities.[94-98] Although these new developments have been quite helpful, breast attenuation continues to be a significant problem in

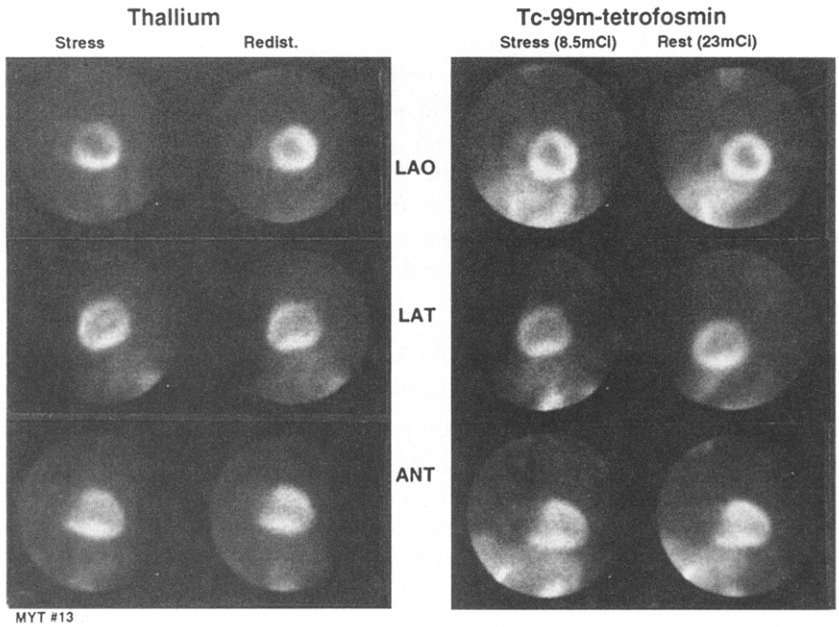

Fig 6. Standard three-view planar stress and redistribution ^{201}Tl images and stress and rest ^{99m}Tc tetrofosmin images of a female patient with longstanding hypertension and atypical chest pain. Note significant breast attenuation of stress ^{201}Tl images. However, ^{99m}Tc tetrofosmin images show unequivocally normal perfusion.

women. This can be reliably eliminated only with the use of an effective attenuation and scatter correction program. This is discussed in more detail in a separate article by Dr. Watson in this issue. Despite several important technical advances in the field of attenuation correction, this technique is not yet ready for routine clinical use.

MYOCARDIAL PERFUSION IMAGING IN ACUTE CORONARY PATIENTS

Because ^{99m}Tc sestamibi and ^{99m}Tc tetrofosmin do not redistribute, these agents can capture the status of myocardial perfusion at the time of injection, which can be imaged even several hours later irrespective of the cardiac interventions performed in the interim. ^{99m}Tc sestamibi imaging has been successfully used for developing the concept of risk area in patients with acute myocardial infarction and its salvage with the use of thrombolysis or angioplasty.[99,100] The same concept has been used for imaging the myocardium at risk during transient coronary obstruction by balloon inflation in patients undergoing elective coronary angioplasty.[101] More recently, ^{99m}Tc sestamibi and ^{99m}Tc tetrofosmin have been used for early triage of patients with chest pain suspected to be of cardiac origin. This technique has evolved with the evolution of the concept of chest pain centers.[102,103] The presence of resting perfusion abnormalities in patients without prior myocardial infarction is diagnostic of unstable coronary syndrome and is highly predictive of impending cardiac events even in the absence of any electrocardiographic changes or cardiac enzyme increase. Such patients warrant admission to a coronary care unit with the institution of aggressive therapy. On the other hand, the absence of resting perfusion abnormality rapidly excludes the possibility of an unstable coronary syndrome, and further evaluation can be performed with a stress test. ^{99m}Tc labeled perfusion tracers are particularly suited for this use because the patients can be injected as soon as possible after presentation to the emergency department even if a delay of several hours is anticipated between the tracer injection and imaging. ^{99m}Tc perfusion imaging may be a cost-effective and highly efficient tool for early triage of patients in chest pain centers.

REFERENCES

1. Zaret BL, Wackers FJT: Nuclear cardiology (two parts). N Engl J Med 329:775-783, 855-863, 1993
2. Zaret BL, Strauss HW, Martin ND, et al: Noninvasive evaluation of regional myocardial perfusion with radioactive potassium: study of patients at rest, exercise, and during anginal pectoris. N Engl J Med 288:809-812, 1973
3. Zaret BL, Stenson RE, Martin ND, et al: Potassium-43 myocardial perfusion scanning for the noninvasive evaluation of patients with false-positive exercise tests. Circulation 48:1234-1241, 1973
4. Wackers FJTh, Sokole EB, Samson G, et al: Value and limitations of thallium 201 scintigraphy in the acute phase of myocardial infarction. N Engl J Med 295:1-5, 1976
5. Kaul S, Boucher CA, Newell JB, et al: Determination of the quantitative thallium imaging variables that optimize detection of coronary artery disease. J Am Coll Cardiol 7:527-537, 1986
6. Deutsch E, Glavan KA, Sodd VJ, et al: Cationic Tc-99m complexes as potential myocardial imaging agents. J Nucl Med 22:897-907, 1981
7. Deutsch E, Bushong W, Glavan KA, et al: Heart imaging with cationic complexes of technetium. Science 214:85-86, 1981
8. Chua T, Kiat H, Germano G, et al: Gated technetium-99m sestamibi for simultaneous assessment of stress myocardial perfusion, post exercise regional ventricular function and myocardial viability: correlation with echocardiography, and rest thallium-201 scintigraphy. J Am Coll Cardiol 35:1185-1192, 1994
9. Nishiyama H, Deutsch E, Adolph RJ, et al: Basal kinetic studies of Tc-99m DMPE as a myocardial imaging agent in the dog. J Nucl Med 23:1093-1101, 1982
10. Nishiyama H, Adolph RJ, Deutsch E, et al: Effect of coronary blood flow on uptake and washout of Tc-99m DMPE and Tl-201. J Nucl Med 23:1102-1110, 1982
11. Deutsch E, Hirth W: In vivo inorganic chemistry of technetium cations. J Nucl Med 28:1491-1500, 1987
12. Sia STB, Holman BL, McKusick K, et al: The utilization of Tc-99m TBI as a myocardial perfusion agent in exercise studies: comparison with Tl-201 and examination of its biodistribution in humans. Eur J Nucl Med 12:333-336, 1986
13. Holman BL, Sporn V, Jones AG, et al: Myocardial imaging with technetium-99m CPI: initial experience in humans. J Nucl Med 28:13-18, 1987
14. Wackers FJT, Berman DS, Maddahi J, et al: Technetium-99m hexakis 2-methoxyisobutyl isonitrile: human biodistribution, dosimetry, safety and preliminary comparison to thallium-201 for myocardial perfusion imaging. J Nucl Med 30:301-311, 1989
15. Taillefer R, Laflamme L, Dupras G, et al: Myocardial perfusion imaging with ^{99m}Tc-methoxy-isobutyl-isonitrile (MIBI): comparison of short and long time intervals between rest and stress injections. Preliminary report. Eur J Nucl Med 13:515-522, 1988
16. Berman DS, Hachamovitch R, Kiat H, et al: Incremental value of prognostic testing in patients with known or suspected ischemic heart disease: a basis for optimal utilization of exercise technetium-99m sestamibi myocardial perfusion single-photon

emission computed tomography. J Am Coll Cardiol 26:639-647, 1995

17. Miller TD, Christian TF, Hopfenspirger MR, et al: Infarct size after acute myocardial infarction measured by quantitative tomographic ^{99m}Tc sestamibi imaging predicts subsequent mortality. Circulation 92:334-341, 1995

18. Kelly JD, Higley B, Archer CM, et al: New functionalized diphosphine complexes of Tc-99m for myocardial perfusion imaging. J Nucl Med 30:773, 1989 (abstr)

19. Kelley JD, Higley B, Archer CM, et al: Technetium-99m complexes of functionalized diphosphines for myocardial imaging, in Nicolini M, Bandoli G, Mazzi U, et al (eds): Technetium and Rhenium in Chemistry and Nuclear Medicine (ed 3). New York, NY, Raven Press, pp 405-412

20. Kelley JD, Forster AM, Higley B, et al: Technetium-99m-tetrofosmin a new radiopharmaceutical for myocardial perfusion imaging. J Nucl Med 34:222-227, 1993

21. Higley B, Smith FW, Smith T, et al: Technetium-99m-1,2 bis[bis (2-ethoxyethyl) phosphino] ethane: human biodistribution, dosimetry and safety of a new myocardial perfusion imaging agent. J Nucl Med 34:30-38, 1993

22. Rigo P, Leclercq B, Itti R, et al: Technetium-99m-tetrofosmin myocardial imaging: a comparison with thallium-201 and angiography. J Nucl Med 35:587-593, 1994

23. Jain D, Wackers FJT, Mattera J, et al: Biokinetics of ^{99m}Tc-tetrofosmin: myocardial perfusion imaging agent: implications for a one day imaging protocol. J Nucl Med 34:1254-1259, 1993

24. Jain D, Zaret BL: Technetium 99m tetrofosmin, in Iskandrian AE, Verani MS (eds): New Developments in Cardiac Nuclear Imaging. Armonk, NY, Futura Publishing, 1998, pp 29-58

25. Rossetti V, Vanoli G, Paganelli G, et al: Human biodistribution, dosimetry, and clinical use of technetium-99m-Q12. J Nucl Med 35:1571-1580, 1994

26. Gerson MC, Millard RW, Roszell NJ, et al: Kinetic properties of Tc-99m Q12 in canine myocardium. Circulation 89:1291-1300, 1994

27. Gerson MC, Millard RW, McGoron AJ, et al: Myocardial uptake and kinetic properties of Tc-99m Q3 in dogs. J Nucl Med 35:1698-1706, 1994

28. Rohe RC, Thomas SR, Stabin MG, et al: Biokinetics and dosimetry analysis in healthy volunteers for a two-injection (rest-stress) protocol of the myocardial perfusion imaging agent technetium 99m-labeled Q3. J Nucl Cardiol 2:395-404, 1995

29. Gerson MC, Lukes J, Deutsch E, et al: Comparison of imaging properties of technetium 99m Q12 and technetium 99m Q3 in humans. J Nucl Cardiol 2:224-230, 1995

30. Hendel RC, Verani MS, Miller DD, et al: Diagnostic utility of tomographic myocardial perfusion imaging with technetium 99m furifosmin (Q12) compared with thallium 201: results of a phase III multicenter trial. J Nucl Cardiol 3:291-300, 1996

31. Hendel RC: Technetium 99m furifosmin, in Iskandrian AE, Verani MS (eds): New Developments in Cardiac Nuclear Imaging. Armonk, NY, Futura Publishing, 1998, pp 59-78

32. Hendel RC, McSherry B, Karimeddini M, et al: Diagnostic value of new myocardial perfusion agent, teboroxime (SQ 30217), utilizing a rapid planar imaging protocol: preliminary results. J Am Coll Cardiol 16:855-861, 1990

33. Johnson G 3rd, Glover DK, Hebert CB, et al: Myocardial technetium 99m-labeled teboroxime clearance derived from canine scans differentiates severity of stenosis after dipyridamole. J Nucl Cardiol 1:338-350, 1994

34. Dahlberg ST, Gilmore MP, Leppo JA: Interaction of technetium 99m-labeled teboroxime with red blood cells reduces the compound's extraction and increases apparent cardiac washout. J Nucl Cardiol 1:270-279, 1994

35. Tartagni F, Fallani F, Corbelli C, et al: Dynamic planar myocardial perfusion imaging in patients with one-vessel disease with intracoronary injection of technetium 99m teboroxime during papaverine-induced coronary hyperemia. Am Heart J 132:1042-1047, 1996

36. Narra RK, Nunn AD, Kuczynski BL, et al: A neutral technitium-99m complex for myocardial imaging. J Nucl Med 30:1830-1837, 1989

37. Pasqualini R, Duttani A, Bellande E, et al: Bis(dithiocarbamato) nitrido technetium-99m radiopharmaceuticals: a class of neutral myocardial imaging agents. J Nucl Med 35:334-341, 1994

38. Ghezzi C, Fargret D, Arvieux CC, et al: Myocardial kinetics of TcN-Noet: a neutral lipophilic complex tracer of regional myocardial blood flow. J Nucl Med 36:1069-1077, 1995

39. Vanzetto G, Calnon DA, Ruiz M, et al: Myocardial uptake and redistribution of ^{99m}Tc-N-NOET in dogs with either sustained coronary low flow or transient coronary occlusion: comparison with ^{201}Tl and myocardial blood flow. Circulation 96:2325-2331, 1997

40. Fagret D, Marie PY, Brunotte F, et al: Myocardial perfusion imaging with technetium-99m-Tc NOET: comparison with thallium-201 and coronary angiography. J Nucl Med 36:936-943, 1995

41. Piwnica-Worms D, Kronauge JF, Delmone L, et al: Effect of metabolic inhibition on technetium-99m-MIBI kinetics in cultured chick myocardial cells. J Nucl Med 31:464-472, 1990

42. McGoron AJ, Gerson MC, Biniakiewicz D, et al: Extraction and retention of technetium-99m Q12, technetium-99m sestamibi, and thallium-201 in isolated rat heart during coronary acidemia. Eur J Nucl Med 24:1479-1486, 1997

43. Platts EA, North TL, Pickett RD, et al: Mechanism of uptake of technetium-tetrofosmin. I: uptake into isolated adult rat ventricular myocytes and subcellular localization. J Nucl Cardiol 2:317-326, 1995

44. Younes A, Songadele JA, Maublant J, et al: Mechanism of uptake of technetium-tetrofosmin. II: uptake into isolated adult rat heart mitochondria. J Nucl Cardiol 2:327-333, 1995

45. Carvallo PA, Chiu ML, Kronague JF, et al: Subcellular distribution and analysis of technetium-99m-MIBI in isolated perfused rat hearts. J Nucl Med 33:1516-1521, 1992

46. Glover DK, Ruiz M, Yang JY, et al: Myocardial ^{99m}Tc-tetrofosmin uptake during adenosine-induced vasodilatation with either a critical or mild coronary stenosis: comparison with ^{201}Tl and regional myocardial blood flow. Circulation 96:2332-2338, 1997

47. Bernard BF, Krenning EP, Breeman WAP, et al: ^{99m}Tc-MIBI, ^{99m}Tc-tetrofosmin and ^{99m}Tc-Q12 in vitro and in vivo. Nucl Med Biol 25:233-240, 1998

48. Mansi L, Rambaldi PF, Marino G, et al: Tc-99m tetrofosmin uptake in breast tumors. J Nucl Med 36:83, 1995

49. De Jong M, Bernard BF, Breeman WAP, et al: Comparison of uptakes of 99mTc-Mibi, 99mTc-tetrofosmin and 99mTc-

Q12 into human breast cancer cell lines. Eur J Nucl Med 23:1361-1366, 1996

50. Pinwica-Worms D, Holman BL: Noncardiac applications of hexakis-(alkylisonitrile)-technetium-99m complexes. J Nucl Med 31:1166-1167, 1990

51. Johnson G 3rd, Allton IL, Nguyen KN, et al: Clearance of technetium ^{99m}N-NOET in normal, ischemic-reperfused, and membrane-disrupted myocardium. J Nucl Cardiol 3:42-54, 1996

52. Uccelli L, Giganti M, Duatti A, et al: Subcellular distribution of technetium-99m-N-NOEt in rat myocardium. J Nucl Med 36:2075-2079, 1995

53. Sinusas AJ, Shi QX, Saltzberg MT, et al: Technetium-99m tetrofosmin to assess myocardial blood flow: experimental validation in an intact canine model of ischemia. J Nucl Med 35:664-671, 1994

54. Glover DK, Okada RD: Myocardial kinetics of Tc-MIBI in canine myocardium after dipyridamole. Circulation 81:628-637, 1990

55. Glover DK, Ruiz M, Edwards NC, et al: Comparison between ^{201}Tl and ^{99m}Tc sestamibi uptake during adenosine-induced vasodilation as a function of coronary stenosis severity. Circulation 91:813-820, 1995

56. Shanoudy H, Raggi P, Beller GA, et al: Comparison of technetium-99m tetrofosmin and thallium-201 single-photon emission computed tomographic imaging for detection of myocardial perfusion defects in patients with coronary artery disease. J Am Coll Cardiol 31:331-337, 1998

57. Sinusas AJ, Bergin JD, Edwards NC, et al: Redistribution of ^{99m}Tc-sestamibi and ^{201}Tl in the presence of a severe coronary artery stenosis. Circulation 89:2332-2341, 1994

58. Richter WS, Cordes M, Calder D, et al: Washout and redistribution between immediate and two-hour myocardial images using technetium-99m sestamibi. Eur J Nucl Med 22:49-55, 1995

59. Jain D, Wackers FJT, McMahon M, et al: Is there any redistribution with ^{99m}Tc-tetrofosmin imaging? A quantitative study using serial planar imaging. Circulation 86:I-46, 1992 (abstr)

60. Johnson G 3rd, Nguyen KN, Pasqualini R, et al: Interaction of technetium-99m-N-NOET with blood elements: potential mechanism of myocardial redistribution. J Nucl Med 38:138-143, 1997

61. Sridhara BS, Braat S, Rigo P, et al: Comparison of myocardial perfusion imaging with technetium-99m tetrofosmin versus thallium-201 in coronary artery disease. Am J Cardiol 72:1015-1019, 1993

62. Braat SH, Leclercq B, Itti R, et al: Myocardial imaging with technetium-99m-tetrofosmin: comparison of one-day and two-day protocols. J Nucl Med 35:1581-1585, 1994

63. Zaret BL, Rigo P, Wackers FJT, et al: Myocardial perfusion imaging with technetium-99m tetrofosmin: comparison to thallium-201 imaging and coronary angiography in a phase III multicenter trial. Circulation 91:313-319, 1995

64. Sasaki Y, Nishimura T, Kubo A, et al: Evaluation of the clinical usefulness of a new myocardial imaging agent, ^{99m}Tc-tetrofosmin (PPN1011)—a report of multicenter phase III clinical trials. Kaku Igaku 30:257-271, 1993

65. Leppo JA, DePuey EG, Johnson LL: A review of cardiac imaging with sestamibi and teboroxime. J Nucl Med 32:2012-2022, 1991

66. Berman D, Germano G, Lewin H, et al: Comparison of post-stress ejection fraction and relative left ventricular volumes by automatic analysis of gated myocardial perfusion single-photon emission computed tomography acquired in the supine and prone positions. J Nucl Cardiol 5:40-47, 1998

67. Hendel RC, Parker MA, Wackers FJT, et al: Reduced variability of interpretation and improved image quality with technetium-99m myocardial perfusion agent: comparison of thallium-201 and technetium-99m-labeled tetrofosmin. J Nucl Cardiol 1:509-514, 1994

68. Samady H, Wackers F, Deman P, et al: Low level exercise combined with adenosine myocardial perfusion imaging improve image quality, diagnostic accuracy and side effect profile. Circulation 96:I-735, 1997 (abstr, suppl)

69. Candell-Riera J, Santana-Boado C, Castell-Conesa J, et al: Simultaneous dipyridamole/maximal subjective exercise with ^{99m}Tc-MIBI SPECT: improved diagnostic yield in coronary artery disease. J Am Coll Cardiol 29:531-536, 1997

70. Ohtsuki K, Obaldo J, Jadvar H, et al: Comparison of Tc-99m tetrofosmin imaging and Tc-99m sestamibi imaging for assessing coronary artery disease. J Nucl Med 1999 (in press)

71. Berman DS, Kiat H, Friedman JD, et al: Separate acquisition rest thallium-201/stress technetium-99m sestamibi dual-isotope myocardial perfusion single-photon emission computed tomography: a clinical validation study. J Am Coll Cardiol 22:1455-1464, 1993

72. Mahmood S, Gunning M, Bomanji JB, et al: Combined rest thallium-201/stress technetium-99m-tetrofosmin SPECT: feasibility and diagnostic accuracy of a 90-minute protocol. J Nucl Med 36:932-935, 1995

73. Samady H, Lee J, Natale D, et al: Fast ninety minute Tc-99m tetrofosmin stress-rest imaging protocol: value and limitations. J Am Coll Cardiol 31:175A, 1998 (abstr, suppl A)

74. Matsunari I, Boning G, Ziegler SI, et al: Attenuation-corrected rest thallium-201/stress technetium 99m sestamibi myocardial SPECT in normals. J Nucl Cardiol 5:48-55, 1998

75. Jain D, Lahiri A, Raftery EB: Lung thallium uptake on rest, stress, and redistribution cardiac imaging. Am J Card Imaging 4:303-309, 1990

76. Boucher CA, Zir LM, Beller GA, et al: Increased lung uptake of thallium-201 during exercise myocardial imaging: clinical, hemodynamic and angiographic implications in patients with coronary artery disease. Am J Cardiol 46:189-196, 1980

77. Gill JB, Ruddy TD, Newell JB, et al: Prognostic importance of thallium uptake by the lungs during exercise in coronary artery disease. N Engl J Med 317:1485-1489, 1987

78. Giubbini R, Campini R, Milan E, et al: Evaluation of technetium-99m-sestamibi lung uptake: correlation with left ventricular function. J Nucl Med 36:58-63, 1995

79. Hurwitz GA, Fox SP, Driedger AA, et al: Pulmonary uptake of sestamibi on early post-stress images: angiographic relationships, incidence and kinetics. Nucl Med Commun 14:15-22, 1993

80. Barr SA, Jain D, Wackers FJT, et al: Are there correlates of increased thallium lung uptake on planar tetrofosmin perfusion imaging? Circulation 88:582, 1993 (abstr, Suppl I)

81. Acampa W, Cuocolo A, Sullo P, et al: Direct comparison of technetium 99m-sestamibi and technetium 99m-tetrofosmin cardiac single photon emission computed tomography in patients with coronary artery disease. J Nucl Cardiol 5:265-274, 1998

82. Munch G, Neverve J, Matsunari I, et al: Myocardial technetium-99m-tetrofosmin and technetium-99m-sestamibi kinetics in normal subjects and patients with coronary artery disease. J Nucl Med 38:428-432, 1997

83. Wackers FJ: Science, art, and artifacts: how important is quantification for the practicing physician interpreting myocardial perfusion studies? J Nucl Cardiol 1:S109-117, 1994

84. Naruse H, Daher E, Sinusas A, et al: Quantitative comparison of planar and SPECT normal data files of thallium-201, Tc-99m sestamibi, Tc-99m tetrofosmin and Tc-99m furifosmin. J Nucl Med 37:1783-1788, 1996

85. Widding A, Hesse B, Gadsboll N: Technetium-99m sestamibi and tetrofosmin myocardial single-photon emission tomography: can we use the same reference data base? Eur J Nucl Med 24:42-45, 1997

86. Stratmann HG, Mark AL, Amato M, et al: Risk stratification with pre-hospital discharge exercise technetium-99m sestamibi myocardial tomography in men after acute myocardial infarction. Am Heart J 136:87-93, 1998

87. Desideri A, Candelpergher G, Zanco P, et al: Exercise technetium 99m sestamibi single-photon emission computed tomography late after coronary artery bypass surgery: long-term follow-up. Clin Cardiol 20:779-784, 1997

88. Boyne TS, Koplan BA, Parsons WJ, et al: Predicting adverse outcome with exercise SPECT technetium-99m sestamibi imaging in patients with suspected or known coronary artery disease. Am J Cardiol 79:270-274, 1997

89. Iskander S, Iskandrian AE: Risk assessment using single-photon emission computed tomographic technetium-99m sestamibi imaging. J Am Coll Cardiol 32:57-62, 1998

90. Sciagra R, Bisi G, Santoro GM, et al: Comparison of baseline-nitrate technetium-99m sestamibi with rest-redistribution thallium-201 tomography in detecting viable hibernating myocardium and predicting postrevascularization recovery. J Am Coll Cardiol 30:384-391, 1997

91. Greco C, Tanzilli G, Ciavolella M, et al: Nitroglycerin-induced changes in myocardial sestamibi uptake to detect tissue viability: radionuclide comparison before and after revascularization. Coron Artery Dis 7:877-884, 1996

92. Arrighi JA, Ng CK, Dey HM, et al: Effect of left ventricular function on the assessment of myocardial viability by technectium-99m sestamibi and correlation with positron emission tomography in patients with healed myocardial infarcts or stable angina pectoris, or both. Am J Cardiol 80:1007-1013, 1997

93. Ciavolella M, Greco C, Tavolaro R, et al: Acute oral trimetazidine administration increases resting technetium99m sestamibi uptake in hibernating myocardium. J Nucl Cardiol 5:128-133, 1998

94. Amanullah AM, Berman DS, Erel J, et al: Incremental prognostic value of adenosine myocardial perfusion single-photon emission computed tomography in women with suspected coronary artery disease. Am J Cardiol 82:725-730, 1998

95. Taillefer R, DePuey EG, Udelson JE, et al: Comparative diagnostic accuracy of Tl-201 and Tc-99m sestamibi SPECT imaging (perfusion and ECG-gated SPECT) in detecting coronary artery disease in women. J Am Coll Cardiol 29:69-77, 1997

96. Travin MI, Duca MD, Kline GM, et al: Relation of gender to physician use of test results and to the prognostic value of stress technetium 99m sestamibi myocardial single-photon emission computed tomography scintigraphy. Am Heart J 134:73-82, 1997

97. Amanullah AM, Berman DS, Hachamovitch R, et al: Identification of severe or extensive coronary artery disease in women by adenosine technetium-99m sestamibi SPECT. Am J Cardiol 80:132-137, 1997

98. Smanio PE, Watson DD, Segalla DL, et al: Value of gating of technetium-99m sestamibi single-photon emission computed tomographic imaging. J Am Coll Cardiol 30:1687-1692, 1997

99. O'Keefe JH Jr, Grines CL, DeWood MA, et al: Factors influencing myocardial salvage with primary angioplasty. J Nucl Cardiol 2:35-41, 1995

100. Christian TF: The use of perfusion imaging in acute myocardial infarction: applications for clinical trials and clinical care. J Nucl Cardiol 2:423-436, 1995

101. Haronian HL, Sinusas AJ, Remetz MS, et al: Effects of altered left ventricular geometry on quantitative technetium 99m sestamibi defect size in humans: perfusion imaging during coronary angioplasty. J Nucl Cardiol 1:150-158, 1994

102. Kim SC, Adams SL, Hendel RC: Role of nuclear cardiology in the evaluation of acute coronary syndromes. Ann Emerg Med 30:210-218, 1997

103. Heller GV, Stowers SA, Hendel RC, et al: Clinical value of acute rest technetium-99m tetrofosmin tomographic myocardial perfusion imaging in patients with acute chest pain and nondiagnostic electrocardiograms. J Am Coll Cardiol 31:1011-1017, 1998

Fatty Acids for Myocardial Imaging

James R. Corbett

Radioiodinated free fatty acids are tracers that can be used to assess both myocardial perfusion and metabolism. There have been several fatty acids and structurally modified fatty acids studied since Evans' initial report of radiolabeled I-123 oleic acid in 1965. The radiolabeling of a phenyl group added to the long chain fatty acids in the ω-terminal position opposite the carboxyl terminal group prevents nonspecific deiodination and the rapid release of free iodine as the tracer undergoes β-oxidation. The additional inclusion of a methyl or dimethyl group to the chain slows oxidation resulting in prolonged myocardial retention. The longer retention of the radiolabel permits longer image acquisitions more compatible with single photon emission computed tomography (SPECT) imaging, especially with single-detector imaging systems. Several protocols have been implemented using these compounds, particularly 15-(para-iodophenyl)-3-R,S-methyl pentadecanoic BMIPP, to detect abnormal fatty acid metabolism in ischemic heart disease as well as in nonischemic and hypertrophic cardiomyopathies. Successful management of patients with ischemic cardiomyopathies depends on the accurate identification of hibernating myocardium. The studies covered in this review suggest that both IPPA and BMIPP, especially when combined with markers of myocardial perfusion, may be excellent tracers of viable and potentially functional myocardium. Future studies with larger numbers of patients are needed to confirm the results of these studies and to compare their efficacy with that of other available imaging modalities. Cost and distribution issues will have to be resolved for these metabolic tracers to compete in the commercial marketplace. Otherwise they will likely be available only on a limited basis for research use. As progress is made with these issues and with the development of newer imaging systems, the use of radioiodinated and fluorinated fatty acids is likely to be increasingly attractive.

MANY IMAGING MODALITIES have been developed to evaluate heart disease noninvasively. Radiotracers that can assess myocardial perfusion during exercise or pharmacological stress are the most widely used agents in nuclear cardiology. The study of myocardial metabolism with radiolabeled fatty acids has been pursued for more than 30 years. Evans et al[1] in 1965 first reported the feasibility of photoscanning the heart with radiolabeled fatty acids using iodine-131 oleic acid. Fatty acids are the principle substrate for the production of ATP in the myocardium under aerobic conditions. Carbon-11 palmitate was extensively studied in the early 1980s using PET imaging.[2] Radioiodinated fatty acids have been the most widely studied single photon tracers of myocardial metabolism.

This review concentrates on those radiolabeled fatty acids that have been studied clinically, especially single photon labeled fatty acids (Table 1). Iodine-123 labeled fatty acids including the alkyl fatty acids (16-I-hexadecanoic acid [IHXA], 17-I-heptadecanoic acid [IHDA]), the unbranched omega terminal iodophenyl fatty acids (15-(para-iodophenyl)-pentadecanoic acid [p-IPPA]), and the methyl branched para-iodophenyl fatty acids (15-(para-iodophenyl)-3-R,S-methyl pentadecanoic [BMIPP] and 15-(para-iodophenyl)-3,3-dimethyl pentadecanoic [DMIPP]) are covered.[3-8] The increased availability of positron emission tomography (PET) imaging with either dedicated or hybrid systems increases the relevance of these tracers, especially those with relatively stable myocardial distributions such as 18-F-thia-heptadecanoic acid (FTHA). Because BMIPP is the only radiolabeled fatty acid currently available for clinical use in some parts of the world, it is currently the most widely studied of these tracers and will be reviewed in the greatest detail.

MYOCARDIAL FATTY ACID METABOLISM

Uptake of radiolabeled fatty acids by the myocardium is generally avid, first-pass extraction of 40% to 60% of the blood content, and proportional to perfusion so that diagnostic quality images may be acquired beginning within 3 to 5 minutes after injection.[9,10] Transported to the heart as nonesterified fatty acids (NEFA), triglycerides or in chylomicrons, within the heart they pass along concentration gradients to the interstitium.[9] In well-oxygenated hearts at rest or under low to intermediate work loads, oxidation of fatty acids is quantitatively the most important source of energy

From the Department of Cardiovascular Nuclear Medicine, University of Michigan Medical Center, Ann Arbor, MI.

Address reprint requests to James R. Corbett, MD, Director, Cardiovascular Nuclear Medicine, University of Michigan Medical Center, B1 G412 UH, Box 0028, 1500 E. Medical Center Drive, Ann Arbor, MI 48109-0028.

0001-2998/99/2903-0004$10.00/0

Table 1. Radiolabeled Fatty Acid Analogs for Evaluation of Myocardial Fatty Acid Metabolism

Iodine-for-methyl group analogs
16-iodohexadecanoic acid (IHXA)
17-iodoheptadecanoic acid (IHDA)
1-carbon-palmitate (CPA)
Aromatic fatty acid analogs
15-(p-iodophenyl)-pentadecanoic acid (IPPA)
15-(o-iodophenyl)-pentadecanoic acid
Isosteric analogs
15-(p-iodophenyl)-6-tellura pentadecanoic acid
17-iodo-9-tellura heptadecanoic acid
14-fluoro-6-thia-heptadecanoic acid (FTHA)
Branch-chain fatty acid analogs
14-(p-iodophenyl)-beta methyltetradecanoic acid
15-(p-iodophenyl)-3-methlpentadecanoic acid (BMIPP)
15-(p-iodophenyl)-3,3-dimethyl pentadecanoic acid (DMIPP)

in the form of adenosine triphosphate (ATP).[11] Under these conditions, fatty acids supply as much as 70% of oxidatively metabolized substrate.[10] The extraction of free fatty acids by the myocyte is regulated by several variables including chain length, the availability of other metabolic substrates, circulating levels of hormones, cardiac workload, and the presence or absence of ischemia.[12-16]

Activation of fatty acids is an energy-dependent step necessary for their sequestration within the myocardium.[17] Cytosolic free fatty acids are activated at the outer mitochondrial membrane by the acyl-CoA synthetase isozyme family mediated activation to fatty acyl-CoA (Fig 1).[11] Nonesterified fatty acids can back-diffuse into the vascular space and be lost. However, once activated, fatty acids may be transported across the inner mitochondrial membranes and undergo stepwise β-oxidation. Activated intramitochondrial fatty acyl-CoA is transported across the inner mitochondrial membranes by the acyl-carnitine/carnitine transporter (carnitine shuttle) in a two-step process. This facilitated diffusion through the inner mitochondrial membrane is the rate-limiting step for the oxidation of fatty acids. With high cardiac work loads or during myocardial ischemia, esterified fatty acids are diverted into storage pools as cytosolic triglycerides and membrane phospholipids.

Inside the mitochondria, fatty acids are metabolized in three stages by enzymes in the mitochondrial matrix. In the first stage, dissociated fatty acyl-CoA rapidly undergoes stepwise β-oxidation.[11] During this stage, starting from the carboxyl end of the fatty acyl chain, the fatty acid undergoes oxidative removal of two-carbon units in the form of acetyl-CoA. The carboxyl-terminal two-carbon fragment is split off as acetyl-CoA, and this process is repeated for each remaining two-carbon fragment. The second stage of fatty acid metabolism is characterized by oxidative phosphorylation of acetyl-CoA to CO_2 via the citric acid cycle. This is the final common pathway for the oxidation of acetyl-CoA, whether derived from fatty acids, glucose, or pyruvate. In the third stage of fatty acid oxidation, the reduced nicotinamide adenine dinucleotide (NADH) and reduced flavin adenine dinucleotide ($FADH_2$) produced during previous stages of oxidation transfer electrons to the mitochondrial respiratory chain, and through this process electrons are carried to oxygen and ATP is synthesized. Each pass of an activated fatty acid through β-oxidation results in the production of five molecules of ATP, and each molecule of acetyl-CoA that passes through the citric acid cycle produces 12 molecules of ATP. The complete oxidation of the 16 carbon fatty acid palmitate to CO_2 and H_2O results in a net energy production per molecule oxidized of 129 ATP molecules. Only 2 ATP equivalents are necessary for each fatty acid molecule activated.

Oxidation of fatty acids is the most important source of energy at rest or at low to intermediate work loads in well-oxygenated hearts. The rate limiting factor under these conditions is the maximum rate of flux through the citric acid cycle. At higher work loads, free fatty acid extraction and activation increase, producing high intramitochondrial levels of acyl CoA-carnitine, and the rate of transfer across the inner mitochondrial membrane becomes the rate limiting step.[18] When acyl CoA-carnitine accmulates, β-oxidation is slowed and acetyl CoA levels decline. When citric acid cycle flux exceeds the capacity of the carnitine shuttle to provide substrate, other less efficient substrates, especially glucose, are used. Thus, at high cardiac work loads in normal patients, fatty acid metabolism is diminished, leading to the accumulation of intracellular fatty acids and a shift to glycolysis.[19,20]

During myocardial ischemia, fatty acid metabolism is suppressed and anaerobic glycolysis is accelerated (Fig 2).[10,21] Lack of oxygen rapidly depresses β-oxidation, and mitochondrial acyl-CoA, acetyl-CoA, and cytosolic acyl-carnitine levels increase because of their polarity.[22] Beta-oxidation is inhibited, and activated fatty acids are shunted into storage pools as triglycerides and

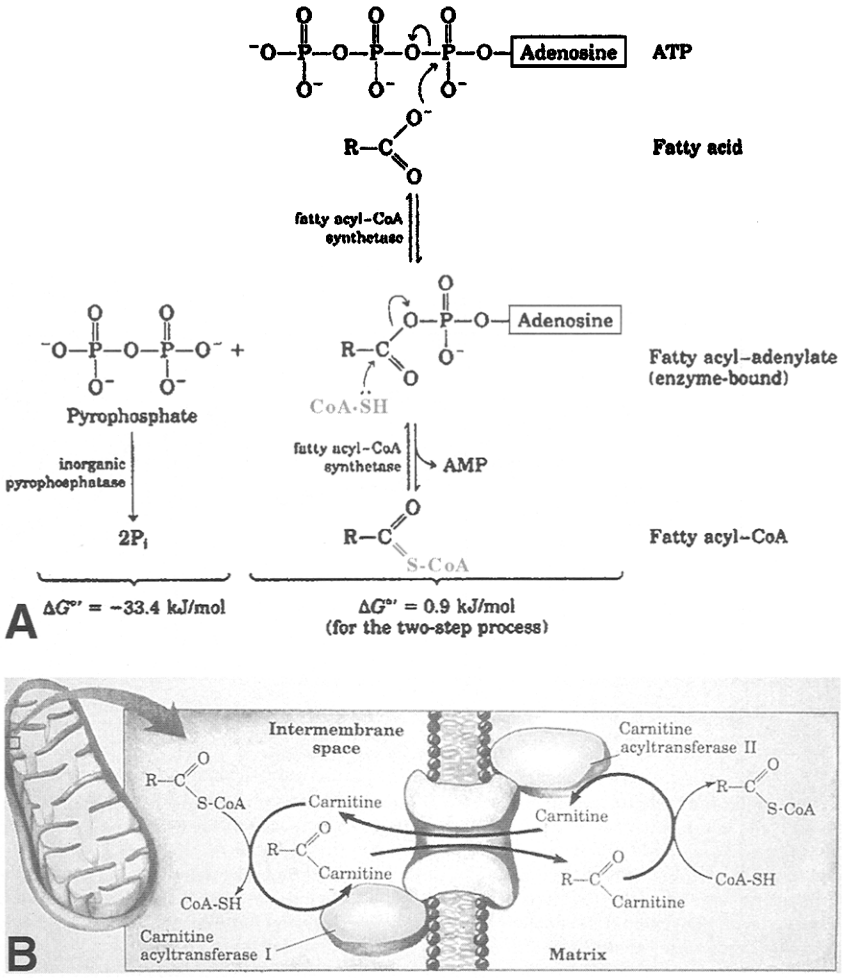

Fig 1. (A) Fatty acid activation by the formation of the fatty acyl-CoA derivative occurs in two steps. First, the carboxylate ion displaces the outer two (β and χ) phosphates of ATP to form a fatty acyl-adenylate, the mixed anhydride of a carboxylic acid, and a phosphoric acid. The other product, PP_i, is immediately hydrolyzed to two P_i, pulling the reaction in the forward direction. (Reprinted with permission.[11]) (B) Fatty acid entry into mitochondria via the acyl-carnitine/carnitine transporter. After its formation at the outer surface of the inner mitochondrial membrane, fatty acyl-carnitine moves into the matrix by facilitated diffusion through the transporter. The acyltransferase I and II enzymes are bound to the outer and inner surfaces, respectively, of the mitochondrial inner membrane. This entry process is the rate-limiting step for the oxidation of fatty acids in mitochondria. (From Principles of Biochemistry by Lehninger, Nelson, Cox ©1993, 1982 by Worth Publishers, Inc. Used with permission.)

phospholipids.[23] Additionally, there is a significant increase in back-diffusion of unmetabolized fatty acids because ischemic tissue is no longer able to activate and trap them. Glucose use is inhibited in ischemic myocardium, but not to the same extent as fatty acid oxidation.

The myocardial kinetics of radiolabeled fatty acids can be understood if one keeps in mind the above information relating to the uptake and metabolism. All of the labeled fatty acids to be discussed must be activated to be retained, ie, trapped, within the myocyte and avoid back-diffusion. Those fatty acids that have a modified structure to block β-oxidation (BMIPP, DMIPP, and FTHA) have prolonged retention and are more easily imaged with currently available single photon emission computed tomography (SPECT) imaging systems. The straight-chain fatty acids (IHXA and IHDA) after activation are metabolized through all of the three stages discussed with the subsequent release of free radiolabel and rapid degradation of image quality. Those fatty acids whose structure has been modified with the radiolabel placed on an added phenyl group (IPPA) are metabolized by β-oxidation; however, once the straight chain is metabolized, the radiolabel is lost as the resulting iodobenzoic acid diffuses out of the cell and is excreted by the kidney as iodohippurate. The remainder of this review will concentrate on the radiolabeled fatty acids themselves and their evaluations in animal and clinical studies.

IODINATED ALKYL FATTY ACIDS

Evans et al[1] in 1965 were the first investigators to radiolabel a fatty acid by saturation of the double-carbon bond of oleic acid with iodine-131 monochloride. Although photoscans of the canine heart were produced, the low specific activity of the final

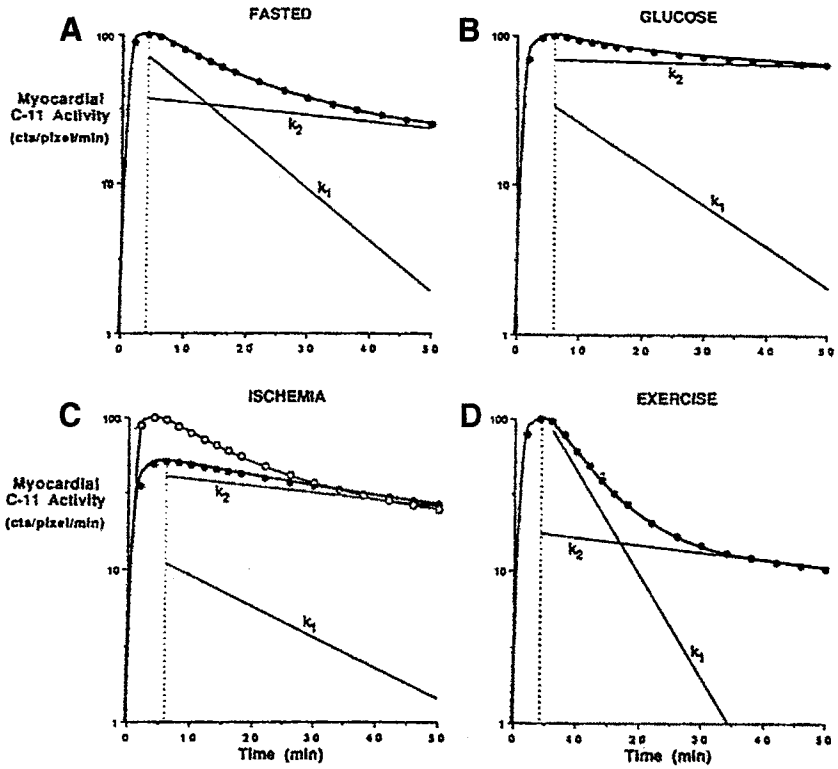

Fig 2. Effects of substrate availability, cardiac work, and ischemia on the clearance curve morphology of ^{11}C-palmitate. (A) In the fasted state, when plasma fatty acid levels are high and glucose levels are low, the myocardium meets its energy requirements by oxidizing predominantly free fatty acid. The relative size and slope of the rapid-clearance phase are high. (B) An increase in glucose concentrations in plasma is associated with a decline in free fatty acid levels after a carbohydrate-rich meal and a shift in myocardial substrate selection from free fatty acids to glucose. (C) Regional myocardial ischemia results in regional impairment of fatty acid oxidation with the regional time activity curve (*solid circles*) showing a corresponding decline in the regional size and slope of the rapid clearance component. The time activity curve derived from ischemia myocardium is compared with that in normal myocardium (*open circles*). (D) The increase in myocardial oxygen consumption in response to exercise and increased cardiac work is reflected by an increase in the relative size and slope of the rapid clearance curve component. (Reprinted with permission from Schelbert HR: Principles of positron emission tomography, in Marcus ML, et al (eds): Cardiac Imaging: A Companion to Braunwald's Heart Disease. Philadelphia, PA, Saunders, 1991.)

product precluded its clinical use. In 1975, Robinson and Lee[3] reported the development of radioiodinated fatty acids by iodide replacement of the terminal bromine in 6-bromohexanoic, 11-bromoundecanoic, and 16-bromo-9-hexadecanoic acids. In 1976, Poe et al[4] showed that iodine-123-hexadecanoic acid (IHXA) was an indicator of myocardial perfusion in experimental canine models. These investigators subsequently used iodine-123 heptadecanoic acid (IHDA) to qualitatively assess region myocardial perfusion in 21 patients.[24] All patients with prior myocardial infarcts studied showed decreased regional tracer uptake.

Among various long-chain free fatty acids labeled with C-11, I-123, Cl-34m, and Br-77, Machulla et al[5] reported that the ω-terminal–labeled fatty acids had more efficient extraction than analogs labeled in the alpha position, and that IHDA had the highest uptake. Further, IHDA showed myocardial extraction and biexponential clearance similar to that of C-11 palmitate. Several other investigators have confirmed these results.[5,25-27] Notohamiprodjo et al[27] showed biexponential clearance curves in patients with mean clearance half-times of 9 ± 3 minutes for the rapid and 43 ± 26 minutes for the slow clearance components. The corresponding half-times for C-11 palmitate were 6 ± 1 minutes and 157 ± 103 minutes, respectively. Poe et al[4] reported similar clearance for IHXA in animal models.

The rapid and slow components of IHXA and IHDA clearances are generally thought to represent β-oxidation of fatty acids and fatty acid storage in endogenous lipid pools. It was observed in some

studies that the regional elimination of radioactivity with IHDA differed under various pathophysiological conditions, and some investigators have speculated that the myocardial activity clearance of these straight chain iodo-fatty acids represents deiodination and back-diffusion of free iodide rather than β-oxidation. Two hypotheses have been proposed to explain the differences in elimination rates.[28-31] The first hypothesis explains the difference in iodide elimination rates on the basis of beta oxidation, whereas the second hypothesis explains the iodide elimination rates on the basis of differing rates of diffusion of free tracer from the mitochondria after cleavage from the fatty acid. Using an open-chest dog model, Visser et al[30] investigated the metabolic fate of IHDA by directly injecting 3 to 10 mCi into the left atrium. Biopsy specimens were taken over 30 minutes, and tracer counts were obtained in various fractions. The counts increased in the biopsy specimens until the fifth minute and decreased thereafter with a half-time of 36 minutes. The myocardial activity of radiolabeled phospholipids and triglycerides remained constant after an initial increase during the first 5 to 10 minutes, and it was concluded that deiodination and back-diffusion of free radioiodine determined the elimination rate, not beta oxidation. Visser also evaluated the kinetics of metabolites of IHDA during various metabolic interventions.[32] Again using open-chest dogs, IHDA was injected intravenously and biopsy specimens were taken sequentially over a 90-minute period. Three groups were studied: control state, during the infusion of glucose and insulin, and during the infusion of lactate. In the control group, the majority of radioactivity at peak activity resulted from free radioiodine. During the infusion of glucose, although the majority of activity came from free radioiodine, additional activity was found in the phospholipid and triglyceride fractions. With the infusion of lactate, the majority of radioactivity at peak counts was in the triglyceride fraction (43%). Under the variable metabolic conditions studied, myocyte free fatty acid use varied. With increased lactate, simulating ischemia, the enzyme thiokinase is inhibited and in turn inhibits the activation of free fatty acids to fatty acyl-CoA, and fatty acid metabolism is shunted preferentially toward triglyceride storage.

Using dynamic planar imaging, Freundlieb et al[28] were the first to evaluate IHDA in clinical studies. They showed reduced regional tracer uptake in patients with previous myocardial infarction (MI) (Fig 3A). Although high-quality images were obtained early after injection, because of the liberation of free radioiodine into the interstitial space and blood pool, image quality deteriorated rapidly, interfering with the ability to measure metabolic parameters. To correct for the accumulation of free iodine, a split-dose injection method was devel-

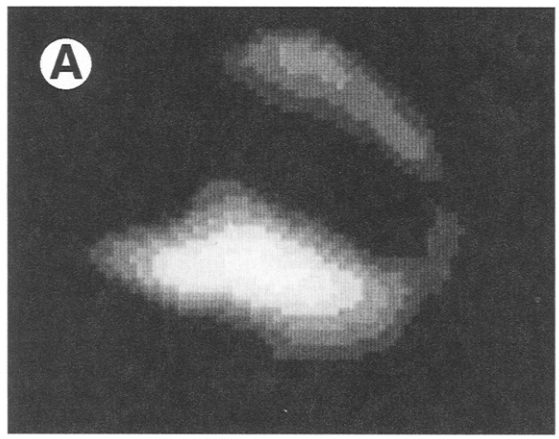

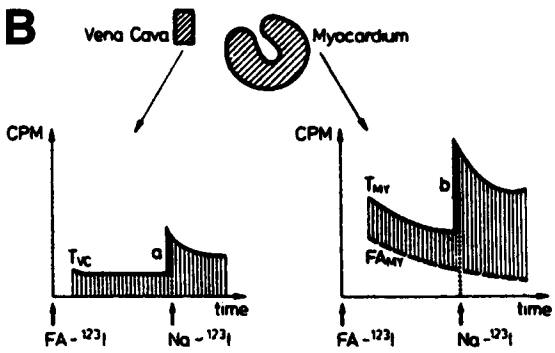

$$\frac{a}{b} = \frac{T_{VC}}{T_{MY} - FA_{MY}}$$

$$FA_{MY} = T_{MY} - \frac{b}{a} T_{VC}$$

Fig 3. (A) Anterior I-123 IHDA scintigram, from patient with congestive heat failure due to anterior MI. (Reprinted with permission.[28]) (B) Correction procedure for nonmyocardial background activity after I-123 IHDA injection. T_{VC} = count rates over control ROI (vena cava); T_{MY} = count rates over myocardial ROI; FA_{MY} = count rates related to organically bound I-123; a and b = increments attributable to $Na^{123}I$ injection. (Reprinted by permission of the Society of Nuclear Medicine from: Freundlieb C, Hoeck A, Vyska K, et al. Myocardial imaging and metabolic studies with (17-123I) iodoheptadecanoic acid. *Journal of Nuclear Medicine* 1980;21:1043-1050.)

oped that included injections of labeled and free radioiodine and provided measurements of tissue clearance half-times (Fig 3B). The average IHDA clearance half-time in normal subjects was relatively uniform at 24 ± 4.7 minutes, whereas in patients with coronary disease there were significant regional differences. Fridrich et al[29] also evaluated IHDA imaging in patients with coronary disease. Their patients had prolonged elimination rates compared with patients who had been revascularized, suggesting impaired myocyte metabolism. Railton et al[33] and Dudczak et al[26] each reported similar observations in two other trials.

Although iodine-123 IHDA and IHXA have potential as myocardial perfusion agents, their ability to access myocardial metabolism in patients has been questioned.[28,30,32] The clinical utility of radiolabeled iodoalkyl fatty acids appears limited by (1) the rapid appearance of free radioiodine requiring special correction procedures to differentiate between myocardial and blood pool activity, (2) the short elimination half-times, making them unattractive agents for SPECT imaging, and (3) the data suggesting that the elimination rate may not reflect beta oxidation but rather deiodination and back-diffusion of the tracer across the membrane. Further, the two-injection protocol and the special correction algorithm developed for planar imaging are not applicable to SPECT, effectively eliminating it as a potential imaging modality for the measurement of metabolic parameters with these radiotracers. Because of the imaging difficulties associated with deiodination of IHDA and IHXA, further investigation was performed in search of a radioiodinated fatty acid that avoided these problems. Ultimately, this resulted in the development of the phenyl fatty-acids to be discussed next.

METHYLBRANCHED FATTY ACIDS

Development and Metabolism

The short myocardial clearance half-time of IPPA as discussed below is disadvantageous even when multidetector SPECT imaging systems are used. If image acquisition is relatively slow compared with tracer clearance, progressive undersampling of raw projection data occurs. Image distortions and a loss of quantitative image accuracy result. Acquisition times may be shortened in an effort to avoid washout effects, but image resolution is significantly degraded. The molecular structure of fatty acids can be modified to slow myocardial metabolism, prolong cardiac retention, and avoid washout effects. Straight-chain alkyl and phenyl fatty acids are rapidly metabolized and cleared from the intracellular space via β-oxidation. Methyl branching was introduced to slow myocardial clearance and improve quantitative image accuracy.[34] The addition of methyl group(s) at the beta-carbon position does slow β-oxidation by interfering with the formation of the beta hydroxy CoA intermediate. Two iodine-labeled modified fatty acids developed at Oak Ridge National Laboratories to provide prolonged myocardial retention are 15-(p-iodophenyl)-3-(R,S)-methyl-pentadecanoic acid (BMIPP) and 15-(p-iodophenyl)-3,3-dimethyl-pentadecanoic acid (DMIPP) (Table 1).[35] Since its commercial introduction in Japan (1993), BMIPP (Cardiodine) has been widely studied in a variety of clinical cardiac syndromes, especially those relating to the various manifestations of ischemic heart disease.

The kinetics and subcellular distribution of IPPA and the methyl-branched fatty acids BMIPP and DMIPP have been evaluated in fasted and unfasted rat heart models.[36,37] The myocardial clearance half-time values in fasted rats were greatly increased for DMIPP (6 to 7 hours) and BMIPP (30 to 45 minutes) compared with IPPA (5 to 10 minutes). The rates of incorporation of BMIPP and DMIPP into triglycerides and diglycerides were significantly decreased, DMIPP more than BMIPP, compared with IPPA. The radioactivity in the free fatty acid pool, a reflection of unmetabolized iodinated fatty acids and the degree of their intracellular retention within mitochondria and microsomes, was greatest for DMIPP and least for IPPA. BMIPP showed intermediate characteristics between IPPA and DMIPP. DMIPP showed the most prolonged retention and was principally localized within the mitochondrial and microsomal particulate fractions. Thus, these data show that both DMIPP and BMIPP, when compared with IPPA, have prolonged myocardial retention with greater accumulations in the subcellular microsomal fractions.

Knapp et al[8] compared the biodistribution and myocardial retention of BMIPP and DMIPP in fasted rats. Although BMIPP displayed relatively slow myocardial washout with approximately 40% clearance at 60 minutes, DMIPP showed much slower clearance and greater retention, with only 24% washout at 4 hours. In addition, DMIPP showed more favorable heart-to-blood activity ra-

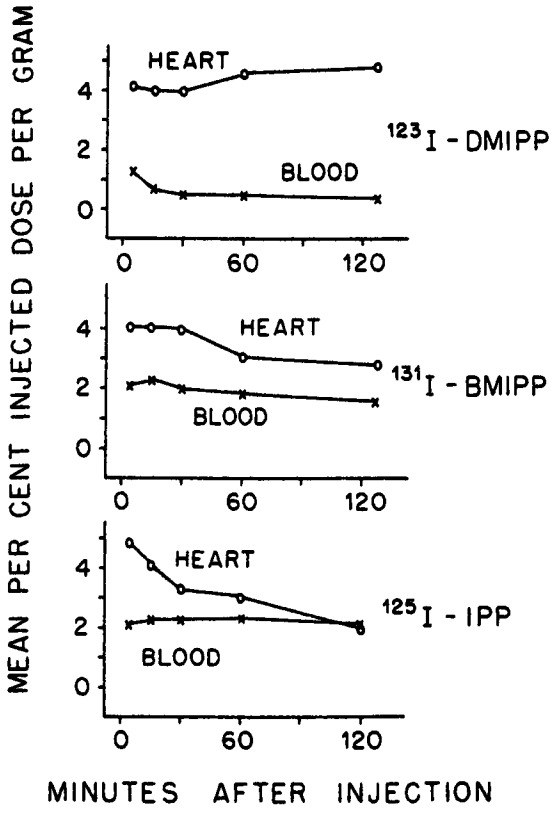

Fig 4. The distribution of [^{123}I]DMIPP, [^{131}I]BMIPP, and [^{125}I]IPPA in tissues of fasted female Fischer rats in triple-label study. (Reprinted by permission of the Society of Nuclear Medicine from: Knapp F, Goodmann M, Callahan A, et al. Radioiodinated 15-(p-iodophenyl)-3,3 dimethylpentadecanoic acid: a useful new agent to evaluated myocardial fatty acid uptake. *Journal of Nuclear Medicine* 1986;27:521-531.)

tios 15 minutes after injection: >10:1 for DMIPP compared with 3:1 to 4:1 for BMIPP (Fig 4). The investigators speculated that DMIPP should be a useful clinical and research tool for the evaluation of abnormal regional fatty acid uptake, and that because of its prolonged retention, it should be an excellent agent for use in SPECT imaging.

The importance of ATP in the myocardial extraction and retention of BMIPP has been shown (Fig 5). The initial step in beta oxidation is the production of fatty acyl-CoA, an energy-dependent (ATP-requiring) enzymatic reaction. Fujibayashi et al[38] assessed the effect of depleting ATP levels on the myocardial extraction of BMIPP versus thallium-201 in mice, and showed that treatment with 2,4 dinitrophenol (DNP), an electron transport uncoupler, resulted in significant reductions in cellular ATP and adenosine diphosphate (ADP) and accumulation of cellular adenosine 3′,5′,-cyclic monophosphate (AMP).[38] Further, they showed that BMIPP uptake was reduced in mice pretreated with DNP and that these reductions correlated with those of ATP. Thallium-201 uptake was not affected. These investigators suggested that the myocardial accumulation of BMIPP is more related to ATP content than to myocardial blood flow.

Two possible pathways have been proposed for the catabolism of BMIPP.[36] The first pathway involves the direct beta-oxidation of BMIPP. However, monomethyl-substitution at the β-carbon would be expected to interfere with oxidation at the stage of formation of the β-keto acid intermediate resulting in the myocardial accumulation of beta-hydroxy BMIPP. The second pathway begins with alpha oxidation, producing alpha-hydroxy-BMIPP as an intermediate. After loss of propionic acid, further degradation proceeds through successive cycles of beta-oxidation to the end-product (p-iodophenyl)-acetic acid. To further assess the metabolism of radioiodinated BMIPP, Yamamichi et al[39] studied the metabolites of BMIPP in an isolated perfused rat heart model. The principal metabolite

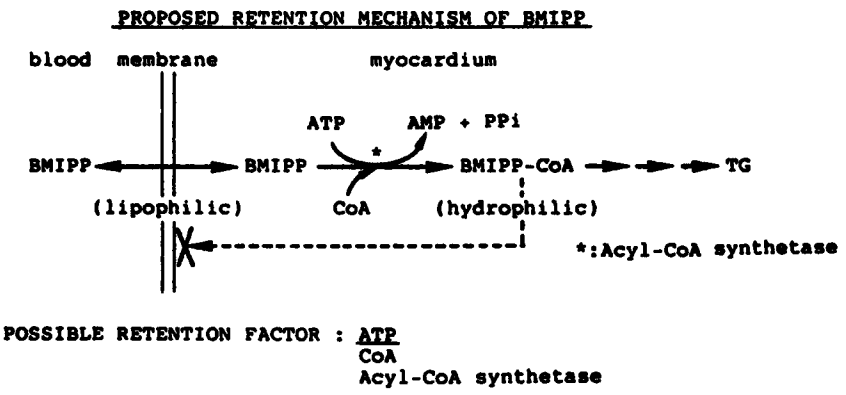

Fig 5. Proposed retention mechanism of BMIPP in viable metabolically active myocardium. (Reprinted by permission of the Society of Nuclear Medicine from: Fujibayashi Y, Yonekura Y, Takemura Y, et al. Myocardial accumulation of iodinated beta-methyl branched fatty acid analogue, iodine-125-15-(p-iodophenyl)-3-(R,S,)methylpentadecanoic acid (BMIPP) in relation to ATP conc. *Journal of Nuclear Medicine* 1990;31:1818-1822.)

of [I-123]-BMIPP identified was 14-(p-iodophenyl)-2-(R,S)-methyltetradecanoic acid (AMIPT). AMIPT is the initial metabolite derived after α-hydroxylation followed by oxidative decarboxylation. This process essentially moves the impeding beta-methyl group to the alpha position. AMIPT with its α-methyl group can subsequently be processed by classic β-oxidation. The remaining α-methyl substituted fragment passes through the beta-oxidative chain. Two other metabolites consistent with this process were identified, 12-(p-iodophenyl)-dodecanoic acid ($PIPC_{12}$) and 2-(p-iodophenyl)-acetic acid (PIPA), the products of the first and final cycles of β-oxidation. These studies confirmed the earlier observations of Knapp et al[36] that BMIPP has prolonged myocardial retention, and further confirmed their hypothesis that it does undergo β-oxidative metabolism in the myocyte after an initial α-oxidation and oxidative decarboxylation.[36,39] In contrast, DMIPP has even greater myocardial retention with no significant metabolism.

The effect of metabolic substrate on BMIPP metabolism has been studied using an open-chest dog model.[40] Nohara et al[40] directly sampled BMIPP and its metabolites from the left anterior descending coronary artery and the great cardiac vein during the infusions of lipid (intralipid) and glucose under conditions of normal myocardial perfusion. During lipid infusion BMIPP extraction was decreased ($P < .05$), wash-out increased ($P < .05$) but retention remained unchanged. Also, back-diffusion of BMIPP increased and the levels of metabolites decreased ($P < .05$). During the infusion of glucose, the extraction, retention, and wash-out of BMIPP did not differ significantly compared with controls; there was an insignificant decrease in extraction and increase in wash-out. The back-diffusion of BMIPP increased, whereas the intermediate metabolites decreased significantly during the infusions of both lipid and glucose. The effect of glucose on these metabolic parameters tended to be greater than those of lipid.

The myocardial uptake of BMIPP was studied by Reinhardt et al[41] in a rabbit model of regional myocardial hypoperfusion. The myocardial uptake of BMIPP was compared with that of Tl-201 and microspheres in control animals and after circumflex artery ligation. Using both dual-tracer autoradiography and segmental tissue analysis, these investigators showed that the activity profiles of BMIPP and Tl-201 were comparable and normal-to-defect contrasts were similar. The uptake of BMIPP correlated strongly with microsphere coronary blood flow, $y = 0.058 + 0.881x$, $r = .94$. Reinhardt concluded that BMIPP accurately delineates areas of hypoperfusion distal to coronary occlusions.

Hosokawa et al[42] studied the effects of mild and severe myocardial ischemia on the kinetics of BMIPP. Using an open-chest dog model in controls and 20 minutes of reperfusion following 10 minutes and 30 minutes of occlusion, these investigators injected BMIPP directly into the left anterior descending (LAD) and sampled the great cardiac vein and aorta for back-diffusion and metabolites. The extraction and retention of BMIPP were the same for all three groups. The early wash-out of radioactivity was significantly increased after severe ischemia ($61 \pm 8\%$ from $50 \pm 13\%$, $P < .05$). The metabolites of BMIPP from myocardium include back-diffusion of unmetabolized BMIPP, alpha oxidation, intermediate oxidation, and full oxidation with the release of 2-(p-iodophenyl) acetic acid (PIPA). Mild ischemia had no significant effect on these metabolites. During mild ischemia BMIPP back-diffusion ($r = -.92$) and full oxidation with release of PIPA ($r = .78$) correlated significantly with lactate production. However, during severe ischemia back-diffusion increased from $25.1 \pm 8.0\%$ to $34.7 \pm 8.7\%$ ($P < .05$) and full oxidation decreased from $21.4 \pm 10.9\%$ to $14.8 \pm 7.3\%$. These investigators concluded that BMIPP showed promise as a sensitive marker of ischemic heart disease.

Clinical Studies with BMIPP—Coronary Heart Disease

Clinical studies with BMIPP have evaluated its potential clinical utility in the assessment of coronary heart disease (CHD), especially in patients with unstable angina pectoris, MI and myocardial viability concerns, and in patients with hypertrophic cardiomyopathies. Dudczak et al[43] studied 15 patients with documented CHD and four controls using rest BMIPP imaging (2 to 4 mCi). Seven patients had previous MI. Cardiac uptake was slightly lower than liver uptake, and the cardiac clearance rate was slower than hepatic clearance. Myocardial uptake of BMIPP was reduced in both infarcted segments and many segments supplied by stenosed coronary arteries. Ventricular BMIPP elimination rates in regions showing reduced up-

take were generally abnormal as compared with undiseased regions, and biochemical analysis of plasma and urine samples for BMIPP metabolites provided data consistent with its beta-oxidation and incorporation into triglycerides.

De Geeter et al[44] studied mismatches between BMIPP and sestamibi uptake in 26 patients within 2 weeks after acute MI (subacute MI). Abnormal segments were categorized according to relative tracer uptake: group I—increased sestamibi uptake compared with BMIPP, group II—equally reduced sestamibi and BMIPP uptake, and group III—increased BMIPP relative to sestamibi uptake. Increased sestamibi uptake relative to BMIPP uptake occurred in 197 myocardial segments that had been reperfused by either thrombolytic therapy or mechanical revascularization (group I). BMIPP and sestamibi uptake were equally reduced in 226 segments (group II). Group III segments (n = 54) with relatively increased BMIPP uptake were more likely to be supplied by occluded coronary arteries, myocardial territories that were sites of previous infarctions, or segments with akinesis or dyskinesis. These investigators speculated that BMIPP uptake was relatively decreased compared with perfusion in group I segments because of delayed recovery of fatty acid metabolism after reperfusion. These investigators speculated that BMIPP uptake was increased compared with perfusion because of enhanced fatty acid metabolism induced by passive systolic wall stretch in areas of akinesis or dyskinesis, an interesting but not necessarily intuitive explanation.

Matsunari et al[45] compared exercise stress and rest BMIPP and thallium-201 images in 26 patients with coronary artery disease and previous myocardial infarcts. Five hundred and twenty segments were analyzed using a 20-segment model of the left ventricle and classified on the basis of the results of stress thallium imaging (Fig 6). The following observations were made:

1. The clearance of BMIPP early after rest injections (2 to 4 and 12 to 14 minutes) from segments with reversible thallium defects was relatively increased in comparison with segments with fixed defects ($P < .05$).
2. BMIPP defects were more prominent after stress than rest injections, and early stress BMIPP images showed more severe defects than exercise thallium images ($P < .05$).
3. In 163 myocardial segments with reversible thallium defects, early (20 minute) resting BMIPP uptake was lower than 3-hour redistribution thallium uptake in 90 segments.
4. In 187 segments with fixed thallium defects, 117 showed equally decreased early resting

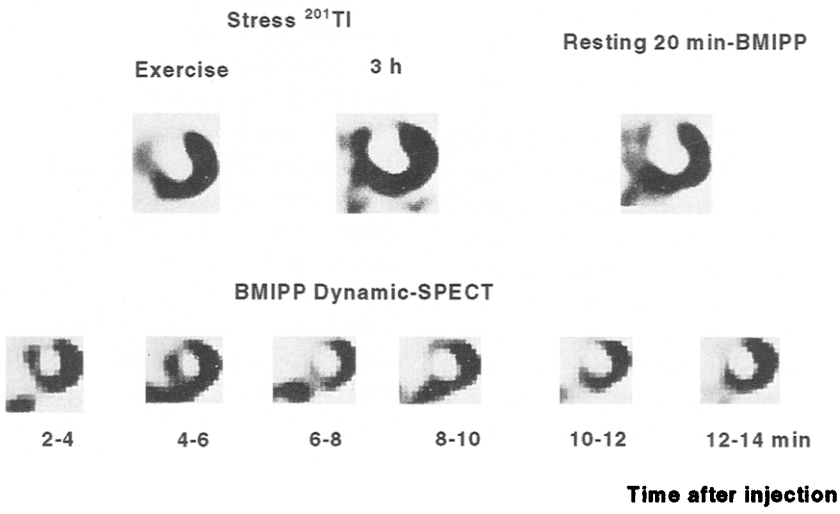

Fig 6. (A) Short-axis tomograms of exercise-redistribution Tl-201 SPECT and resting 20-minute BMIPP SPECT of a patient with an anterior septal wall infarction. The exercise-redistribution ^{201}Tl images show a reversible defect in the septal wall. On resting 20-minute BMIPP SPECT, there is decreased uptake in the septal wall compared with 3-hour Tl-201. (B) Serial changes in the accumulation pattern in BMIPP dynamic SPECT of the same patient as shown above are observed. A significant clearance of BMIPP from the septal wall is noted. (Reprinted by permission of the Society of Nuclear Medicine from: Kobayashi H, Kusakabe K, Momose M, et al. Evaluation of myocardial perfusion and fatty acid uptake using a single injection of iodine-123-BMIPP in patients with acute coronary syndromes. *Journal of Nuclear Medicine* 1998;39:1117-1122.)

BMIPP and 3-hour redistribution thallium uptake.

Matsunari suggested that the enhanced early clearance of BMIPP after rest injections in segments showing reversible ischemia (exercise and redistribution thallium imaging) could be explained by enhanced back-diffusion resulting from impaired fatty acid metabolism and trapping. When exercise stress BMIPP images were obtained, more severe defects were generally observed than with either rest BMIPP or stress thallium images. This observation was thought to be caused by the synergistic effect of decreased coronary blood flow and impaired fatty acid metabolism during exercise-induced ischemia on the uptake and retention of BMIPP.

Acute coronary syndromes. Kobayashi et al[46] studied rest BMIPP imaging 3 to 6 days after admission in patients with acute coronary syndromes including unstable angina (n = 30) and acute MI (n = 15) to evaluate the possibility of obtaining simultaneous evaluations of myocardial perfusion and fatty acid metabolism with a single injection of BMIPP. Dynamic SPECT imaging was performed beginning 2 minutes after BMIPP injection (five times, 3-minute acquisitions), and conventional SPECT imaging was performed beginning 30 minutes after injection and compared with rest Tl-201 imaging performed 2 to 7 days later. There was generally an excellent correspondence between 2 to 5-minute BMIPP images and thallium images in both the unstable angina group (kappa statistic $\kappa = 0.823$) and the acute MI group ($\kappa = 0.765$). At 30 minutes after injection, BMIPP imaging and thallium did not correspond nearly as well, and there were 27 of 30 unstable angina patients and 8 of 15 MI patients with mismatching patterns of tracer retention, BMIPP retention generally reduced compared with thallium in mismatching segments. These investigators concluded that the initial distribution of BMIPP 2 to 5 minutes after injection reflects myocardial perfusion and the 30 minutes after injection reflects myocardial metabolism.

Nakata et al[47] studied the importance of antecedent ischemia in the preservation of myocyte viability and cardiac function with rest BMIPP and thallium imaging in 32 patients with first acute MI treated with direct percutaneous transluminal coronary angioplasty (PTCA). Twenty patients with preexisting angina and 12 patients without were studied. SPECT imaging was performed within 3 weeks after the onset of symptoms. Regional wall motion was assessed at discharge and 2 to 6 months later with serial contrast left ventriculography (CVG). Regional function improved significantly at follow-up CVG in the patients with antecedent angina pectoris but did not in patients without angina, 107 ± 31 to 70 ± 31 SD/chord ($P < .001$) group A versus 109 ± 62 to 106 ± 52 SD/chord group B (P = NS). Thallium defect severity (severity index) was significantly lower in group A than group B, 62 ± 45 versus 104 ± 65 ($P < .05$). The thallium severity index was significantly lower than the BMIPP severity index in group A, 62 ± 45 versus 96 ± 59 ($P < .001$). BMIPP severity indices were not significantly different in groups A and B. There was a significant inverse correlation between the ratio of thallium to BMIPP severity index within 3 weeks of MI and improved regional wall motion during follow-up in reperfused patients, $y = -53x + 65$, $r = .667$. These investigators concluded that preinfarction angina is associated with functional improvement in patients undergoing direct PTCA for acute MI.

MI and Viability Assessments. Because of its prolonged myocardial retention and the ability to assess both myocardial perfusion and myocyte metabolism, BMIPP is a potentially attractive agent for the evaluation of dysfunctional or hibernating myocardium. Using a protocol that had previously been developed for use with Tl-201, Kropp et al[48,49] used BMIPP to assess myocardial viability. Tomographic images were obtained immediately after the injection of 5 mCi of BMIPP during symptom-limited maximal exercise (SPECT-I), with delayed imaging 3 hours later (SPECT-II), and immediately after reinjection of 2 mCi BMIPP (SPECT-III). The difference in uptake between SPECT I and II images was considered to represent myocardial metabolism and the uptake in SPECT III images was considered to assess myocardial viability. Twenty patients who had recently undergone coronary angiography and contrast ventriculography were studied. Infarct territories showed persistent defects on all three SPECT scans. Of the stenosed coronary territories without prior infarctions, 95% showed reduced uptake in SPECT I and II. Uptake in the SPECT-III images obtained immediately after the reinjection of 2 mCi BMIPP returned to 98% of normal, an impressive demonstration of

BMIPP's potential for differentiating viable and infarcted myocardium.

Tamaki et al[50] compared rest BMIPP SPECT with both Tl-201 perfusion SPECT and contrast ventriculography assessments of wall motion. Twenty-eight patients with CHD and prior MI (interval from 10 days to 8 years; mean, 14.0 months) were studied. A total of 196 myocardial segments were analyzed, and in 75% of these segments, BMIPP and thallium showed similar uptake. Discordant BMIPP and thallium uptake was shown in 25% of segments with lower BMIPP uptake compared with thallium in all cases. More discordant segments were observed in patients with infarcts less than 4 weeks old than in older infarcts (59% versus 31%, $P < .01$). BMIPP often showed reduced uptake compared with thallium. Myocardial territories that had not been revascularized showed greater discordance of BMIPP uptake compared with previously revascularized territories. Preserved BMIPP uptake correlated with retention of regional wall function. Thus, Tamaki suggested that decreased BMIPP uptake compared with thallium-201 indicates a persistent metabolic abnormality and predicts failure of functional recovery after revascularization.

Franken et al[51] studied the ability of a combination of radiotracers including Tc-99m sestamibi (perfusion) and BMIPP (metabolism) to assess myocardial viability in the setting of subacute myocardial infarction. Twenty-two patients with acute myocardial infarcts 4 to 10 days after successful coronary thrombolysis or angioplasty were evaluated with SPECT imaging. Wall thickening with intravenous dobutamine compared with resting wall motion (2-D echocardiography) verified the presence or absence of viability. Using a five-segment model of the LV, 110 myocardial segments were analyzed. Five patients had totally normal wall motion and thickening at rest. The remaining 17 patients had 32 regions of ventricular dysfunction at rest. Wall motion was normal in all 72 segments with normal tracer uptake. However, wall motion was normal in only 6 of 29 segments with mismatched uptake, BMIPP uptake reduced compared with sestamibi. Rest tomographic imaging showed 38 myocardial segments with reduced tracer uptake; 29 segments had greater reductions in BMIPP than sestamibi, and 9 segments had equally reduced uptake. No segment showed reduced sestamibi uptake compared with BMIPP. Wall motion scores were more abnormal in regions with matching defects than in regions with mismatched defects, 2.11 ± 0.78 versus 1.34 ± 0.81 ($P = .014$). None of the nine segments with matched defects had ionotropic reserve, whereas 15 of 23 discordant segments (6 hypokinetic and 9 akinetic) showed ionotropic reserve ($P < .001$). The positive predictive value for wall motion improvement in mismatched segments was 79% (11 of 14 segments), and the negative predictive value for the absence of improvement in matched segments was 100% (6 of 6 segments). Thus, wall motion may recover under resting conditions before normalization of myocardial fatty acid metabolism occurs. Defects mismatched for perfusion and metabolism are most likely indicative of viability, whereas matched defects are likely representative of scar.

In other studies, Franken et al[52] and Knapp et al[53] assessed the prognostic value of combined BMIPP and sestamibi SPECT to predict functional outcome. Eighteen patients with recent myocardial infarcts (7 ± 3 days) and resting regional wall motion abnormalities were studied. Mechanical revascularization was obtained in 13 patients: 7 with PTCA, and 6 surgically. Wall motion, assessed 6 months after infarction with 2-D echocardiography, improved in half of the patients and was unchanged in half. Functional outcome was not predicted by clinical data, catheterization data, or the type of revascularization performed. There was, however, a highly significant association between functional outcome and the relative uptakes of BMIPP and sestamibi. Wall motion improved in 27 of 33 segments (82%) with mismatched defects (BMIPP < sestamibi) and was unchanged in 19 of 21 segments (90%) with matched defects (Fig 7). Sestamibi had a positive predictive value of 84% and a negative predictive value of 72% when using 50% of the maximal LV activity as criteria for myocardial viability. These values improved to 95% and 89%, when the relative uptake of BMIPP was considered (mismatched versus matched defects). The positive and negative predictive values of low-dose dobutamine echocardiography and improved systolic wall thickening were only 80% and 62%. When more than 75% of a patient's dysfunctional segments showed a mismatched pattern, the probability for functional improvement was 90% (9 of 10 patients). None of eight patients with less than 75% mismatching segments improved functionally.

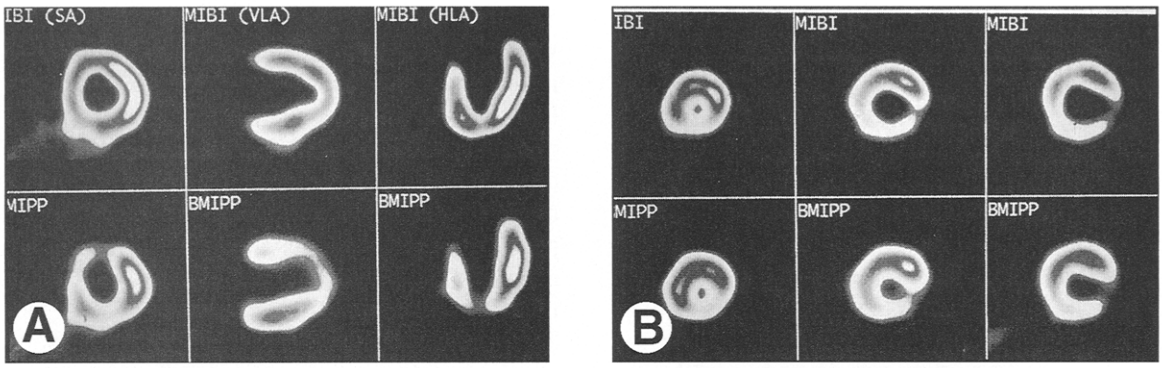

Fig 7. (A) Example of mismatched defects. Sestamibi (MIBI) and BMIPP obtained in a patient with left ventricular dysfunction 1 week after acute anterior myocardial infarction. The study shows reduced BMIPP but normal sestamibi uptake in the infarct-related coronary artery territory, indicating the presence of viable but jeopardized myocardium. HLA images are shown apex down. (Reprinted with permission.[53]) (B) Sestamibi (MIBI) and BMIPP left ventricular short-axis slices obtained in a patient with recent acute inferolateral myocardial infarction. There is a mild-to-moderate matched defect of both tracers in the infarct-related coronary artery territory, suggesting the absence of residual viability. Regional dysfunction did not improve after revascularization of this patient. (Reprinted by permission of the Society of Nuclear Medicine from: Knapp F, Franken P, Kropp J. Cardiac SPECT with iodine-123-labeled fatty acids: evaluation of myocardial viability with BMIPP. *Journal of Nuclear Medicine* 1995;36:1022-1030.)

Several more recent studies have evaluated BMIPP as a tracer of myocardial viability early and late after MI.[54-58] Dendale et al[54] studied 15 patients early after MI comparing sestamibi and BMIPP SPECT with low-dose dobutamine magnetic resonance imaging. Wall thickening at rest was significantly related to the uptake of sestamibi but not BMIPP ($P < .001$). There was a significant correlation between contractile reserve and abnormalities of BMIPP metabolism; 14 of 16 segments with but only 6 of 18 without contractile reserve had mismatched reductions in sestamibi and BMIPP uptake ($P < .002$). Fujiwara et al[57] studied 23 patients with acute MI treated with direct angioplasty using BMIPP 30 minutes after injection and sestamibi 1 and 3 hours after injection and compared these results with those from CVG immediately after intervention and 1 month later. Recovery of regional function was associated with perfusion/metabolism mismatch, as had been reported previously. An interesting finding was that reverse redistribution of sestamibi also correlated with functional recovery. Yamagishi et al[58] compared Tl-201/BMIPP SPECT, exercise Tl-201 SPECT, and N-13 ammonia/F-18 fluorodeoxyglucose (FDG) PET in 46 patients within 6 weeks of MI. Again BMIPP mismatch correlated with other markers of regional viability. Sloof et al[56] and Hambye et al[57] studied patients later after MI using BMIPP and either Tl-201 or sestamibi perfusion/metabolism mismatch correlated with functional recovery. Sloof's study was interesting in that patients with chronic ischemic heart disease not only showed perfusion metabolism mismatch, but 74% of FDG SPECT viable segments showed BMIPP mismatch with BMIPP uptake higher than perfusion. Segmental BMIPP uptake reduced compared with perfusion occurred in 69% of FDG nonviable segments. The mechanism for these disparate findings is unclear and awaits confirmation.

Imaged either alone or in combination with a myocardial perfusion tracer such as Tl-201 or Tc-99m sestamibi, BMIPP appears to be useful as a marker of myocardial viability in acute and chronic ischemic LV dysfunction. Reduced uptake of both tracers is reflective of scar, whereas mismatched defects with less BMIPP uptake in comparison with myocardial perfusion is generally indicative of jeopardized myocardium with impaired fatty acid metabolism. BMIPP SPECT enhanced the accuracy of myocardial viability assessments in comparison with either dobutamine echocardiography or myocardial perfusion imaging alone. These studies confirmed earlier investigations with BMIPP and strengthened the case for the use of BMIPP as a marker of myocardial viability. Because it has been shown that the initial distribution of BMIPP in the first several minutes after injection is comparable to that of perfusion tracers, it can be argued that the use of BMIPP alone imaged early and late after injection is all that is required to evaluate myocardial viability with a high degree of accuracy. Multicenter studies with functional outcomes are needed to confirm these findings before the consid-

erable additional expense for BMIPP imaging can be recommended for clinical use.

Cardiomyopathy. Grover-McKay et al[59] have reported that C-11 palmitate uptake is reduced in the septa of patients with hypertrophic cardiomyopathy when imaged using positron emission tomography (PET). These investigators suggested that septal fatty acid metabolism was normal because the clearance half-times of the early rapid phase and the residual fractions of C-11 palmitate were similar in the lateral and septal walls. They postulated that the decrease in palmitate uptake was caused by reduced blood flow. The difference between the former studies and this study is that C-11 palmitate can be metabolized via beta oxidation, whereas BMIPP must initially undergo alpha oxidation. They also showed that F-18 2-deoxyglucose (FDG) uptake was lower in the septum than in the lateral wall. Decreased septal glucose uptake may result in decreased cellular ATP, which in turn may explain the reduced septal uptake of BMIPP.[38] They concluded that the uncoupling of thallium and BMIPP uptake in hypertrophic cardiomyopathy patients may reflect an intrinsic impairment of myocardial fatty acid metabolism.

Characterized by thickened myocardium and associated abnormal diastolic relaxation, hypertrophic cardiomyopathy (HCM) has also been associated with various abnormalities of glucose and fatty acid metabolism. Results from several clinical trials have shown that BMIPP SPECT is useful for identifying patients with hypertrophic cardiomyopathies.[60-63] Takeishi et al[62] used rest BMIPP and thallium SPECT imaging to study 14 patients with HCM. Imaging was performed 20 minutes and 3 hours after the injection of BMIPP, and quantitative image analysis was performed. Two patients had hypertrophic cardiomyopathies secondary to hypertension, and 12 patients had primary cardiomyopathies, including two patients who had the apical variant. In patients with anteroseptal hypertrophy, there was less anteroseptal BMIPP uptake in comparison to the posterolateral wall uptake (74% versus 85%, $P < .001$). Further, BMIPP was cleared more rapidly from thickened anteroseptal segments (33% versus 27%, $P < .001$). Segments with severe hypertrophy showed less BMIPP uptake (73% versus 82%, $P < .001$) and faster clearance (30% versus 25%, $P < .05$) when compared with less severely hypertrophied segments. The results of BMIPP imaging were often discordant with the results of thallium imaging; ie, thallium imaging often showed normal or even increased anteroseptal myocardial uptake whereas BMIPP uptake and clearance in the corresponding segments were often reduced.

Kurata et al[63] studied 10 patients with asymmetric septal hypertrophy (ASH) (septal thickness >15 mm and septal to posterior wall ratio >1.3), including 5 patients with diffuse hypertrophy and 2 patients with apical hypertrophy. Rest and delayed BMIPP images (30 minutes and 4 hours, respectively) and immediate thallium images were compared. In patients with ASH, there was lower relative regional BMIPP uptake in hypertrophic segments (immediate and delayed) as compared with BMIPP uptake in normal segments and in comparison to thallium uptake. Thallium uptake was generally less heterogeneous in these patients. In the 2 patients with apical hypertrophy, 1 had decreased BMIPP uptake and the other did not. The results of this study were similar to those of Takeishi et al[62] discussed above, and were interpreted as indicating that disproportionately thickened myocardial regions may have impaired fatty acid metabolism that is independent of perfusion. Kurata observed that the apparent LV chamber sizes in patients imaged with BMIPP were larger than those seen in the corresponding thallium studies (16 of 17 patients), especially in patients with diffuse hypertrophy. This was thought to result from diffuse subendocardial impairment of lipid metabolism. An alternate explanation for this observation is provided by the 159 keV photon iodine-123 emits. This higher energy iodine photon results in improved image resolution and may account at least in part for the discrepancies observed in apparent chamber size. This is similar to what has been consistently observed with thallium-201 and Tc-99m sestamibi dual-isotope imaging.

Tadamura et al[64] used rest metabolic imaging using F-18 FDG PET, C-11 acetate PET, and BMIPP SPECT to evaluate 28 subjects with HCM. The purpose of this study was to assess the frequency of myocardial metabolic abnormalities and to clarify the relationship between these metabolic parameters. BMIPP uptake was often impaired without significant reductions in glucose uptake or acetate metabolism. Segmental abnormalities of BMIPP uptake (34%) were more frequent than with either acetate (18%) or FDG (5%) ($P < .0001$). In nonhypertrophic myocardium, the

FDG, BMIPP, and acetate did not differ: 96.5 ± 7.9, 95.6 ± 7.6, and 96.2 ± 7.9, respectively (P = NS). In hypertrophic myocardium, all three metabolic markers were reduced: 90.0 ± 12.3, 73.1 ± 16.1, and 85.2 ± 15.2, respectively ($P < .01$), whereas FDG uptake was relatively maintained even when both BMIPP uptake and acetate metabolism were abnormal. Although BMIPP was the most sensitive marker, among those segments with reduced acetate metabolism (K mono), some showed reduced BMIPP with preserved FDG uptake. When acetate metabolism was maintained, FDG was always normal, and only when acetate was severely abnormal was FDG reduced. These investigators concluded that the first manifestation of abnormal metabolism assessed with these three radiotracers was that of fatty acids assessed with BMIPP. Metabolism of C-11 acetate was the next to become abnormal, and FDG was the last.

Several studies in patients with hypertrophic cardiomyopathy have shown abnormalities of myocardial fatty acid metabolism. Such abnormalities were commonly identified with BMIPP. The specificity of these findings and their clinical significance are yet to be determined. Questions yet to be answered include those related to the prognostic significance of such metabolic abnormalities; the unique characteristics of these abnormalities as compared with those seen in patients with ischemic heart disease; and the meaning of these abnormalities in regard to symptoms, especially chest pain, arrhythmias, and survival.

(p-IODOPHENYL) PENTADECANOIC ACID

Development and Metabolism

To prevent the rapid deiodination of the alkyl fatty acids and stabilize the iodine radiolabel, Machulla developed 15- (p-iodophenyl) pentadecanoic acid (IPPA) as an alternative to the alkyl fatty acid analogs.[5,6] The iodine-123 label attached to the terminal phenyl ring in either the ortho or para position is stabilized against deiodination. Radiolabeled IPPA has been shown to have kinetics similar to the physiological substrate palmitic acid in perfused rat hearts.[65] The uptake of IPPA is related to coronary perfusion, and the catabolism of IPPA generally follows the normal metabolic pathway for beta oxidation.[66] Iodobenzoic acid and its metabolite iodohippurate are the products of IPPA oxidation (Fig 8). Iodobenzoic acid and iodohippurate are rapidly excreted by the kidneys with the iodine moiety still attached, preventing the buildup of free radioiodine. Studies using myocardial biopsy specimens have shown rapid extraction by normal myocardium, with a biexponential clearance including a fast component half-time of 3.5 minutes, a slow component half-time of approximately 130 minutes, and a blood clearance half-time of 2.5 minutes.[67,68] As compared with the alkyl fatty acids, IPPA has the advantages of rapid myocardial uptake, iodine stabilization, and rapid clearance of metabolites from the body.

The uptake and myocardial kinetics of IPPA have been studied in canine models of ischemia and infarction. Rellas et al[69] used open-chest dog models to evaluate the effects of temporary (90-minute)

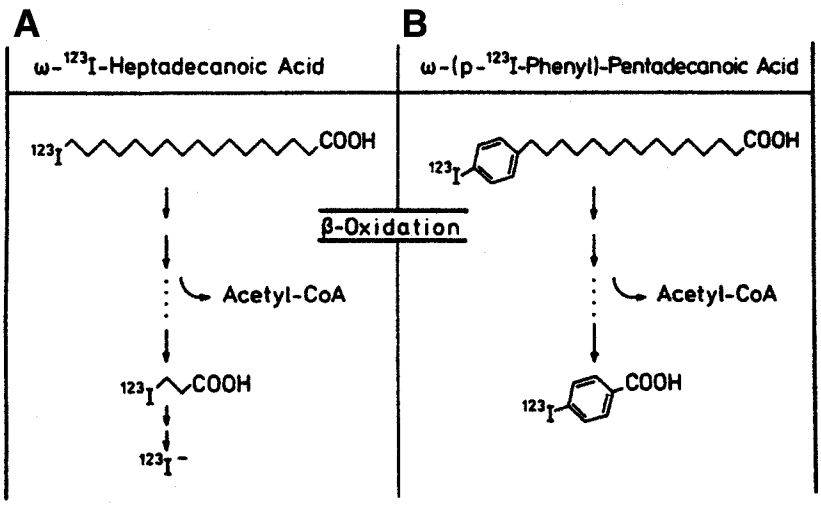

Fig 8. Schematic catabolism of ω-[123]I heptadecanoic acid (A) and ω-(p-[123]I phenyl)-pentadecanoic acid (B). (Reprinted with permission from Springer-Verlag.[6])

and sustained (90 to 120 minutes) occlusions of the LAD coronary artery to determine if IPPA can be used to identify myocardial injury. They studied how uptake and metabolism differed under conditions of ischemia, reperfusion, and infarction. In dogs with temporary LAD occlusions and reperfusion, the uptake of IPPA was blunted and the clearance prolonged. In contrast and compared with controls, dogs with fixed LAD occlusions showed significantly decreased uptake and accelerated clearance. These investigators concluded that IPPA could be used to localize sites of myocardial ischemia and infarction, and that clearance from ischemic tissue of the radioiodinated fatty acid reflects beta oxidation. Hudon et al[22] used planar imaging in canine models to investigate the affect of increasingly severe regional myocardial ischemia over time on the myocardial clearance of IPPA. Open-chest dogs instrumented with ameroid constrictors in the LAD territory were studied 6 hours and 5, 7, and 14 days postoperatively. These animals during atrial pacing showed decreased regional myocardial IPPA washout with prolonged clearance half-time values. There were no changes in half-time values in nonischemic segments. Both of these studies showed that during myocardial ischemia, beta oxidation is impaired, resulting in prolonged myocardial IPPA clearance half-times.

Clinical Studies with IPPA

Identification of ischemic heart disease. The ability of IPPA to evaluate ischemic heart disease has been studied in humans with planar and SPECT imaging. Using planar IPPA imaging after exercise stress, Kennedy et al[70] studied 33 patients with known or suspected coronary heart disease. The study population included 15 control patients and 18 patients with stable angina; 17 of 18 patients with angina had coronary disease documented by coronary angiography. Eleven patients had prior myocardial infarcts documented by electrocardiogram (ECG) and corresponding segmental wall motion abnormalities. Given 1 mL Lugol's solution 30 to 60 minutes before IPPA injection to block thyroid uptake, 2 to 6 mCi of IPPA were injected at rest and peak exercise stress. Using both myocardial uptake and clearance criteria compared with normal data files, the sensitivity and specificity of IPPA imaging were 72% and 100%. Zimmermann et al[71] evaluated IPPA and thallium-201 imaging after bicycle ergometry stress in 41 patients with angiographically documented coronary disease and chronic stable angina. Twenty patients had a history of prior Q-wave infarction. There were no significant differences in heart rate, blood pressure, or work load achieved during the bicycle exercise stress associated with the thallium and IPPA studies. The overall sensitivities and specificities were identical at 88% and 70%, respectively for both IPPA and Tl-201. Both tracers had nearly identical sensitivities for the identification of individual coronary stenoses $\geq$75%, 70%, and 66%, respectively. There were, however, a larger number of fixed defects on visual IPPA analysis, 36 reversible with thallium-201, 28 with IPPA ($P = .02$). With quantitative analysis of IPPA wash-out, the abilities of both tracers to discriminate fixed and reversible defects equalized. Their data suggested that IPPA was at least as sensitive as thallium for detecting CHD, but may underestimate regional myocardial viability without quantitation of myocardial clearance rates.

To compare IPPA and TL-201 myocardial SPECT, Hansen et al[72] used symptom-limited maximal exercise stress. Fourteen normal volunteers (mean age, 29 $\pm$ 3 years) and 33 patients with angiographically documented CHD (mean age, 54 $\pm$ 11 years) were evaluated. All 33 patients had chronic stable angina: 18 patients had single-vessel, 9 double-vessel, and 6 triple-vessel disease. All patients were studied while on antianginal therapy as prescribed. Maximal treadmill exercise was performed, and 6 to 8 mCi IPPA was administered 1 minute before the termination of exercise. Stress and rest imaging were performed beginning 10 and 45 minutes after injections. Twenty-five of the 33 patients also had symptom-limited maximal Tl-201 scintigraphy performed. Imaging was performed beginning 10 minutes after injection. Two types of abnormalities were observed with IPPA imaging in patients with CHD: (1) decreased tracer uptake occurring at rest in patients with prior MI and during exercise in coronary distributions supplied by stenosed coronary arteries (>70%), (2) delayed clearance of IPPA from ischemic myocardium. IPPA clearance was slower in territories supplied by stenosed coronary arteries. Using these two criteria, the overall sensitivity of IPPA imaging was 82% versus 72% for Tl-201 imaging. The investigators postulated that the improved sensitivity of IPPA over Tl-201 was attributable to three factors: (1) the initial myocardial uptake of IPPA,

like that of Tl-201, is directly proportional to coronary blood flow over a broad physiologic range. IPPA uptake and retention are dependent on blood flow for myocardial delivery and oxygen for metabolism, thus IPPA may be a more sensitive physiological marker of intracellular ischemia. (2) The half-time of iodine-123 is one-sixth that of TL-201, allowing larger doses of IPPA to be administered and further improving image quality compared with Tl-201. (3) The higher-energy 159 keV iodine-123 photon results in less soft tissue attenuation and scatter, better resolution, and improved signal-to-noise ratios compared with the 60-83 keV mercury X-rays of Tl-201. The delayed clearance of IPPA in CHD patients is consistent with the known metabolism of fatty acids in ischemic tissue, ie, after uptake once fatty acids have undergone thioesterification with acetyl coenzyme A, they are trapped and no longer have the ability to diffuse out of the cell, available oxygen is shunted toward glucose metabolism, resulting in reduced beta oxidation, and an increasing percent of the intracellular fatty acid pool is incorporated into triglyceride and phospholipid stores.

Pippin et al[20] studied 19 healthy volunteers at rest, after submaximal exercise, and again after maximal exercise stress to assess the effects of different cardiac work loads on myocardial fatty acid uptake and metabolism. The dose of IPPA varied from 0.10 to 0.12 mCi/kg body weight, and averaged 6 to 10 mCi per patient. For submaximal exercise studies, a target rate-pressure product of 20,000 was used, and for maximal exercise studies, the onset of severe fatigue was the reason for discontinuation. IPPA was injected 1 minute before the termination of exercise. The normalized total heart uptake of IPPA increased progressively from rest to submaximal (P = NS) and maximal exercise ($P < .001$) (Table 2). In contrast to the changes

Table 2. Normalized Total Heart IPPA Uptake (×1000)

	Rest	Submaximal Exercise	Maximal Exercise
Men	35.2 ± 3.1	40.1 ± 3.0	55.1 ± 3.4
Women	35.3 ± 4.1	35.9 ± 2.1	48.0 ± 5.4
All	35.2 ± 2.4	38.2 ± 1.9	51.9 ± 3.1

Rest versus submaximal: P = NS
Submaximal versus maximal: $P < .001$
Rest versus maximal: $P < .001$

Note: Values expressed as (counts)(mCi)/(voxels)(m^2) ± SEM.
Abbreviation: N = 10 subjects performing all three work loads.

Table 3. Total Heart IPPA Wash-Out

	Rest (%)	Submaximal Exercise (%)	Maximal Exercise (%)
Men	20 ± 2*	28 ± 1†	15 ± 3
Women	14 ± 3*	18 ± 1†	11 ± 2
All	17 ± 2	24 ± 2	13 ± 2

Rest versus submaximal: $P < .01$
Submaximal versus maximal: $P < .01$
Rest versus maximal: P = NS

Note: All values are group mean ± SEM. Wash-out (%) = (immediate counts − delayed counts) × 100/immediate counts.
*$P < .05$.
†$P < .001$.

in IPPA uptake that occurred, wash-out increased significantly from rest to submaximal exercise ($P < .01$) but then at maximal exercise stress decreased to rates slower than those at rest (P = NS) (Table 3). Pippin concluded that with near-exhaustive exercise, while myocardial metabolism is shifted toward glucose use, fatty acid oxidation is blunted and shifted toward anabolism in the form of triglyceride and phospholipid synthesis. This effect is likely the result of lactate production, reported to increase six-fold during maximal exercise stress.[73] Lactate has been shown to inhibit the thiolase enzyme, reducing the rate of fatty acid oxidation and making glucose the preferred fuel source during hypoxemia and ischemia. In animal experiments, pyruvate has the same effect as lactate.[74]

Assessments of myocardial viability. One of the major challenges before noninvasive imaging is the differentiation of viable, potentially functional tissue, and scarred myocardium with no potential for functional recovery. Viability assessments are most challenging in dysfunctional ventricular territories with prior ischemic damage. Noninvasive imaging modalities currently used to assess myocardial viability include PET imaging with F-18 FDG and C-11 acetate, SPECT with thallium and Tc-99m sestamibi, and dobutamine echocardiography. PET imaging is considered by many to be the gold standard for myocardial viability assessments. The widespread use of PET imaging maybe precluded by the need for an on-site cyclotron and the high cost of these studies. Because radiolabelled fatty acids have the potential to evaluate both coronary perfusion and myocyte metabolism, they have been studied as potential markers of tissue metabolism and viability.

Vyska et al[75,76] used dynamic planar imaging and

compartmental analysis to study the rate constant for influx (k_1) of IPPA. In 15 normal subjects and 30 patients with CHD, there were no significant differences in the k_1 of any of the major myocardial segments. The average k_1 was 0.57 ± 0.13/min at rest and 0.42 ± 0.6/min during exercise. With increased IPPA plasma concentration and increased relative myocardial perfusion, the influx increased in a saturable fashion. In ischemic areas, the mean k_1 was reduced to 57 ± 18% of unaffected areas. The areas of reduced IPPA uptake were larger than the corresponding areas of reduced thallium uptake. In patients studied before and after infarction, areas of reduced thallium uptake postinfarction were accurately predicted by areas of reduced k_1 preinfarction. The uptake of thallium and the IPPA k_1 were both normalized postrevascularization. These investigators later reported that the uptake of IPPA was compatible with a nondiffusional process mediated by the initial interaction of fatty acid, with the 40-kDa membrane fatty acid binding protein of cardiac endothelium.[76]

Murray et al[77] assessed myocardial viability using IPPA in 15 patients with CHD. All subjects were characterized invasively showing resting LV ejection fractions of <35% and obstructive coronary heart disease, with 7% having single-vessel disease, 20% double-vessel disease, and 73% triple-vessel disease. Forty-two dysfunctional coronary territories were evaluated, including 14 LAD, 14 LCx, and 14 RCA distributions. In this study, high temporal resolution planar IPPA imaging at rest was performed for 25 minutes using a multicrystal camera. All patients were revascularized, and intraoperative myocardial biopsy samples were obtained. Tissue containing >50% fibrosis was considered nonviable. Myocardial IPPA clearance rates for normal controls were 21.0 ± 10%. Clearance rates from 3 to 25 minutes postinjection were reduced to 17 ± 2.3% for biopsy viable segments and to 13.4 ± 2.0% for nonviable segments. IPPA had a sensitivity of 92% and a specificity of 86% for detecting viable tissue. These same investigators also compared multicrystal camera rest IPPA clearance rates with the results of transmural myocardial biopsies and reinjection thallium SPECT.[78] All subjects had ischemic cardiomyopathies (LVEF <35%) and underwent transmyocardial biopsies at the time of coronary artery bypass grafting (CABG), 23% had previous anterior wall and 73% inferior wall infarcts. IPPA and reinjection Tl-201 imaging was performed before surgery. There was agreement in 77% of all myocardial segments with reinjection Tl-201. In all cases of discordance, IPPA showed viability. Infarct location did not affect the results. Significant IPPA accumulation or an IPPA wash-out rate from 3 to 25 minutes of ≥16% identified biopsy-viable myocardium regardless of whether the MI was anterior or inferoposterior. Assessed with either first-pass radionuclide ventriculography, echocardiography, or contrast ventriculography after revascularization, 80% of IPPA viable segments showed improved regional systolic function.

Using IPPA and SPECT imaging, Hansen et al[79] evaluated 23 patients revascularized for ischemic cardiomyopathies. Thirteen patients had a history of prior MI and 10 had ECG Q-waves; 5 patients had one-vessel disease, 10 had two-vessel disease, and 8 had three-vessel disease. The average EF before revascularization was 39 ± 14%. IPPA imaging was performed at rest, and five sequential image sets were obtained beginning 4, 12, 20, 28, and 36 minutes postinjection. Myocardial metabolism was evaluated by fitting regional myocardial IPPA activity to monoexponential curves. The fraction of the left ventricle with retained intermediate metabolism determined from clearance half-times was assessed. Operator-assigned regions of interest permitted analysis of hypoperfused myocardium corresponding to specific coronary territories (Fig 9).[80] A significant correlation was found between initial IPPA uptake and postrevascularization LVEF. The fraction of the left ventricle showing IPPA metabolism in the intermediate metabolic range was higher in patients who had increases in global LV function.

Because radiolabeled fatty acids assess both coronary perfusion and myocardial metabolism, they may be superior to conventional tracers for viability assessments. Prospective outcomes studies to evaluate if regional wall motion, global LV systolic function, and patient prognosis improve after imaging-guided revascularization are of the greatest importance.

Nonischemic cardiomyopathy. Patients with nonischemic cardiomyopathies often show normal or near-normal patterns of myocardial perfusion and severe abnormalities of ventricular wall motion. There is limited information available relating to the abnormalities of myocardial metabolism that occur in patients with congestive heart failure

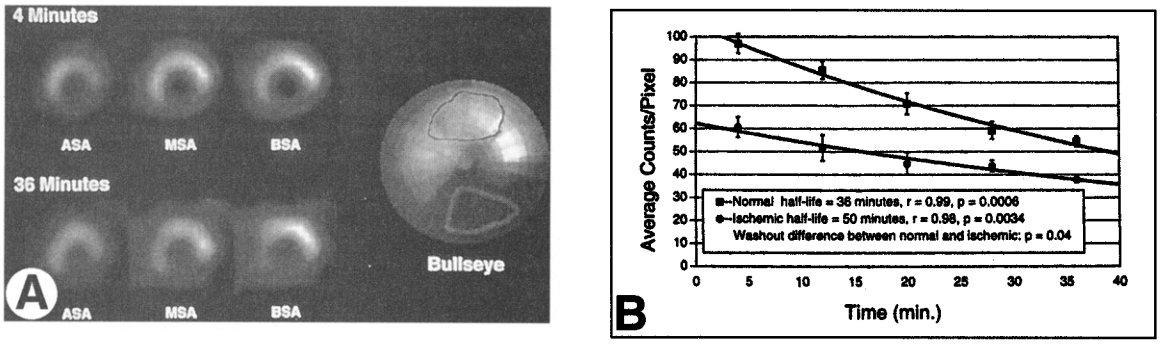

Fig 9. (A) Images from a man who presented with unstable angina and three-vessel CAD. There is moderately decreased activity in the inferolateral wall, which shows relative improvement over time. The bull's-eye plot to the right shows the regions identified as ischemic (black outline) and normal (gray outline). The activity in these regions is plotted in Fig 9B. This patient had inferior hypokinesis which resolved after CABG. (B) Relative activity versus time in ischemic and nonischemic regions from Fig 9A. There is markedly reduced tracer uptake and metabolic activity in the ischemic region. The error bars demonstrate ± 1 SD. (Reprinted by permission of the Society of Nuclear Medicine from: Hansen C. Preliminary report of an ongoing phase I/II dose range, safety and efficacy study of iodine-123-phenyl-pentadecanoic acid for the identification of viable myocardium. *Journal of Nuclear Medicine* 1994;35:38S-42S.)

caused by nonischemic dilated cardiomyopathies.[81,82]

Miche reported the results of dynamic planar imaging with IPPA and thallium-201 after bicycle exercise testing in patients with nonischemic dilated cardiomyopathies.[83] Using quantitative compartmental analysis techniques their group had previously described, they measured IPPA extraction rates.[75] The rate constants for global fatty acid influx they found were significantly higher in patients than controls, $k_1\ min^{-1} = 0.419 \pm 0.096$ versus $k_1\ min^{-1} = 0.39 \pm 0.08$, $P < .05$. There was an inverse correlation between influx rate and measures of global left ventricular function, including cardiac index and ejection fraction ($r = -.9$). The increased influx rates seen in these patients were thought to be related to a compensatory increase in fatty acid metabolism necessary to preserve cellular function in the face of reduced global myocardial perfusion. Although they did report frequent mismatches between myocardial IPPA and thallium uptake, they did not quantify myocardial efflux or β-oxidation.

Ugolini et al[84] performed SPECT imaging with IPPA in 19 patients with nonischemic cardiomyopathies. Imaging was performed 8 and 40 minutes after rest injections. Patients with cardiomyopathies had greater heterogeneity of radiotracer uptake compared with normal controls (27 ± 11% versus 18 ± 5%, $P < .01$), and mean IPPA washout rates were more rapid in cardiomyopathy patients than in normal controls (26 ± 7% versus 18 ± 5%, $P < .01$). Although the severities of IPPA uptake and wash-out abnormalities did not correlate with measures of left ventricular systolic function (ejection fraction), there was a statistically significant positive association between the heterogeneity of IPPA uptake and New York Heart Association functional class ($r = .64$, $P < .01$), but there was no such association between functional class and IPPA washout. Compared with patients with ischemic cardiomyopathies, there was less heterogeneity of tracer distribution in nonischemic patients; ie, severely diminished IPPA uptake did not occur. Patients with ischemic cardiomyopathies had reduced IPPA uptake and wash-out, reflecting impaired beta oxidation. These investigators hypothesized that the elevated levels of circulating catecholamines well known to occur in patients with CHF favor more rapid fatty acid metabolism and wash-out.

The development of IPPA was motivated by the suboptimal imaging characteristics of the radioiodinated alkyl fatty acids, their metabolism, and release of free iodine-123 resulting in a rapid loss of quantifiable image characteristics; tomographic imaging was not feasible. IPPA was a significant improvement over the alkyl fatty acids, providing excellent image quality, and permitting SPECT image acquisition and quantification with estimates of metabolic rates. The rate of IPPA metabolism and clearance is still relatively fast for single-detector SPECT imaging systems. Because of this, an effort was made to develop radiolabeled fatty acid analogue with slowed oxidative metabolism. The methylbranched chain fatty acids reviewed above and the new F-18 thia-heptadecanoic fatty

acid (FTHA) reviewed below resulted from these efforts.

F-18 FLUORO-6-THIA-HEPTADECANOIC ACID

F-18 fluoro-6-thia-heptadecanoic acid (FTHA) is a new radiolabeled fatty acid that may be suitable for PET cardiac imaging. The metabolism of this fatty acid analogs is inhibited by the sulfur heteroatom.[85] The sulfur substitute at the six carbon position allows metabolic trapping and partial metabolism but blocks β-oxidation beyond that point with prolonged cardiac retention.[86] DeGrado et al,[86] in a mouse model, showed rapid blood clearance, avid cardiac uptake (39.8 ± 3.0% injected dose at 5 minutes), and with slow clearance of the tracer label from the heart ($T_{1/2}$, about 2 hours). Further, pretreatment with a carnitine palmitoyl-transferase I inhibitor reduced myocardial uptake by 80% to 90%, proving the importance of trapping and β-oxidation in the myocardial retention of FTHA. These investigators found that the rapid cardiac uptake, excellent target-to-background ratios, and prolonged myocardial retention dependent on metabolic trapping were characteristics suggesting the potential of FTHA as a quantitative PET tracer of myocardial metabolism.

Mäki et al[87] studied patients with stable coronary heart disease using dynamic PET imaging at rest in the fasted state and during euglycemic hyperinsulinemia. Rapid myocardial FTHA uptake was observed in both metabolic states. The fractional myocardial uptake constant K_i was 0.11 ± 0.04 mL/g/min fasted and 0.12 ± 0.03 mL/g/min during insulin clamp, P = NS. The mean myocardial uptake indices decreased by 76% during insulin clamping, 5.8 ± 1.7 μmol/100g/min versus 1.4 ± 0.5 μmol/100g/min ($P < .005$) (Fig 10). As within the heart, the femoral muscle uptake was significantly higher in the fasted state. These investigators concluded that FTHA PET is feasible and provides physiologically reasonable rates of myocardial and skeletal muscle free fatty acid uptake in both the fasted and insulin clamp states.

The basic studies with FTHA suggested the feasibility of its use as a tracer of cardiac fatty acid metabolism. There are only very limited clinical data available regarding the use of FTHA. Schulz et al[88] compared the utility of FTHA to F-18 FDG as a marker of myocardial viability in 21 patients with advanced coronary heart disease and ischemically reduced LV function. Normalized to the region of maximal Tc-99m sestamibi uptake, myocardial

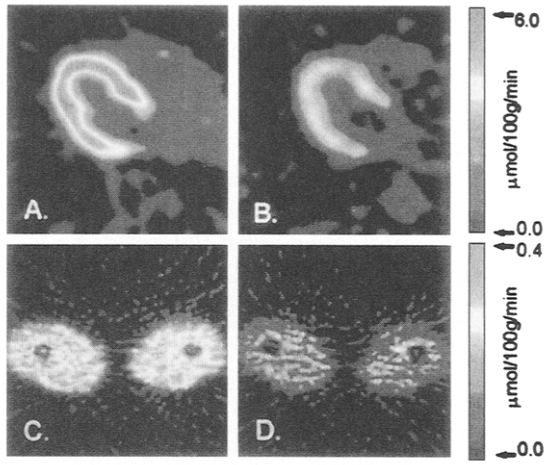

Fig 10. Examples of parametric images measured with FTHA. Midventricular transaxial slices (A, B) and cross-section of femoral region (C, D). Figs A and C were measured in fasting state. Figs B and D were measured during insulin clamp. (Reprinted by permission of the Society of Nuclear Medicine from: Mäki MT, Haaparanta M, Nuutila P, et al. Free fatty acid uptake in the myocardium and skeletal muscle using fluorine-18-fluoro-6-thia-heptadecanoic acid. *Journal of Nuclear Medicine* 1998;39:1320-1327.)

uptakes of FTHA and FDG were analyzed quantitatively. FTHA uptake paralleled that of sestamibi (r = .80) but not FDG (r = .57). Mean regional myocardial uptake in regions of severe hypoperfusion was similar to that of sestamibi (38.1 ± 16.3% and 36.8 ± 9.4, 54.6 ± 25.0%, P = NS), but significantly lower than FDG (54.6 ± 25.0%, $P < .001$). In 52 regions with severely reduced perfusion but preserved glucose metabolism (FDG uptake ≥70%), FTHA uptake was similarly preserved in only 8 regions (43.8 ± 25.0%, $P < .001$). These investigators concluded that FTHA is of limited value in identifying hibernation myocardium, and the underestimation of viability may be caused by dependence of uptake on flow and the suppression of β-oxidation in regions of chronic ischemia. Using the same methodology, this same team of investigators reported the use of FTHA in a patient with left bundle branch block.[89] They found retention of septal FTHA uptake in a patient with severely reduced FDG uptake, and suggested that this finding may be caused by divergent metabolic effects of the alter ventricular conduction resulting from left bundle branch block on myocardial glucose metabolisms (reduced) and fatty acid β-oxidation (preserved).

Although Schulz's[88] report on the use of FTHA in the assessment of myocardial viability was less than encouraging, the potential clinical utility of

FTHA is still unknown. The myocardial uptake and retention of FTHA appear to be similar to those of BMIPP. Considering the very positive reports appearing related to BMIPP, it seems likely that there may be similar results with FTHA. Although the FTHA's fluorine-18 label will limit its use primarily to imaging systems capable of coincidence detection, with the increasing availability of dedicated PET systems and hybrid SPECT/PET systems this will be a diminishing limitation. A tracer such as FTHA could play an important role in metabolic assessments of the heart. At present, the studies of FTHA's clinical utility are far too few and preliminary to know what role it may have in clinical or investigative cardiac imaging.

ACKNOWLEDGMENT

The authors acknowledge and thank Laurie J. Enz and Mary K. Dempsey for their expert secretarial and editorial assistance in the preparation of this manuscript.

REFERENCES

1. Evans J, Gunton R, Baker R, et al: Use of radioiodinated fatty acid for photoscans of the heart. Circ Res 16:1-10, 1965

2. Schelbert H, Henze E, Keen R, et al: C-11 palmitate for the noninvasive evaluation of regional myocardial fatty acid metabolism with positron computed tomography. III. In vivo demonstration of the effects substrate availability on myocardial metabolism. Am Heart J 105:492-504, 1983

3. Robinson G, Lee A: Radioiodinated fatty acids for heart imaging: iodine monochloride addition compared with iodide replacement labeling. J Nucl Med 16:17-21, 1975

4. Poe N, Robinson G, Graham S, et al: Experimental basis for myocadial imaging with 123 I-labeled hexadecanoic acid. J Nucl Med 17:1077-1082, 1976

5. Machulla H, Stoecklin G, Kupfernagel C, et al: Comparative evaluation of fatty acids labeled with C-11, C1-34m, Br-77, and I-123 for metabolic studies of the myocardium: concise communication. J Nucl Med 19:298-302, 1978

6. Machulla H, Marsmann M, Dutschka K: Biochemical concept and synthesis of a radioiodinated phenyl fatty acid to in vivo metabolic studies of the myocardium. Eur J Nucl Med 5:171-173, 1980

7. Goodman M, Kirsch G, Knapp Jr F: Synthesis and evaluation of radioiodinated terminal p-iodophenyl-substituted alpha- and beta-methyl-branched fatty acids. J Med Chem 27:390-397, 1984

8. Knapp F, Goodmann M, Callahan A, et al: Radioiodinated 15-(p-Iodophenyl)-3,3 dimethylpentadecanoic acid: a useful new agent to evaluated myocardial fatty acid uptake. J Nucl Med 27:521-531, 1986

9. Frederickson D, Gordon R: Transport of fatty acids. Physiol Rev 38:585-630, 1958

10. van der Vasse G, Stam H: Lipid and carbohydrate metabolism in the ischemic heart. Basic Res Cardiol 82:149-153, 1987

11. Lehninger A, Nelson D, Cox M: Principles of Biochemistry (ed 2). New York, NY, Worth Publishers, 1993

12. Bing R: Cardiac metabolism. Physiol Rev 45:171-213, 1965

13. Opie L: Metabolism of the heart in health and disease. Part I. Am Heart J 76:685-698, 1968

14. Neely J, Morgan H: Relationship between carbohydrate and lipid metabolism and the energy balance of heart muscle. Ann Rev Physiol 36:413-459, 1974

15. Neely J, Whitmer K, Mochizuki S: Effects of mechanical activity and hormones on myocardial glucose and fatty acid utilization. Circ Res 38:22-29, 1976

16. Liedtke A: Alterations of carbohydrate and lipid metabolism in the acutely ischemic heart. Prog Cardiovasc Dis 23:321-336, 1981

17. Rose C, Goresky C: Constraints on the uptake of labeled palmitate by the heart. The barriers at the capillary and sarcolemmal surfaces and the control of intracellular sequestration. Circ Res 41:534-545, 1977

18. Neely J, Rovetto M, Oram J: Myocardial utilization of carbohydrate and lipids. Prog Cardiovasc Dis 15:289-329, 1972

19. Schelbert H: Blood flow and substrate use in myocardium. Ann Intern Med 98:339-359, 1983

20. Pippin J, Jansen D, Henderson E, et al: Myocardial fatty acid utilization of various workloads in normal volunteers: iodine-123 phenylpentadecanoic acid and single photon emission computed tomography to investigate myocardial metabolism. Am J Cardiac Imaging 6:99-108, 1992

21. Grover-McKay M, Schelbert HR, Schwaiger M, et al: Identification of impaired metabolic reserve by atrial pacing in patients with significant coronary artery stenosis. Circulation 74:281-292, 1986

22. Hudon M, Lyster D, Jamieson W, et al: The metabolism of 15-p-(123I)-iodophenylpentadecanoic acid in a surgically induced canine model of regional ischemia. Eur J Nucl Med 16:199-204, 1990

23. Rosamond TL, Abendschein DR, Sobel B, et al: Metabolic fate of radiolabeled palmitate in ischemic canine myocardium: implications for positron emission tomography. J Nucl Med 28:1322-1329, 1987

24. Poe N, Robinson Jr D, Zielenski F, et al: Myocardial imaging with 123 I heptadecanoic acid. Radiology 124:419-424, 1977

25. Kloster G, Stöcklin G, Smith E, et al: ω-Halofatty acids: a probe for mitochondrial membrane integrity. In vitro investigations in normal and ischaemic myocardium. Eur J Nucl Med 9:305-311, 1984

26. Dudczak R, Kletter K, Frichaut H, et al: The use of I-123 labeled heptadecanoic acid as a metabolic tracer: preliminary report. Eur J Nucl Med 9:81-85, 1984

27. Notohamiprodjo G, Schmid A, Spohr G, et al: Comparison of 11-C-palmitic acid (CPA) and 123-I-heptadecanoic acid (IHA) turnover in human heart. J Nucl Med 26:P88, 1985

28. Freundlieb C, Hoeck A, Vyska K, et al: Myocardial imaging and metabolic studies with (17-123I) iodoheptadecanoic acid. J Nucl Med 21:1043-1050, 1980

29. Fridrich L, Gassner A, Sommer G, et al: Dynamic 123

I-HAD myocardial scintigraphy after aortocoronary bypass grafting. Eur J Nucl Med 12:S24-S26, 1986

30. Visser F, van Eenige M, Westera G, et al: Metabolic fate of radioiodinated heptadecanoic acid in the normal canine heart. Circulation 1985:565-571, 1985

31. Duwel C, Visser F, van Eenige M, et al: Metabolic testing of the heart with lactate and glucose during labeled FFA scintigraphy. Acta Cardiologica 43:111-120, 1988

32. Visser F, van Eenigne M, Duwel C, et al: Radioiodinated free fatty acids; can we measure myocardial metabolism? Eur J Nucl Med 12:520-523, 1986

33. Railton R, Rogers J, Small D, et al: Myocardial scintigraphy with I-123 heptadecanoic acid as a test for coronary heart disease. Eur J Nucl Med 13:63-66, 1987

34. Livni E, Elmaleh D, Levy S, et al: Beta-methyl (1-C-11)heptadecanoic acid: a new myocardial metabolic tracer for positron emission tomography. J Nucl Med 23:169-175, 1982

35. Goodman M, Kirsch G, Knapp Jr F: Synthesis of radioiodinated ω-(p-iodophenyl)-substituted methyl-branched long-chain fatty acids. J Med Chem 27:390-397, 1984

36. Knapp F, Ambrose K, Goodmann M: New radioiodinated methyl-branched fatty acids for cardiac imaging. Eur J Nucl Med 12:S39-S44, 1986

37. Ambrose K, Owen B, Goodman M, et al: Evaluation of the metabolism in rat hearts of two new radioiodinated 3-methyl branched fatty acid myocardial imaging agents. Eur J Nucl Med 12:486-491, 1987

38. Fujibayashi Y, Yonekura Y, Takemura Y, et al: Myocardial accumulation of iodinated beta-methyl branched fatty acid analogue, iodine-125-15-(p-iodophenyl)-3-(R,S,)methylpentadecanoic acid (BMIPP), in relation to ATP conc. J Nucl Med 31:1818-1822, 1990

39. Yamamichi Y, Kusuoka H, Morishita K, et al: Metabolism of iodine-123-BMIPP in perfused rat hearts. J Nucl Med 36:1042-1050, 1995

40. Nohara R, Hosokawa R, Hirai T, et al: Effect of metabolic substrate on BMIPP metabolism in canine myocardium. J Nucl Med 39:1132-1137, 1998

41. Reinhardt CP, Weinstein H, Marcel R, et al: Comparison of iodine-125-BMIPP and thallium-201 in myocardial hypoperfusion. J Nucl Med 36:1645-1653, 1995

42. Hosokawa R, Nohara R, Fujibayashi Y, et al: Myocardial kinetics of iodine-123-BMIPP in canine myocardium after regional ischemia and reperfusion: implications for clinical SPECT. J Nucl Med 38:1857-1863, 1997

43. Dudczak R, Schmoliner R, Angelberger P, et al: Structurally modified fatty acids: clinical potential as tracers of metabolism. Eur J Nucl Med 12:S45-S48, 1986

44. De Geeter F, Franken P, Knapp Jr F, et al: Relationship between blood flow and fatty acid metabolism in subacute myocardial infarction: a study by means of 99mTc-sestamibi and 123I-beta-methyl-iodo-phenyl pentadecanoic acid. Eur J Nucl Med 21:283-291, 1994

45. Matsunari I, Saga T, Junichi T, et al: Kinetics of iodine-123-BMPP in patients with prior myocardial infarction: assessment with dynamic rest and stress images compared with stress thallium-201 SPECT. J Nucl Med 35:1279-1285, 1994

46. Kobayashi H, Kusakabe K, Momose M, et al: Evaluation of myocardial perfusion and fatty acid uptake using a single injection of iodine-123-BMIPP in patients with acute coronary syndromes. J Nucl Med 39:1117-1122, 1998

47. Nakata T, Hashimoto A, Kobayashi H, et al: Outcome significance of thallium-201 and iodine-123-BMIPP perfusion-metabolism mismatch in preinfarction angina. J Nucl Med 39:1492-1499, 1998

48. Kropp J, Likungu J, Kirchhoff P, et al: Single photon emission tomography imaging of myocardial oxidative metabolism with 15-(p-[^{123}I]iodophenyl) pentadecanoic acid in patients with coronary artery disease and aorto-coronary bypass graft surgery. Eur J Nucl Med 18:467-474, 1991

49. Kropp J, Kohler U, Knapp Jr F, et al: 15-(p-[I-123]iodophenyl)-3-R,S-methylpentadecanoic acid to evaluate ischemia in patients with coronary artery disease. Eur J Nucl Med 18:650, 1991 (abstr)

50. Tamaki N, Kawamoto M, Yonekura Y, et al: Regional metabolic abnormality in relation to perfusion and wall motion in patients with myocardial infarction: assessment with emission tomography using an iodinated branched fatty acid analog. J Nucl Med 33:659-667, 1992

51. Franken P, DeGeeter F, Dendale P, et al: Abnormal free fatty acid uptake in subacute myocardial infarction after coronary thrombolysis: correlation with wall motion and inotropic reserve. J Nucl Med 35:1758-1765, 1994

52. Franken P, Demour D, Desadelerr C, et al: Free fatty acid uptake in myocardium with postischemic dysfunction: comparison with dobutamine echocardiography to predict long term functional recovery. J Nucl Med 35:50P, 1994 (abstr)

53. Knapp F, Franken P, Kropp J: Cardiac SPECT with iodine-123-labeled fatty acids: evaluation of myocardial viability with BMIPP. J Nucl Med 36:1022-1030, 1995

54. Dendale P, Franken PR, van der Wall EE, et al: Wall thickening at rest and contractile reserve early after myocardial infarction: correlation with myocardial perfusion and metabolism. Coron Artery Dis 8:259-264, 1997

55. Hambye AS, Dobbeleir A, Franken PR: SPET-generated colour-coded polar maps to quantify 99Tcm-MIBI and 123I-BMIPP uptake in chronically dysfunctional myocardium: comparison with coronary anatomy and wall motion. Nucl Med Commun 18:1135-1147, 1997

56. Sloof GW, Visser FC, Bax JJ, et al: Increased uptake of iodine-123-BMIPP in chronic ischemic heart disease: comparison with fluorine-18-FDG SPECT. J Nucl Med 39:255-260, 1998

57. Fujiwara S, Takeishi Y, Atsumi H, et al: Prediction of functional recovery in acute myocardial infarction: comparison between sestamibi reverse redistribution and sestamibi/BMIPP mismatch [see comments]. J Nucl Cardiol 5:119-127, 1998

58. Yamagishi H, Akioka K, Takagi M, et al: Relation between the kinetics of thallium-201 in myocardial scintigraphy and myocardial metabolism in patients with acute myocardial infarction. Heart 80:28-34, 1998

59. Grover-McKay M, Schwaiger M, Krivokapich J, et al: Regional myocardial blood flow and metabolism at rest in mildly symptomatic patients with hypertrophic cardiomyopathy. J Am Coll Cardiol 13:317-324, 1989

60. Nishmura T, Uehara T, Shimonagata T, et al: Clinical experience of 123-I-BMIPP myocardial infarction and hypertrophic cardiomyopathy. Ann Nucl Med 7:35-40, 1993

61. Morita K, Yanagimoto S, Otsuka N, et al: I-123-BMIPP scintigraphy in seven cases with cardiomyopathy. Ann Nucl Med 7:101-107, 1993

62. Takeishi H, Chiba J, Abe S, et al: Heterogeneous

myocardial distribution of iodine-123 15-(p-iodophenyl)-3-R, S-methylpentadecanoic acid (BMIPP) in patients with hypertrophic cardiomyopathy. Eur J Nucl Med 19:775-782, 1992

63. Kurata C, Tawarahara K, Taguchi T, et al: Myocardial emission computed tomography with iodine-123-labeled beta-methyl-branched fatty acid in patients with hypertrophic cardiomyopathy. J Nucl Med 33:6-13, 1992

64. Tadamura E, Kudoh T, Hattori N, et al: Impairment of BMIPP uptake precedes abnormalities in oxygen and glucose metabolism in hypertrophic cardiomyopathy. J Nucl Med 39:390-396, 1998

65. Reske S, Sauer W, Machulla H, et al: 15-(p-(I-123)phenyl) pentadecanoic acid as a tracer of lipid metabolism. Comparison with 1-C-14 palmitic acid in murine tissues. J Nucl Med 25:1335-1342, 1984

66. Caldwell J, Martin G, Link J, et al: Iodophenylpentadecanoic acid-myocardial blood flow relationship during maximal exercise with coronary occlusion. J Nucl Med 31:99-105, 1990

67. Kulkarni P, Parkey R: A new radioiodination method utilizing organothallium intermediate: radioiodination of phenyl pentadecanoic acid (PPA) for potential applications in myocardial imaging. J Nucl Med 23:105, 1982

68. Chien K, Han A, White J, et al: In vivo esterification of a synthetic 125-I labeled fatty acid into cardiac glycerolipids. Am J Physiol 245:H693-H697, 1983

69. Rellas J, Corbett J, Padmaker K, et al: Iodine-123 Phenylpentadecanoic acid: detection of acute myocardial infarction and injury in dogs using an iodinated fatty acid and single-photon emission tomography. Am J Cardiol 52:1326-1332, 1983

70. Kennedy PL, Corbett JR, Kulkarni PV, et al: Iodine 123-phenylpentadecanoic acid myocardial scintigraphy: usefulness in the identification of myocardial ischemia. Circulation 74:1007-1015, 1986

71. Zimmermann R, Rauch B, Kapp M, et al: Myocardial scintigraphy with iodine-123-phenylpentadecanoic acid and thallium-201 in patients with coronary artery disease: a comparative dual-isotope study. Eur J Nucl Med 19:946-954, 1992

72. Hansen C, Corbett J, Pippen J, et al: Iodine-123 Phenylpentadecanoic acid and single photon emission computed tomography in identifying left ventricular regional metabolic abnormalities in patients with coronary heart disease: comparison with thallium-201 myocardial tomography. J Am Coll Cardiol 12:78-87, 1988

73. Duwel C, Visser F, Eenige M, et al: The influence of lactate and dipyridamole on myocardial fatty acid metabolism in man, traced with I-123-iodoheptadecanoic acid. Nucl Med 29:8-34, 1990

74. Eisenhut M, Lehmann W, Sutterle A: Metabolism of 15-(-(123iodophenyl) pentadecanoic acid in the rat heart: identification of new metabolites by high pressure liquid chromatography and fast atom bombardment mass spectrometry. Nucl Med Biol 6:747-754, 1993

75. Vyska K, Machulla H, Stremmel W, et al: Regional myocardial free fatty acid extraction in normal and ischemic myocardium. Circulation 78:1218-1233, 1988

76. Vyska K, Stremmel W, Notohamiprodjo G, et al: Fatty acid uptake in normal human myocardium. Circ Res 69:857-870, 1991

77. Murray G, Schad N, Ladd W, et al: Metabolic cardiac imaging in severe coronary artery disease: assessment of viability with iodine-123-iodophenylpentadecanoic acid and multicrystal gamma camera and correlation with biopsy. J Nucl Med 33:1269-1277, 1992

78. Murray G, Schad N, Magill L, et al: Myocardial viability assessment with dynamic low-dos iodine-123-Iodophenylpentadecanoic acid metabolic imaging: comparison with myocardial biopsy and reinjection SPECT thallium after myocardial infarction. J Nucl Med 35:43S-48S, 1994

79. Hansen C, Heo J, Oliner C, et al: Prediction of improvement in left ventricular function with iodine-123-IPPA after coronary revascularization. J Nucl Med 36:1987-1993, 1995

80. Hansen C: Preliminary report of an ongoing phase I/II dose range, safety and efficacy study of iodine-123-phenylpentadecanoic acid for the identification of viable myocardium. J Nucl Med 35:38S-42S, 1994

81. Geltman EM, Smith JL, Beecher D, et al: Altered regional myocardial metabolism in congestive cardiomyopathy detected by positron tomography. Am J Med 74:773-785, 1983

82. Geltman E: Metabolic findings in cardiomyopathies, in Marcus ML, Schelbert HR, Skorton DJ, et al (eds): Cardiac Imaging: A Companion to Braunwald's Heart Disease. Philadelphia, PA, Saunders, 1991, pp 1244-1255

83. Miche E, Notohamiprodjo G, Baller D, et al: The significance of free fatty acid extraction in dilated cardiomyopathy. Circulation 88:I-407, 1993

84. Ugolini V, Hansen C, Kulkarni P, et al: Abnormal myocardial fatty acid metabolism in dilated cardiomyopathy detected by iodine-123 phenylpentadecanoic acid and tomographic imaging. Am J Cardiol 62:923-928, 1988

85. Rahman MD, Ziering DL, Mannarelli SJ, et al: Effects of sulfur-containing analogues of stearic acid on growth and fatty acid biosynthesis in the protozoan Crithidia fasciculata. J Med Chem 31:1656-1659, 1988

86. DeGrado TR, Coenen HH, Stocklin G: 14(R,S)-[18F]fluoro-6-thia-heptadecanoic acid (FTHA): evaluation in mouse of a new probe of myocardial utilization of long chain fatty acids. J Nucl Med 32:1888-1896, 1991

87. Mäki MT, Haaparanta M, Nuutila P, et al: Free fatty acid uptake in the myocardium and skeletal muscle using fluorine-18-fluoro-6-thia-heptadecanoic acid. J Nucl Med 39:1320-1327, 1998

88. Schulz G, von Dahl J, Kaiser HJ, et al: Imaging of beta-oxidation by static PET with 14(R,S)-[18F]-fluoro-6-thiaheptadecanoic acid (FTHA) in patients with advanced coronary heart disease: a comparison with 18FDG-PET and 99Tcm-MIBI SPET. Nucl Med Commun 17:1057-1064, 1996

89. Altehoefer C, vom Dahl J, Bares R, et al: Metabolic mismatch of septal beta-oxidation and glucose utilization in left bundle branch block assessed with PET [see comments]. J Nucl Med 36:2056-2059, 1995

The Current Role of Infarct Avid Imaging

Ban-An Khaw

Tc-99m pyrophosphate is the grandfather of infarct avid agents. Its value is its clinical availability and ease of use. However, its shortcomings are the delay of 2 to 3 days for reliable interpretation in nonreperfused myocardial infarction (MI) and the overarching bone activity. Antimyosin provides exquisite specificity for the detection of myocardial necrosis irrespective of the cause of the injury. Therefore, diagnosis of equivocal MI or confirmation of diffuse myocardial necrosis would benefit from the availability of In-111 labeled antimyosin Fab. The drawback of antimyosin, like that of Tc-99m pyrophosphate, is the delay, in this case because of the protracted blood clearance of the antibody protein macromolecules. Tc-99m glucaric acid, on the other hand, may fulfill the original role envisioned for antimyosin, which was to enable early, rapid diagnosis of acute MI. However, the window for the use of Tc-99m glucaric acid appears to be limited to within the first day of the acute event. Therefore, there is a potential use of both Tc-99m glucaric acid and In-111 antimyosin in tandem with Tc-99m glucaric acid, which would not only facilitate early detection and diagnosis of acute MI and diagnosis of equivocal MI, but also may permit stratification of the infarct age.

AMONG THE approximately 8 million annual emergency room visits associated with various forms of chest pain in the United States,[1] only 1.5 million will be diagnosed as acute myocardial infarction (MI). Confirmation of acute MI is relatively easy using the classical clinical symptoms, electrocardiogram, and serum enzyme assessments. However, approximately one third to one fourth will be missed by the existing traditional diagnostic methods.[2] Furthermore, the window for maximal patient benefit from thrombolytic therapy is within the first 6 hours of chest pain. Therefore, requirement of an infarct avid imaging agent should include speed and accuracy.

Currently, there are no FDA-approved infarct avid imaging agents that are useful for diagnosing acute MI within the time frame necessary to direct decisions for early thrombolytic therapy to achieve maximal myocardial salvage. Although myocardial perfusion agents may permit early diagnosis of acute MI,[3-5] they cannot reliably differentiate reversibly ischemic but viable myocardium from irreversibly compromised myocardium, nor can perfusion agents distinguish a fresh infarct from scar tissues of an old infarct. Infarct avid imaging techniques, however,[6-8] may allow early diagnosis within 4 to 6 hours of the onset of chest pain.

Among the many infarct-avid imaging agents that have been proposed, three stand apart; technetium-99m (Tc-99m) labeled pyrophosphate,[6,9-11] indium-111 (In-111) labeled antimyosin,[7,12-14] and Tc-99m labeled glucaric acid.[15,16] Tc-99m pyrophosphate has been on the market for over 2 decades. In-111 antimyosin was recently approved by the FDA for commercial marketing, however, the FDA-approved indication restricts its use only to ischemic disease indications. The last reagent, Tc-99m glucarate, is still in its initial clinical trial stages.[17] The current role of each reagent in infarct avid imaging will be presented in chronological order.

Tc-99m PYROPHOSPHATE

Tc-99m pyrophosphate was initially developed for diagnosis of bone lesions. It was serendipitously observed to localize in acute myocardial infarction. The mechanism of localization of Tc-99m pyrophosphate is believed to be binding to hydroxyapatite. Buja et al[18] observed that the quantity of Tc-99m pyrophosphate binding to the necrotic myocardium correlated with the amount of calcium deposited in the tissue.[18] However, Dewanjee and Kahn[19] found that Tc-99m pyrophosphate localization occurred primarily in the cytosolic fraction and that hydroxyapatite was not the primary target. Irrespective of the exact mechanism of localization of Tc-99m pyrophosphate, experimental and clinical reports affirm that this radiopharmaceutical localizes in infarcted[9-11] or severely injured myocardium.[20,21] Optimal localization of Tc-99m pyrophosphate in the infarcted myocardium occurs 1 to 5 days after the acute coronary event.[22]

From the Center for Cardiovascular Targeting, Bouvé College of Health Sciences, Department of Pharmaceutical Sciences, Northeastern University, and the Department of Radiology and The Cardiac Unit, Massachusetts General Hospital, and Harvard Medical School, Boston.

Address reprint requests to Ban-An Khaw, PhD, the Center for Cardiovascular Targeting, Department of Pharm. Sci., Bouvé College of Health Sciences, Northeastern University, Boston, MA 02115.

0001-2998/99/2903-0005$10.00/0

Nonreperfused infarcts were not visualized by gamma imaging with Tc-99m pyrophosphate on day 1 by Kondo et al,[23] when the radiotracer was injected 5 to 8 hours after the onset of acute MI. These same patients re-imaged at 22 to 57.7 hours showed infarct visualization in 5 out of the 6 patients with persistent coronary artery occlusion. On the other hand, in reperfused MI patients, visualization of the infarcts was possible in 19 out of 22 patients within the first day. In these 19 patients, Tc-99m pyrophosphate uptake averaged only 2.42 ± 0.61 on a scale of 0 to 4, where 2 was considered normal. Nevertheless, the use of Tc-99m pyrophosphate for diagnosis of acute MI at 2 to 3 days is well established (Fig 1).

Whether Tc-99m pyrophosphate is specific for the delineation of irreversibly damaged myocardium however, is not certain. Tc-99m pyrophosphate has been observed to be sequestered by viable but severely injured myocardium.[20,21] It is also taken up in patients with stable angina without clinical evidence of myocardial necrosis,[24] in patients with unstable angina,[25] and in patients several months[26] to 1 year[27] after the acute event. Protracted Tc-99m pyrophosphate uptake in these cardiovascular disorders suggests that there might be ongoing myocyte cell death, or alternatively, that pyrophosphate binds to both severely ischemic as well as necrotic myocardium. Because elevation of intracellular calcium is a common denominator in both ischemic and infarcted myocardium,[28] localization of Tc-99m pyrophosphate in severely ischemic and infarcted myocardium is a distinct possibility.

Regardless of the exact mechanism of Tc-99m pyrophosphate localization, if this reagent can delineate severely ischemic or necrotic myocardium very acutely such that the attending physicians can reach an unequivocal diagnostic endpoint early, pyrophosphate would be extremely useful. As it is, pyrophosphate is a useful early infarct avid radiopharmaceutical agent only in reperfused MI. In nonreperfused infarcts, Tc-99m pyrophosphate is useful as a confirmatory diagnostic reagent 2 to 3 days after the acute event. Even though Tc-99m pyrophosphate is very easy to use and requires only a delay of 2 to 3 hours after intravenous (IV) administration for image acquisition, its disadvantage resides in the inability to delineate the infarcted myocardium very acutely before reperfusion. Therefore, in the acute phase, the use of Tc-99m pyrophosphate is most appropriate for confirmation of successful thrombolytic therapy.

ANTIMYOSIN ANTIBODIES

Although oncological applications of antibodies dominate the field of immunoscintigraphy, antimyosin antibody has led the way in nononcological applications. In vivo targeting of canine acute MI with polyclonal antimyosin antibody was first reported in 1976.[29] $F(ab')_2$ fragments labeled with Iodine-125 (I-125) were used to show the feasibility of targeting acute MI in vivo.[29] In vivo gamma imaging of experimental acute MI with antimyosin $F(ab')_2$ labeled with Iodine-131 (I-131) was accomplished 2 years later.[30]

Preclinical Studies

Localization of antimyosin antibody in the necrotic (oncotic) myocardium is based on the hypothesis that normal myocardial cells with intact cell

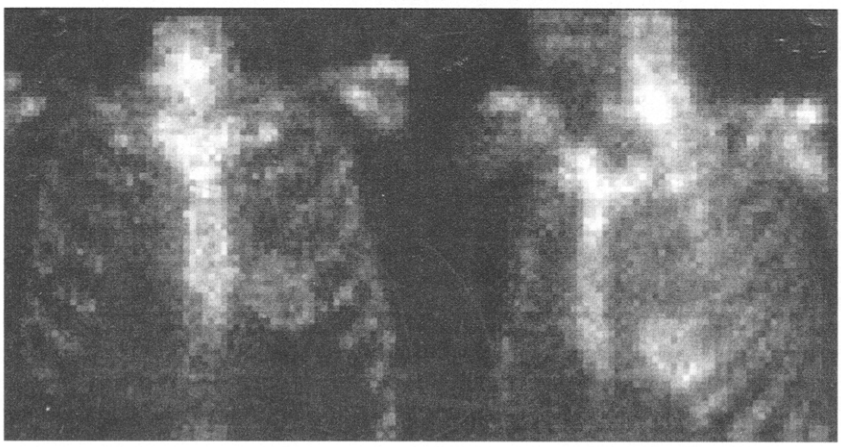

Fig 1. Anterior and left anterior oblique gamma image of a patient with reperfused acute MI injected with Tc-99m pyrophosphate on day 3. The images were obtained 3 hours after IV administration of the radiotracer. Myocardial activity is clearly discerned separate from the bone activity.

membrane will prevent extracellular macromolecules from entering the cell. Necrotic myocardial cells with cell membrane disruption can no longer prevent the influx of extracellular macromolecules or the egress of intracellular components. Therefore, an antibody specific for an intracellular cardiac protein that is insoluble in physiological fluids should be able to enter the cardiac cells with cell membrane disruption and bind to the homologous antigen. Because myosin is an insoluble component of the contractile myofibrils, it will not be washed out of the necrotic cells.[29] If a specific antibody such as antimyosin antibody were introduced into the extracellular milieu, the antibody should be able to bind with the now-exposed cardiac myosin. If the antimyosin antibody were appropriately radiolabeled, then one should be able to image the regions of cell membrane disruption.[31]

Radiolabeled antimyosin antibody (Fig 2A) was observed to be highly specific for the delineation of the necrotic myocardium whereas similarly radiolabeled nonspecific immunoglobulin G (IgG) Fab was not able to delineate the infarcted myocardium (Fig 2B).[32] Furthermore, when radiolabeled specific antimyosin Fab was injected into sham-operated noninfarcted dogs, myocardial targeting of the radioactivity was not observed. Such exquisite specificity of radiolabeled antimyosin antibody for the necrotic myocardium was moreover documented by showing that high affinity of antimyosin antibodies is a necessary condition for the successful in vivo visualization of the infarcts. By using Fab fragments of three monoclonal antimyosin antibodies with different apparent affinities: R11D10 ($Ka = 1.5 - 2.5 \times 10^9$ L/mol), 2G42D5 ($Ka = 3 \times 10^9$ L/mol), and 3H31E6 ($Ka = 3 - 6 \times 10^5$ L/mol),[32] we were able to show that experimental MI could not be visualized with radiolabeled antimyosin Fab with the lowest affinity (Fig 3A). Yet the remaining two antimyosin Fabs with similar high affinities easily delineated the infarcts that were visualized by gamma imaging (Figs 3B and 3C). Infarct (I) to blood (B) activity ratios from computer planimetry of the gamma images of dogs with acute MI injected with high- or low-affinity antimyosin Fabs showed that both high-affinity antimyosin antibodies had similar mean I-B ratios (1.501 ± 0.267, and 1.701 ± 0.376, P = NS). These mean I-B ratios were significantly higher than the mean I-B ratio of the low-affinity antimyosin Fab (0.85 ± 0.115, $P < .0001$), which was similar to

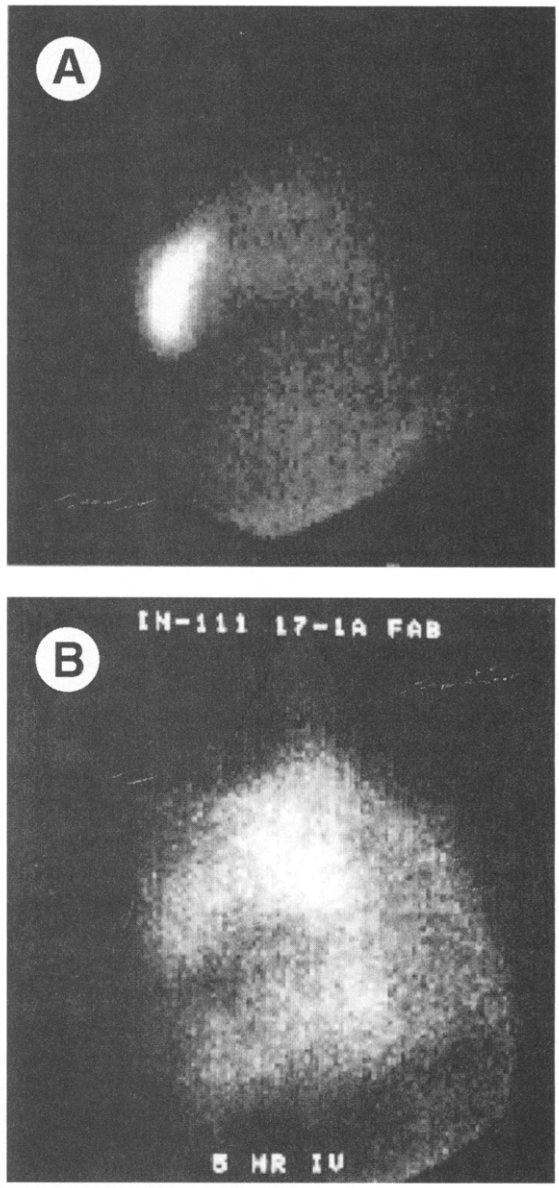

Fig 2. (A) Left lateral gamma image of a dog with acute experimental MI imaged with radiolabeled monoclonal antimyosin Fab. The image was obtained 5 hours after administration of the radiolabeled antimyosin Fab. (B) Left lateral gamma image of a dog with acute experimental MI injected with In-111 labeled nonspecific antibody Fab. Image was acquired also at 5 hours after IV administration. The heart is not visualized. (Reprinted with permission.[32])

that of nonspecific control Fab (0.7605 ± 0.0148).[32] Therefore, specificity of antimyosin antibodies alone is not a sufficient condition for successful in vivo gamma imaging of acute MI. Sufficient, high affinity is also a necessary condition.

Although specificity and sufficiently high affin-

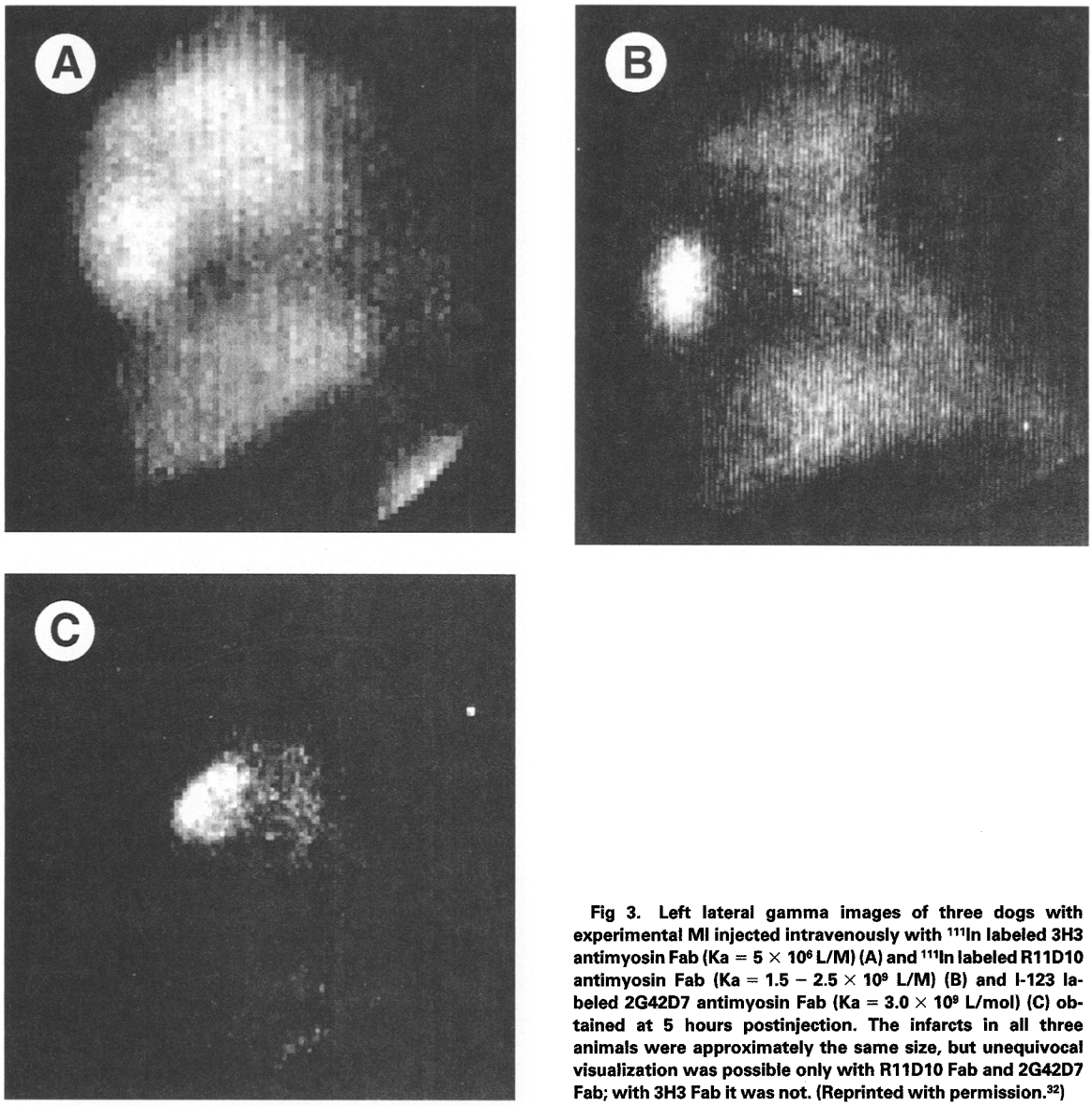

Fig 3. Left lateral gamma images of three dogs with experimental MI injected intravenously with ^{111}In labeled 3H3 antimyosin Fab (Ka = 5 × 10^6 L/M) (A) and ^{111}In labeled R11D10 antimyosin Fab (Ka = 1.5 − 2.5 × 10^9 L/M) (B) and I-123 labeled 2G42D7 antimyosin Fab (Ka = 3.0 × 10^9 L/mol) (C) obtained at 5 hours postinjection. The infarcts in all three animals were approximately the same size, but unequivocal visualization was possible only with R11D10 Fab and 2G42D7 Fab; with 3H3 Fab it was not. (Reprinted with permission.[32])

ity have been established as necessary and sufficient conditions, it remains to be established that development of cell membrane lesions is also an absolute requirement that enables the antibody to recognize and bind to the intracellular cardiac myosin. Because in vivo demonstration of this would be very difficult, in vitro experiments were devised. Hypoxic neonatal murine myocytes in primary cultures, treated with antimyosin antibody attached covalently to 1-μm diameter polystyrene beads, showed attachment of these beads to myofilaments through lesions in the cell membrane (Fig 4B).[33] Normal myocytes with intact sarcolemma prevented accumulation of these antimyosin beads (Fig 4A). Higher magnification of the necrotic cells, at 100,000×, enabled visualization of the binding of the antimyosin beads to the myofilaments containing cardiac myosin (Fig 4C). Therefore, both in vivo and in vitro studies showed the specificity of antimyosin antibody for delineation of myocardial cells with cell membrane disruption that translated into a very specific diagnostic method for identification of irreversibly injured myocardium.

Although the specificity of antimyosin for delineation of the necrotic myocardium has been estab-

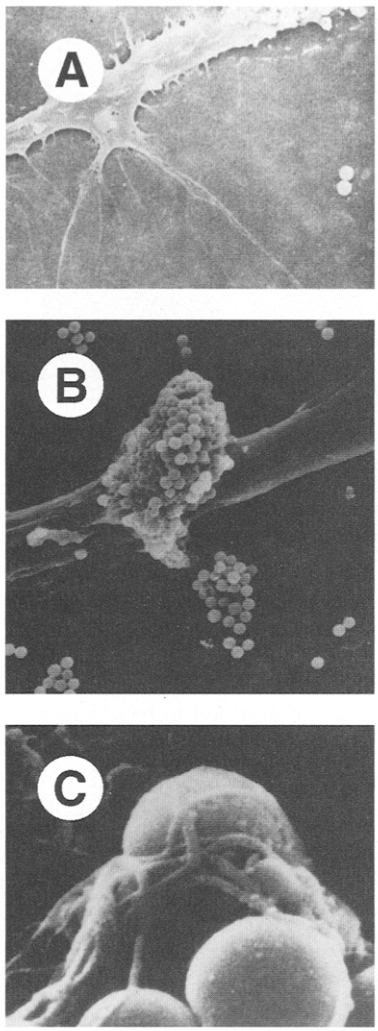

Fig 4. Scanning electron micrographs of murine neonatal primary myocytes in culture treated with antimyosin-linked 1-μ-diameter fluorescent polystyrene beads. (A) A normal myocyte showing the intact cell membrane and a lack of antimyosin-bead binding. (B) A necrotic myocyte with a region of sarcolemmal disruption showing antimyosin-bead binding in that region. (C) 100,000× magnification showing binding of antimyosin beads with myofilaments containing myosin. (Reprinted with permission from Khaw BA, Scott J, Fallon JT, et al: Myocardial injury: quantitation by cell sorting initiated with anti-myosin fluorescent spheres. Science 217: 1050-1053, 1982. Copyright 1982 American Association for the Advancement of Science.)

lished as discussed above, its relationship to other independent radiopharmaceutical parameters for cardiac imaging needs to be addressed. Because antimyosin is an infarct avid agent and the perfusion markers are cold spot agents, there appears to be an inverse relation between antimyosin uptake and either Tl-201 distribution or sestamibi distribution in experimental acute MI.[34,35] The distribution of radiolabeled antimyosin to radiolabeled microsphere regional myocardial blood flow shows an inverse exponential relationship.[31] The microsphere regional myocardial blood flow data indicate that as myocardial perfusion drops below a critical level, myocardial damage is initiated and that antimyosin targeting begins to occur. Above that critical level of perfusion, the cardiocytes may be compromised but membrane disruption may not have ensued. No antimyosin localization is expected or observed in these myocardial regions. Therefore, antimyosin positivity is an indicator of myocardial cell death and not an indicator of an ischemic episode.

Clinical Studies

Based on the premise that localization of radiolabeled monoclonal antimyosin Fab in patients reflects acute MI, studies have been undertaken in patients who have and who have not received thrombolytic therapy. In most studies, the interpretation of the antimyosin gamma images is quite simple if the images are obtained 18 to 24 hours after IV administration. The radioactivity is localized to discrete regions corresponding to the territories of the involved coronary vessels (Fig 5). Myocardial infarcts with and without successful thrombolytic therapy also showed almost equal radiotracer uptake.[13] However, reduced tracer uptake has been observed by Johnson et al[36] in MI patients having no collateral circulation. Another problematic area is in the interpretation of antimyosin images of patients with minimal myocardial injury. The presence of residual blood pool activity even at 24 hours may be construed as myocardial in origin. In such a case, re-imaging at 48 hours usually resolves the dilemma[13] (Fig 6).

Clinical studies have reported a sensitivity of antimyosin for diagnosis of Q-wave acute MI with antimyosin Fab to be between 87% and 98%.[13,37-40] In a multicenter trial of 50 patients, Johnson et al[41] reported positive antimyosin delineation of the infarcts in 46 patients (sensitivity 92%). In a larger phase III trial of 492 patients, undertaken at 26 centers,[42] 190 of 202 patients (94% sensitivity) with Q-wave MI were positive by antimyosin imaging and 48 of 57 patients (84% sensitivity) with non–Q-wave MI. A specificity of 93% was reported in patients with chest pain but no clinical evidence of infarction. Specificity of In-111 anti-

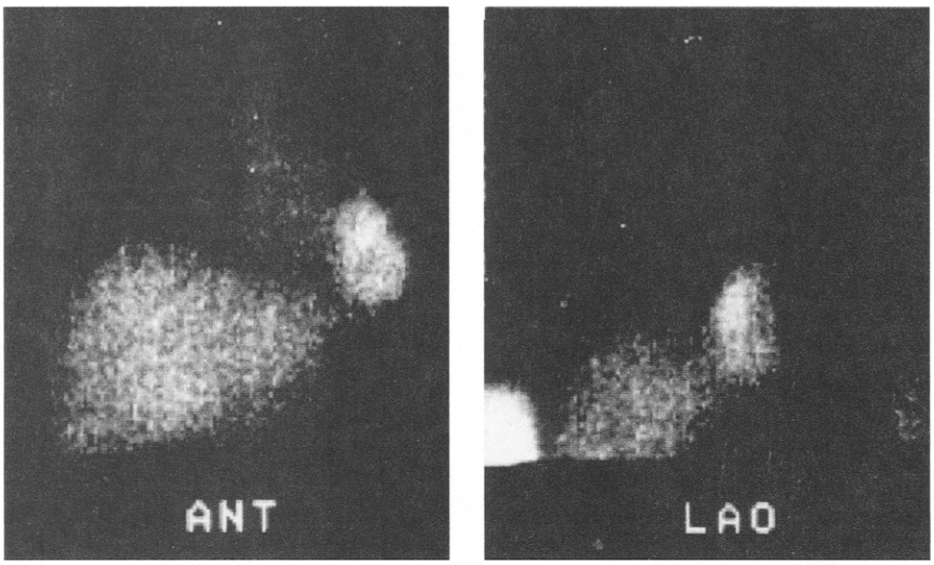

Fig 5. Anterior and 45° LAO images of a patient with anterior MI. The images were obtained 24 hours after IV administration of In-111 labeled antimyosin Fab. Note the cardiac activity clearly separate from liver activity.

myosin antibody imaging for detection of acute MI was further shown by Jain et al[43,44] and Hendel et al[45] in case reports of antemortem confirmation of antimyosin infarct delineation to the postmortem histochemically and histologically demarcated infarction (Figs 7A to 7C).

Because of the high sensitivity and specificity of antimyosin imaging for diagnosis of acute MI, the agent is highly useful for definitive diagnosis of equivocal MI. In a study by Jain et al,[46] 75 patients with suspected acute MI were admitted into the protocol. Seven of 75 had no electrocardiograph (ECG) changes diagnostic of acute MI. However, all 7 were positive for presence of myocardial necrosis by antimyosin imaging criteria. Figure 8 shows one such example where the diagnosis was equivocal by ECG and serum enzyme methods and the patient was diagnosed to have had an MI only after antimyosin imaging.

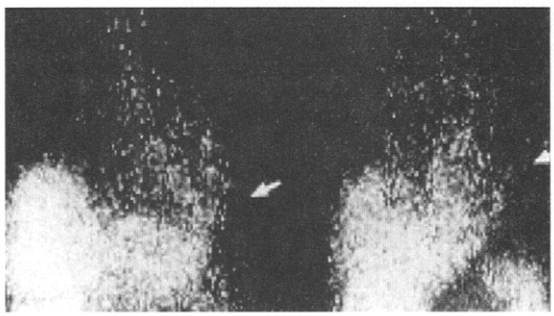

Fig 6. Anterior and LAO 45° gamma images of a patient with minimal myocardial injury in the anterior myocardium visualizable only at 48 hours after IV administration of In-111 antimyosin Fab. Arrows point to patchy myocardial activities.

Because of the specificity and sensitivity of antimyosin immunoscintigraphy for detection of acute myocardial necrosis, antimyosin also has been used for the detection of right ventricular (RV) infarction. RV infarction is reported to occur in up to 50% of patients dying of inferior wall MI. Because diagnosis of RV infarction is difficult unless RV dysfunction occurs from extensive RV damage, or ST-segment elevation occurs in RV precordial leads, use of Tc-99m labeled pyrophosphate scintigraphy has been recommended. Tc-99m pyrophosphate imaging may confirm presence of RV infarction, but a negative pyrophosphate scan does not necessarily exclude diagnosis of RV MI.[47] Johnson et al[48] studied 34 patients with posteroinferior MI with simultaneous In-111 antimyosin and Tl-201 imaging by single photon emission tomography (SPECT). RV MI was detected in 12 patients, only 3 of whom had ECG evidence of RV MI. In one patient, diagnosis of RV MI was made solely on the basis of the antimyosin scans. This patient was misdiagnosed with an anterior wall ischemia caused by ST-segment elevation in leads V1-3.

Despite the high sensitivity and specificity of antimyosin imaging for acute MI, the delay of 12 to 24 hours between radiotracer administration and unequivocal diagnostic image acquisition poses the

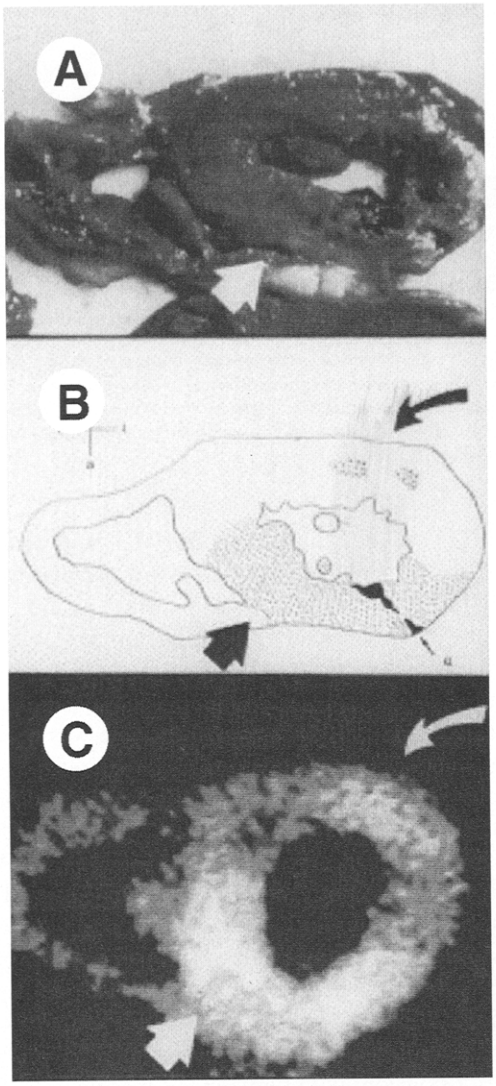

Fig 7. Slice of the heart (A) showing anterior wall infarction (*arrow*) with rupture of the free anterior wall, schematic representation of the histologically identified region of infarction (B), and the gamma image of the above slice showing antimyosin delineation of the infarct (C). (Reprinted with permission.[43])

most serious obstacle for routine use of antimyosin. This delay is partly the result of a protracted blood pool clearance that impedes its use in very acute MI. This delay places the diagnostic time outside the window for maximal patient benefit from thrombolytic therapy. On the other hand, if a qualitative diagnostic end-point is the desired result, infarcts may be detected earlier than 18 to 24 hours. Infarcts can be visualized over and above the blood pool activity anywhere from 6 to 14 hours after IV administration of antimyosin (Fig 9).

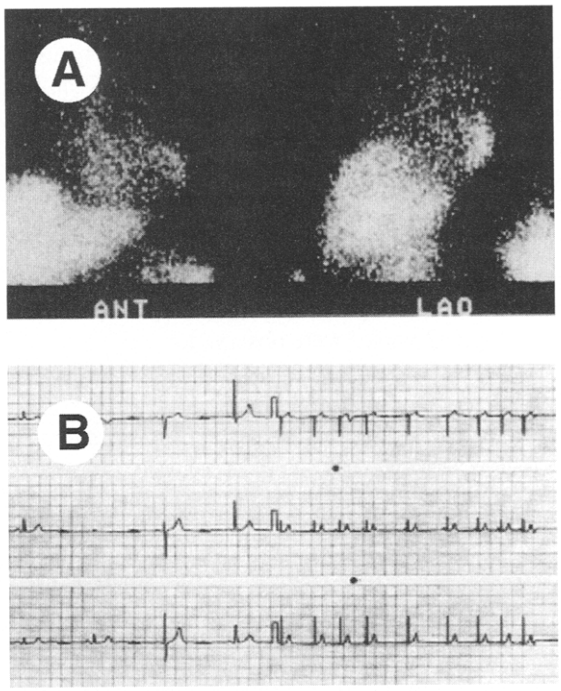

Fig 8. (A and B) Anterior and LAO images of a patient with equivocal MI as seen in the ECG. Antimyosin images showed posterior localization of the radioactivity especially in the LAO view indicating a posterior MI. The heart can be identified in spite of extensive liver activity.

Another potential application of antimyosin imaging is in the diagnosis of postoperative MI.[49] Five percent of patients undergoing coronary bypass surgery develop postoperative MI based on the appearance of new Q-waves, and 40% have ST-T changes.[50] Bulkley and Hutchins[51] observed that among 58 patients who died within 30 days after coronary bypass surgery, 48 patients had evidence of subendocardial contraction band necrosis in the

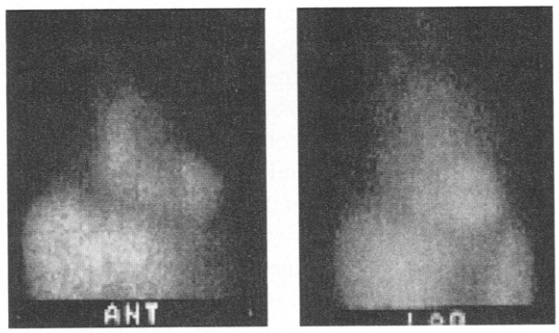

Fig 9. Anterior and LAO images of a patient with anteroapical MI obtained 13 hours after IV administration. Although there is still substantial myocardial blood pool activity, activity localizing to the anteroapical region in the anterior gamma image can be discerned.

areas of the patent bypass grafts. Therefore, antimyosin may provide a diagnostic means early after the surgery when serum enzymes and ECG can be equivocal. Antimyosin scintigraphy was performed by van Vlies et al[49] on 23 stable angina patients who underwent coronary bypass surgery and who had no history of MI. Antimyosin uptake was observed in 19 patients, diffuse uptake in 7, and localized uptake in 12. Although 14 of the 19 patients had ST segment changes, no postoperative pathologic Q-waves were observed.

Thus, it appears that In-111 antimyosin antibody is highly specific for delineation of irreversibly injured myocardium, and has a sensitivity averaging 95%. However, as an agent for early diagnosis of acute MI for directing thrombolytic therapy, this agent does not appear to be adequate. Because thrombolytic therapy is most effective if initiated during the first 6 hours of chest pain, a delay of 6 to 7 hours to obtain a rule-in diagnosis may not be appropriate, especially in light of the importance of initiating thrombolytic therapy as early as possible after symptom onset.[52,53] Therefore, an agent that can delineate the infarcted myocardium within a few hours after IV administration, so that images can be used to direct thrombolytic therapy and postthrombolytic care, would be highly desirable.

Tc-99m GLUCARATE

Glucaric acid is a natural six-carbon dicarboxylic acid sugar that is found in high concentrations in certain green vegetables and can be labeled with Tc-99m.[52] It was developed by Pak et al[54] as a transchelator for radiolabeling Fab′ fragments with Tc-99m. Serendipitously, it was observed that Tc-99m labeled glucaric acid localized in reperfused canine experimental myocardial infarcts within minutes after IV administration[55] (Fig 10). Glucaric acid, being a small molecule with a molecular weight of 210 d, clears from the blood with a very short $T_{1/2}$. This may permit the development of a target-to-background ratio that enables early visualization. The preliminary results of Fornet et al[8] suggested that Tc-99m glucaric acid might identify both zones of reversible and irreversible myocardial injury. However, subsequent studies by Orlandi et al[16] as well as by us,[56] established unequivocally that Tc-99m glucarate is not sequestered by the ischemic tissues. Orlandi et al[16] reported that 20 minutes of ischemia (no triphenyl tetrazolium chloride [TTC] infarction) in dogs did not cause Tc-99m glucarate localization. This was confirmed additionally by Narula et al[56] using 5 and 15 minutes of left anterior descending coronary artery (LAD) occlusion in a rabbit model of ischemia.

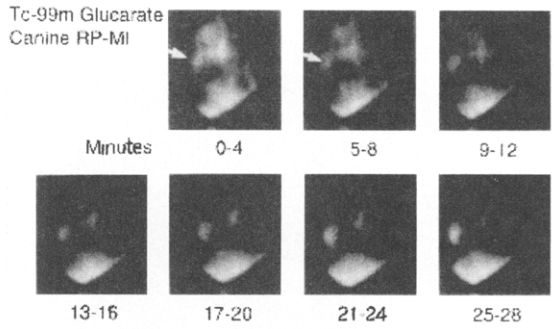

Fig 10. Serial left lateral gamma images of a dog with acute MI injected intravenously with Tc-99m glucarate. The infarct can be visualized as early as 4 to 8 minutes (*arrows*) after IV administration of the radiotracer. (Reprinted with permission.[55])

In the canine reperfused MI model reported by Orlandi et al,[16] Tc-99m glucarate uptake was positive as early as 3 hours of reperfusion, and was significantly higher at 48 hours, but no uptake was seen at 10 days. We were able to visualize canine reperfused acute MI within 4 to 10 minutes after IV administration of Tc-99m glucarate[55] (Fig 10). Visualization of nonreperfused rabbit infarcts required about a 1-hour delay, whereas reperfused rabbit infarcts were visualized within 30 minutes. In nonreperfused acute MI in rats, optimal uptake occurred acutely at 4 hours of persistent coronary artery occlusion, with diminishing localization after 24 hours and no localization of Tc-99m glucarate at 75 hours and 7 days.[57] These studies all indicate that glucarate may be useful as an acute diagnostic reagent in reperfused as well as nonreperfused acute MI.

In another study, Yaoito et al,[58] compared Tc-99m glucaric acid uptake with tritiated deoxyglucose uptake in acute MI and multiple episodes of ischemia in rabbits. In the multiple-episode model of ischemia in which the LAD was occluded for 20 minutes followed by 5 minutes of reperfusion 3 times, uptake ratios of Tc-99m glucaric acid and ^{3}H-deoxyglucose in the normal myocardium, surrounding margin, and the center of the ischemic myocardium were similar, whereas in the infarcted myocardium, the Tc-99m glucaric acid activity in the infarct center was the greatest. ^{3}H-deoxyglu-

cose uptake in the infarct center was similar to, but less than, that in the margin of the infarct. Although Tc-99m glucaric acid accumulated in mildly damaged myocardium, only severe myocardial injury could be visualized by in vivo imaging at 1 hour after IV administration. Therefore, it appears that only infarcts could be visualized by gamma imaging, whereas tissue counting could show areas of slight radiotracer uptake in the ischemic zones. Whether this increase in Tc-99m glucaric acid radiotracer uptake in the ischemic zone is attributable to the presence of microcenters of necrosis is not currently known.

Recently, Narula et al[56] reported that Tc-99m glucarate can be used for hyperacute localization and visualization of experimental MI in reperfused and nonreperfused rabbit infarct models.[56] When uptake of Tc-99m glucarate and In-111 antimyosin Fab, administered simultaneously into rabbits with acute MI, were compared, a direct correlation was obtained in either nonreperfused or reperfused infarcts. Target to nontarget ratios of Tc-99m glucarate were substantially higher than the corresponding In-111 antimyosin Fab (AM-Fab) uptake ratios in the same tissue samples.[56] This difference was more pronounced in nonreperfused MI. When uptake ratios of Tc-99m glucarate were compared with In-111 AM-Fab uptake ratios in the canine reperfused MI model, a direct correlation also was obtained ($r^2 = 0.98$).[55] Because antimyosin is highly specific for delineation of myocardial necrosis, and a direct correlation is obtained between Tc-99m glucarate and In-111 antimyosin Fab, the former must also delineate acute myocardial necrosis. The correlation coefficient of almost 1 (0.98) strongly supports the theory that the two infarct avid agents must be delineating the same infarcted tissues. However, Tc-99m glucarate generated higher target to nontarget ratios than In-111 antimyosin Fab within the same time period. Therefore, visualization of the infarct should occur faster with Tc-99m glucarate than with In-111 AM-Fab. Figure 11 shows that Tc-99m glucaric acid already delineated the infarct as early as 30 minutes after radiotracer administration, whereas the simultaneously administered In-111 AM-Fab showed only blood pool activity at the same time. By 5 hours, both radiotracers showed infarct delineation in canine reperfused MI.[56]

The mechanism for the necrotic tissue specificity of Tc-99m labeled glucarate is attributable to its affinity for targeting the histone of the necrotic myocytes.[56] When the radioactivity from the infarcted tissues at 1 and 3 hours after IV administration of Tc-99m glucarate was fractionated into

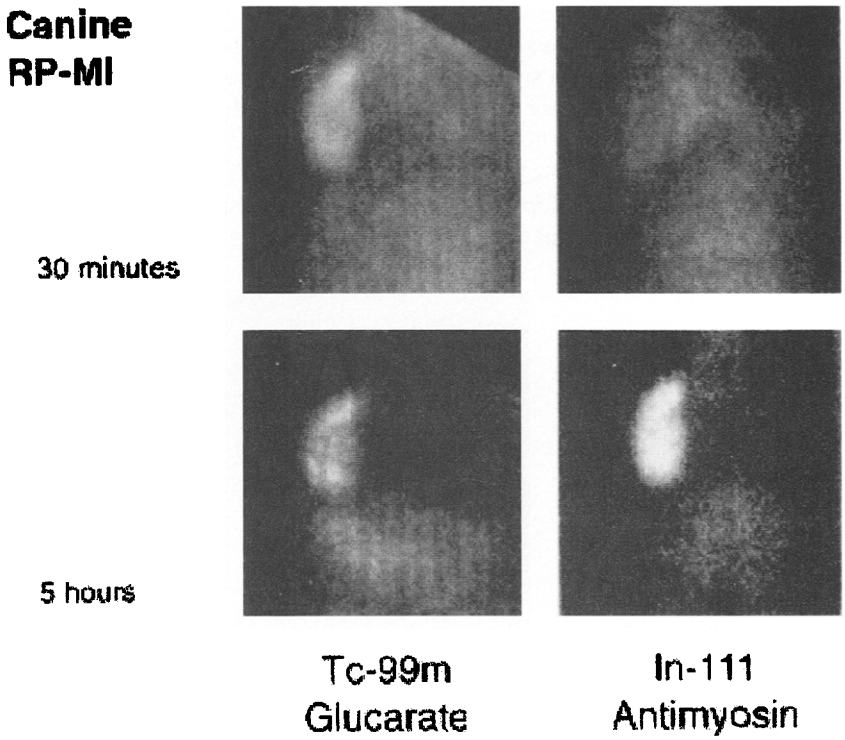

Fig 11. (A) Left lateral gamma images of a dog with reperfused MI imaged at 30 minutes after IV administration of Tc-99m glucarate (*left top panel*) and the corresponding In-111 antimyosin image (*right top panel*). By 5 hours after radiotracer administration, the infarct delineated by both Tc-99m glucarate and In-111 antimyosin is the same. (Reprinted with permission.[55])

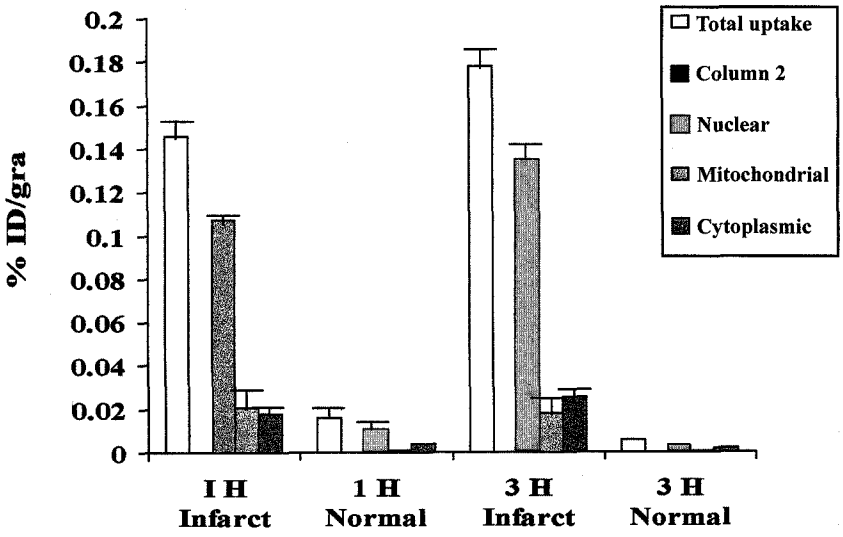

Fig 12. Subcellular distribution of Tc-99m glucarate activity in the infarcted rabbit myocardium at 1 and 3 hours after IV administration of the radiotracer. Total uptake as well as activities in the nuclear, mitochondrial, and cytoplasmic fractions are shown. Greater than 75% of the total infarct activity was associated with nuclear fraction.

nuclear, mitochondrial, and cytosolic fractions, >75% of the infarct activity was associated with the nuclear fraction (Fig 12). Further fractionation of the nuclear activity into nucleoproteins and DNA showed that the predominant radioactivity was associated with the nucleoproteins that consisted primarily of histones. Therefore, it appears that when acute myocardial necrosis occurs, the nucleohistones become accessible to Tc-99m glucaric acid. The initial entry of Tc-99m glucaric acid into the infarct zone appears to be via collateral circulation and/or diffusion. However, the highly basic nucleohistones may act as a sink for concentrating the acidic glucaric acid once the integrity of the sarcolemma has been lost. This high avidity for the nucleohistones together with the fast blood clearance should allow development of target-to-background ratios that permit early visualization of the infarcted myocardium. This very acute localization capability of Tc-99m glucarate also has been seen in patients. Figure 13 shows the anterior and LAO images of a patient who underwent successful thrombolysis within 3.5 hours of chest pain. Tc-99m glucaric acid was administered at 4.5 hours.[59] Studies from Europe have shown that hyperacute visualization of acute MI is feasible with Tc-99m glucaric acid. Large MIs can be visualized earlier than small MIs, but Mariani et al[59] observed that small nonreperfused MI may be visualized within 3 hours of IV administration of this reagent. It appears that Tc-99m glucaric acid is highly specific for acute MI but not for MI older than 2 to 3 days. This observation is consistent with the avidity of Tc-99m glucarate for the nucleoproteins because it appears that at 2 to 3 days, the targets of Tc-99m glucarate may no longer be present because of

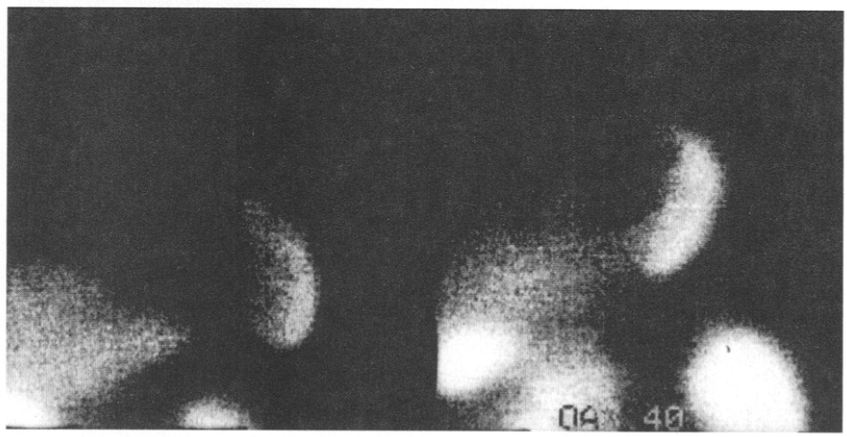

Fig 13. Anterior and LAO (40°) gamma image of a patient with reperfused anterior MI injected with Tc-99m glucarate. The image was obtained at about 3.5 hours after IV administration of the radiotracer.

autolysis in the infarct. The exact duration for Tc-99m glucarate positivity in patients with acute MI is not known. Mariani et al[59] observed that in reperfused MI, positivity wanes after peak serum creatine kinase (CK) levels have been reached. Whether the same time frame will hold for nonreperfused MI must await additional studies.

It appears that Tc-99m glucarate may provide a very acute MI imaging method. Large MI should be visualizable by gamma imaging in about 1 hour after IV administration, and a small MI should be detectable by 3 hours. This diagnostic time frame may be compatible for directing thrombolytic therapy in the emergency department.

REFERENCES

1. Pasternak RC, Braunwald E: Acute myocardial infarction. In: Isselbacher KJ, Braunwald E, Wilson JD, et al (eds): Harrison's Principles of Internal Medicine (ed 13). McGraw-Hill, New York, NY, 1994, p 1066

2. McCaarthy BD, Beshansky JR, D'Agostino RB, et al: Missed diagnosis of acute myocardial infarction in the emergency department: results from a multicenter study. Ann Emerg Med 22:579, 1993

3. Bailey IK, Griffith LSC, Rouleau J, et al: Thallium-201 myocardial perfusion imaging at rest and during exercise: comparative sensitivity to electrocardiography in coronary artery disease. Circulation 55:79-87, 1977

4. Van Train KF, Garcia EV, Maddahi J, et al: Multicenter trial validation for quantitative analysis of same-day rest-stress technetium-99m-sestamibi myocardial tomograms. J Nucl Med 35:609-618, 1994

5. Kelly JD, Forster AM, Higley B, et al: Technetium-99m-tetrofosmin as a new radiopharmaceutical for myocardial perfusion imaging. J Nucl Med 34:222-227, 1993

6. Parkey RW, Bonte FJ, Meyer SL, et al: A new method for radionuclide imaging of acute myocardial infarction in humans. Circulation 50:540-546, 1974

7. Khaw BA, Gold HK, Yasuda T, et al: Scintigraphic quantification of myocardial necrosis in patients after intravenous injection of myosin specific antibody. Circulation 74:501-508, 1986

8. Fornet B, Yasuda T, Wilkinson R, et al: Detection of acute cardiac injury with technetium-99m glucaric acid. J Nucl Med 30:1743, 1989

9. Kronenberg MW, Wooten NE, Friesinger GC, et al: Scintigraphic characteristics of experimental myocardial infarct extension. Circulation 60:1130-1140, 1979

10. Cowley MJ, Mantle JA, Rogers WJ, et al: Technetium-99m stannous pyrophosphate myocardial scintigraphy: reliability and limitations in assessment of acute myocardial infarction. Circulation 56:192-198, 1977

11. Willerson JT, Parkey RW, Bonte FJ, et al: Acute subendocardial myocardial infarction in patients; its detection by technetium-99-m stannous pyrophosphate myocardial scintigrams. Circulation 51:436-441, 1975

12. Khaw BA, Strauss HW, Moore R, et al: Myocardial damage delineated by In-111 antimyosin Fab and Tc-99m-pyrophosphate. J Nucl Med 28:76-82, 1987

13. Khaw BA, Yasuda T, Gold HK, et al: Acute myocardial infarct imaging with Indium-111-labeled monoclonal antimyosin Fab. J Nucl Med 28:1671-1678, 1987

14. Khaw BA, Fallon JT, Strauss HW, et al: Myocardial infarct imaging with Indium-111-diethylene triamine pentaacetic acid-anticanine cardiac myosin antibodies. Science 209:295-297, 1980

15. Yaoita H, Juweid M, Wilkinson R, et al: Detection of myocardial reperfusion injury with Tc-99m glucarate. J Nucl Med 5:795, 1990

16. Orlandi C, Crane PD, Edwards DS, et al: Early scintigraphic detection of experimental myocardial infarction in dogs with technetium-99m-glucaric acid. J Nucl Med 32:263-268, 1991

17. Mariani G, Villa G, Rossettin PF, et al: Scintigraphy with ^{99m}Tc-D-glucaric acid in patients with acute myocardial infarction. J Nucl Cardiol 1:S59, 1997

18. Buja LM, Tofe AJ, Kulkarni PV, et al: Sites and mechanisms of localization of techentium-99m phosphorus radiopharmaceuticals in acute myocardial infarcts and other tissues. J Clin Invest 60:724-740, 1977

19. Dewanjee MK, Kahn PC: Mechanism of localization of ^{99m}Tc-labeled pyrophosphate and tetracycline in infarcted myocardium. J Nucl Med 17:639-646, 1976

20. Bianco JA, Kemper AJ, Taylor A, et al: Technetium-99m (Sn^{2+}) pyrophosphate in ischemic and infarcted dog myocardium in early stages of acute coronary occlusion: histochemical and tissue-counting comparisons. J Nucl Med 24:485, 1983

21. Khaw BA, Strauss HW, Moore R, et al: Myocardial damage delineated by In-111 antimyosin Fab and Tc-99m-pyrophosphate. J Nucl Med 28:76-82, 1987

22. Parkey RW, Kulkarni PV, Lewis SE, et al: Effect of coronary blood flow and site of injection on Tc-99m Ppi detection of early canine myocardial infarction. J Nucl Med 22:133-137, 1981

23. Kondo M, Takahashi M, Matsuda T, et al: Clinical significance of early myocardial ^{99m}Tc-pyrophosphate uptake in patients with acute myocardial infarction. Am Heart J 11:350-356, 1987

24. Mason JW, Myers RW, Alderman EL, et al: Technetium-99m pyrophosphate myocardial uptake in patients with stable angina pectoris. Am J Cardiol 40:1-5, 1977

25. Jaffe AS, Klein MS, Patel BR, et al: Abnormal technetium-99m pyrophosphate images in unstable angina: ischemia versus infarction? Am J Cardiol 44:1035, 1979

26. Olson HG, Lyons KP, Aronow WS, et al: Follow-up technetium-99m stannous pyrophosphate myocardial scintigrams after myocardial infarction. Circulation 56:181, 1977

27. Olson HG, Lyons KP, Aronow WS, et al: Prognostic value of a persistently positive technetium-99m stannous pyrophosphate myocardial scintigram after myocardial infarction. Am J Cardiol 43:889, 1979

28. Schwartz A, Wood JM, Allen JC, et al: Biochemical and

morphologic correlates of cardiac ischemia. I. Membrane systems. Am J Cardiol 32:46, 1973

29. Khaw BA, Beller GA, Haber E, et al: Localization of cardiac myosin-specific antibody in myocardial infarction. J Clin Invest 58:439-446, 1976

30. Khaw BA, Beller GA, Haber E: Experimental myocardial infarct imaging following intravenous administration of Iodine-131 labeled antibody $(Fab')_2$ fragments specific for cardiac myosin. Circulation 57:743-750, 1978

31. Khaw BA, Mattis JA, Melincoff G, et al: Monoclonal antibody to cardiac myosin; scintigraphic imaging of experimental myocardial infarction. Hybridoma 3:11-23, 1984

32. Khaw BA, Petrov A, Narula J: Complementary roles of antibody affinity and specificity in in vivo diagnostic cardiovascular targeting: how specific is antimyosin for irreversible myocardial damage? J Nucl Cardiol (in press)

33. Khaw BA, Scott J, Fallon JT, et al: Myocardial injury: quantitation by cell sorting initiated with anti-myosin fluorescent spheres. Science 217:1050-1053, 1982

34. Khaw BA, Strauss HW, Pohost GM, et al: The relationship of immediate and delayed thallium-201 distribution to localization of I-125-antimyosin antibody in acute experimental myocardial infarction. Am J Cardiol 51:1428-1432, 1983

35. Khaw BA, Mousa S: Comparative assessment of experimental myocardial infarction with Tc-99m hexakis-t-butyl-isonitrile (sestamibi), In-111 antimyosin and Tl-201. Nucl Med Commun 12:853-863, 1991

36. Johnson LL, Seldin DW, Becker LC, et al: Antimyosin imaging in acute transmural myocardial infarction: results of a multicenter clinical trial. J Am Coll Cardiol 13:27, 1989

37. Braat SH, de Zwaan C, Teuke J, et al: Value of indium-111 monoclonal antimyosin antibody for imaging in acute myocardial infarction. Am J Cardiol 60:725-726, 1987

38. Cox PH, Schonfeld D, Remme WF, et al: A comparative study of myocardial infarct detection using Tc-99m-pyrophosphate and In-111 antimyosin. Int J Card Imaging 2:197-198, 1987

39. Volpini M, Giubbini R, Gei P, et al: Diagnosis of acute myocardial infarction by indium-111 antimyosin antibody and correlation with traditional techniques for the evaluation of extent and localization. Am J Cardiol 63:7-13, 1989

40. Antunes ML, Seldin DW, Wall RM, et al: Measurement of acute Q-wave myocardial infarct size with SPECT imaging of In-111 antimyosin. Am J Cardiol 63:777-783, 1989

41. Johnson LL, Seldin DW, Becker LC, et al: Antimyosin imaging in acute transmural myocardial infarction: results of a multicenter clinical trial. J Am Coll Cardiol 13:27-35, 1989

42. Berger H, Lahiri A, Leppo J, et al: Antimyosin imaging in patients with ischemic chest pain: initial results of phase III multicenter trial. J Nucl Med 28:805, 1988 (abstr)

43. Jain D, Lahiri A, Crawley JCW, et al: Indium-111 antimyosin imaging in a patient with acute myocardial infarction: postmortem correlation between histopathologic and autoradiographic extent of myocardial necrosis. Am J Card Imaging 2:158-161, 1988

44. Jain D, Crawley JC, Lahiri A, et al: Indium-111-antimyosin images compared with TTC staining in a patient six days after myocardial infarction. J Nucl Med 31:231-233, 1990

45. Hendel RC, McSherry BA, Leppo JA: Myocardial uptake of indium-111-labeled antimyosin in acute subendocardial infarction: clinical, histochemical and autoradiographic correlation of myocardial necrosis. J Nucl Med 31:1851-1853, 1990

46. Jain D, Lahiri A, Raftery E: Immunoscintigraphy for detecting acute myocardial infarction without electrocardiographic changes. Br Med J 300:151-153, 1990

47. Khaw BA, Narula J: Antimyosin scintigraphy in cardiovascular diseases. Trends Cardiovasc Med 2:197-204, 1992

48. Johnson LL, Seldin DW, Tresgallo ME, et al: Right ventricular infarction and function from dual isotope indium-111 antimyosin/thallium-201 SPECT and gated blood pool scintigraphy. J Nucl Med 32:1018, 1991 (abstr)

49. van Vlies B, van Royen ED, Visser CA, et al: Frequency of myocardial indium-111 antimyosin uptake after uncomplicated coronary bypass surgery. Am J Cardiol 66:1191-1195, 1990

50. Hultgren HN, Shettigar UR, Pfeifer JF, et al: Acute myocardial infarction ischemic injury during surgery for coronary artery disease. Am Heart J 94:146-153, 1977

51. Bulkley BH, Hutchins GM: Myocardial consequences of coronary artery bypass graft surgery: the paradox of necrosis in areas of revascularization. Circulation 56:906-913, 1977

52. Califf RM, Topol EJ, George BS, et al: One-year outcome after therapy with tissue plasminogen activator, report from the Thrombolysis and Angioplasty in Myocardial Infarction trial. Am Heart J 119:777, 1990

53. The TIMI Study Group: Comparison of invasive and conservative strategies after treatment with intravenous tissue plasminogen activator in acute myocardial infarction: results of the Thrombolysis in Myocardial Infarction (TIMI) phase 11 trial. N Engl J Med 320:618, 1989

54. Pak KY, Nedelman MA, Kanke M, et al: An instant method for labeling antimyosin Fab′ with technetium-99m: evaluation in an experimental myocardial infarct model. J Nucl Med 33:144-149, 1992

55. Khaw BA, Nakazawa A, O'Donnell SM, et al: Avidity of ^{99m}Tc-glucarate for the necrotic myocardium: in vivo and in vitro assessment. J Nucl Cardiol 4:283-290, 1997

56. Narula J, Petrov A, Pak KY, et al: Very early noninvasive detection of acute experimental non-reperfused myocardial infarction with technetium-99m-labeled glucarate. Circulation 95:1577-1584, 1997

57. Ohtani H, Callahan RJ, Khaw BA, et al: Comparison of technetium-99m-glucarate and thallium-201 for the identification of acute myocardial infarction in rats. J Nucl Med 33:1988-1993, 1992

58. Yaoito H, Fischman AJ, Wilkinson R, et al: Distribution of deoxyglucose and technetium-99m-glucarate in the acutely ischemic myocardium. J Nucl Med 34:1303-1308, 1993

59. Mariani G, Villa PF, Rosettin C, et al: Direct scintigraphic imaging of acute myocardial infarction with Tc-99m-glucaric acid in humans. Eur J Nucl Med 23:1045, 1996

Gated SPECT Imaging

M. Reza Mansoor and Gary V. Heller

Gated SPECT imaging has allowed the simultaneous assessment of both perfusion and function through one study. The popularity of this is amply shown by the unprecedented growth of this imaging modality throughout the country. In addition to the benefits that ventricular function adds to perfusion, gated SPECT imaging also adds to the specificity of perfusion imaging. With recent studies showing the benefit of medical therapy to interventional approaches for the treatment of patients with angina, in particular, patients with chronic stable angina, there has been an increased dependence on noninvasive imaging to assess their ischemic burden. Perfusion, with technetium-99m sestamibi SPECT imaging together with gated SPECT imaging has been the modality of choice in the majority of cases because of the ease of performance of these studies and the increased information provided. This has in large part been attributable to the ability of gated SPECT imaging to provide functional data, significantly increasing the use of radionuclide perfusion imaging. This article reviews the method of acquisition, validation, clinical use, and the newer advances of gated SPECT imaging. It gives an appreciation of the benefit that gated SPECT imaging has added in terms of risk stratification and prognosis in many cardiac patients. Under the more recent uses are myocardial viability and the increased utility of gating in this scenario, ischemic versus nonischemic cardiomyopathies, and the quandary that this testing poses to physicians and the dilemma of gated thallium imaging with its inferior image quality.

GATED SPECT IMAGING was developed in the late 1980s[1] after the routine acceptance of single photon emission computed tomography (SPECT) myocardial perfusion imaging. Gated SPECT imaging has rapidly become standard in many laboratories because it allows simultaneous assessment of perfusion and function, which was not previously possible. This advance has had a major impact on the field of nuclear cardiology. It has made possible insight into the differentiation of attenuation artifact from coronary artery disease and has provided assessment of ventricular function during studies of myocardial perfusion.

ACQUISITION AND PROCESSING

Gated SPECT acquisition is performed at the same time as routine SPECT acquisition. The patient is positioned supine on the SPECT table and monitored with a three-lead electrocardiograph (ECG). The R wave identifies the beginning of the cardiac cycle, the cardiac cycle being represented by the R-R interval. Beat rejection can cover 10% to 100% of the R-R interval that is different from the predefined R-R interval. Images generally are acquired in a continuous "step and shoot" mode, whereas myocardial perfusion data are acquired with a 64 × 64 matrix over a 180° or 360° arc.

The perfusion data are then reconstructed and standard filtered back projection is applied. A transverse image is created and then reoriented to create the short, vertical long, and horizontal long axis images. A dynamic data set of eight frames is then created, and back filtration and reorientation are performed. To increase counts, a slice thickness of 2 may be used and a cine loop created. Several cycles are then superimposed on each other to give the required counts. The images are then displayed in a dynamic format, allowing the reader to assess wall motion in all areas of the myocardium, including the left and right ventricles.

Left ventricular ejection fraction is calculated separately. Most programs that calculate the ejection fraction rely on an edge detection method.[2-4] The computer assesses the end-diastolic and end-systolic frames and calculates the left ventricular ejection fraction (LVEF).

Fifteen to 60 minutes after the patient is injected with the radioisotope, perfusion imaging and gated SPECT imaging are acquired. Although perfusion data reflect the condition at the time of injection, gated SPECT reflects ventricular function during the acquisition study, generally under rest conditions. This is true whether the patient is injected at rest or during stress. However, two exceptions are possible. First, if a patient is injected with radiopharmaceutical during stress and has prolonged ischemia, a transient wall motion abnormality may be observed during the acquisition phase, 15 to 60 minutes later. In a recent article by Johnson et al,[5] it was reported that 36% of patients with stress-

From the Nuclear Cardiology Laboratory, Division of Cardiology, Hartford Hospital, Hartford, CT.

Address reprint requests to M. Reza Mansoor, MD, Division of Cardiology, Hartford Hospital, 80 Seymour Street, Hartford, CT 06102-5037.

0001-2998/99/2903-0006$10.00/0

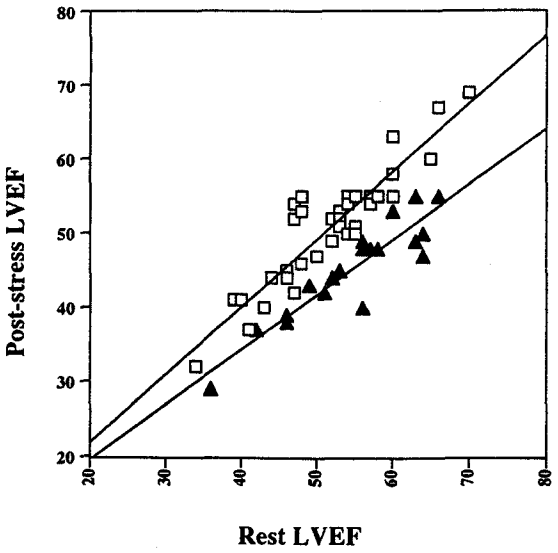

Fig 1. Post-stress versus rest left ventricular ejection fraction in patients with stress induced ischemia. *Triangles* represent post-stress, *squares* represent rest. Reprinted with permission from the American College of Cardiology (Journal of the American College of Cardiology, 1997, 30, 1641-1648).

induced ischemia had a decrease in LVEF of >5% on poststress gated SPECT imaging compared with gated SPECT data acquired after a rest injection in the same patients (Fig 1).

In a similar study, Javaid et al[6] showed a significant change in ejection fraction in patients with ischemia who underwent poststress gated SPECT as compared with postrest gated SPECT imaging. This phenomenon has been termed post-ischemic stunning and has not been observed in nonischemic patients.

Secondly, gated SPECT imaging may reflect a condition under stress if data are acquired during the time of stress. Recent studies have been performed to assess myocardial viability under low-dose dobutamine stress conditions (Levine et al,[7] Iskandrian et al[8]). In these protocols, patients are injected with radiopharmaceuticals under rest conditions, but the study is acquired during dobutamine infusion. It is best to use a dual-headed camera to minimize acquisition time during the dobutamine infusion for this protocol.

VALIDATION OF GATED SPECT IMAGING

Validation of Wall Motion and Wall Thickening

Gated SPECT imaging techniques allow the clinician to assess regional and global wall motion, wall thickening, and ejection fraction. Validation for the use of all these techniques now exists. Visual wall motion analysis by gated SPECT imaging was shown to correlate well with echocardiographic interpretation. Chua et al[9] evaluated 58 patients with ECG and gated SPECT studies. They found a very close correlation between the two techniques in the evaluation of segmental wall motion (r = .91) as well as in the assessment of wall thickening (r = .90). There was a similarly very strong correlation when global wall motion was compared (r = .98) using the two techniques (Fig 2).

Germano et al[10] developed a new technique whereby they measured regional wall motion and wall thickening based on three-dimensional (3-D) endocardial surface detection using a modification of the centerline method, which is based on geometric and partial volume counts. They found that quantitative and visual estimation of wall motion and wall thickening correlated well by both techniques. Cwajd et al[11] described the interobserver and intraobserver variability in a group of 34 patients. When studies were analyzed a month apart by two independent observers, the interobserver and intraobserver agreement was 90% and 88%, respectively. Berman et al[12] also have reported on the cost efficiency of wall motion and wall thickening in providing more diagnostic data with fewer tests.

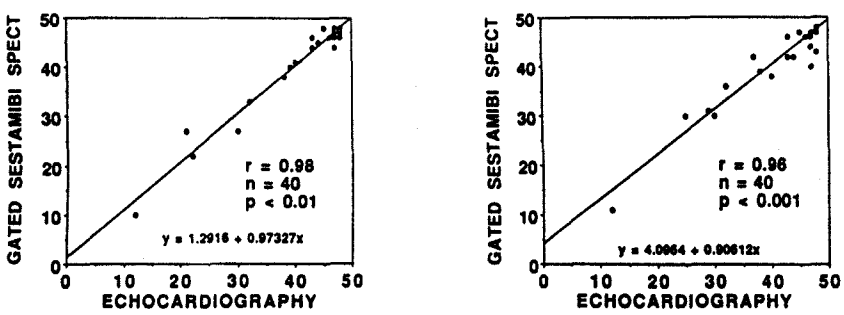

Fig 2. Correlation between gated SPECT (*y axis*) and echocardiographic (*x axis*) global wall motion (*left*) and global wall thickening (*right*) scores. Reprinted with permission from the American College of Cardiology (Journal of the American College of Cardiology, 1994, 23, 1107-1114).

Validation of Ejection Fraction

Computer programs have been developed that detect the endocardial and epicardial boundaries and thus calculate the LVEF. Two techniques have been described and validated by different groups. DePuey et al[2] described a technique by which the endocardial and epicardial borders are drawn manually with computer calculation of the LVEF using Simpson's rule. They compared these gated SPECT studies with planar gated Tc-99m blood pool studies and found a very good correlation between the two techniques (Fig 3). Germano et al[3] have reported a technique in which the computer assesses the endocardial and epicardial surfaces of all gated intervals in the cardiac cycle and calculates the volume changes, and thus the LVEF, all without operator interaction. Nichols et al[4] used yet another technique to automate the calculation of the LVEF. End diastolic and end systolic images were defined by maximum count extremes. The endocardial surfaces were plotted for both these images, and ejection fraction was calculated. This technique was found to correlate strongly with gated blood pool imaging (r = 0.86), the gated SPECT interobserver variability was r = .92, the intraobserver variability was r = .94.

Gated SPECT has also been compared with other modalities such as echocardiography, first-pass radionuclide ventriculography, and contrast ventriculography in an effort to validate its use for measuring ejection fraction. Germano et al[3] compared LVEF by gated SPECT imaging with radionuclide ventriculography and found a very good correlation (r = .91), Piriz et al[13] reported a correlation of r = .86, while Nichols et al[14] compared ejection fraction by gated SPECT and angiographic ventriculography and found a correlation of r = .86. Williams et al[15] compared wall motion and

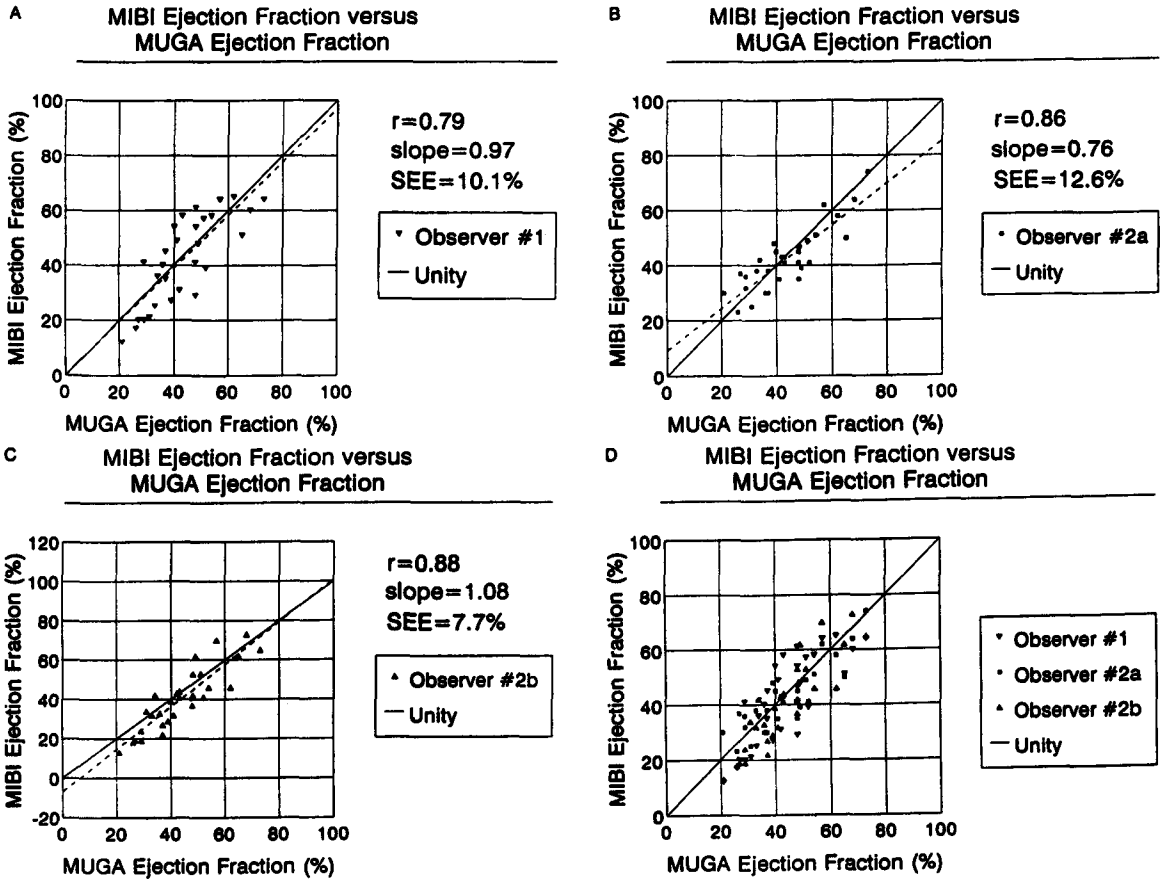

Fig 3. Comparison of LVEF determined from gated SPECT studies and equilibrium radionuclide angiography, with various observers (Reprinted by permission of the Society of Nuclear Medicine from: DePuey EG, Nichols K, Dobrinsky C. Left ventricular ejection fraction assessed from gated technetium-99m sestamibi SPECT. *Journal of Nuclear Medicine* 1993;34:1871-1876.)

ejection fraction by gated SPECT with radionuclide angiography and contrast ventriculography and reported that gated SPECT ejection fraction was more accurate than radionuclide ventriculography when compared with contrast angiography.

Jamil et al[16] recently showed that visually estimated ejection fraction corresponded very closely to the computer-derived ejection fraction. This study was performed in patients with dilated cardiomyopathies. However, the correlation was better with dilated cardiomyopathies of nonischemic origin than in patients with coronary artery disease. In the latter group, more areas of severe underperfusion were noted, which may affect the overall accuracy of the ejection fraction measurement.

Validation of Ventricular Volumes

Another possible use of gated SPECT imaging is in the assessment of ventricular volumes. Everaert et al[17] studied 40 patients using two new programs that depended on 3-D imaging to calculate left ventricular (LV) volumes and found very good concordance between the two techniques (r = .93). Nichols et al[14] compared the LV volume with angiography and showed a high correlation, whereas Iskandrian et al[18] compared the LV volumes by gated SPECT with those of first-pass radionuclide ventriculography showing correlation of r = .89. Germano et al[19] further showed that the gated SPECT volume measurements also were very reproducible.

CLINICAL UTILITY

One of the more common uses of gated SPECT imaging is to improve the accuracy of the diagnosis of coronary artery disease (CAD). It has been recognized that SPECT imaging has a superior sensitivity for the detection of CAD over planar imaging. However, the specificity suffers, and in several studies has been found to be lower than with planar imaging, generally because of attenuation artifact. This commonly occurs as a fixed defect in either the anterior (breast) or inferior (diaphragm) areas. Fixed defects may represent either attenuation artifact, prior myocardial infarction, or hibernating myocardium, and cause significant problems in the interpretation of the study. Only assumptions could be made regarding the etiology of a fixed defect prior to gated SPECT imaging. This resulted in reduced specificity (false positives) and perhaps reduced sensitivity (false negatives). With gated SPECT imaging, evaluation of ventricular wall motion in the area of the perfusion abnormality can be performed. It is assumed that normal function in the area of the perfusion abnormality is consistent with attenuation artifact, whereas abnormal wall motion suggests CAD.

Appropriate classification of fixed defects should result in improved specificity. This was indeed shown to be the case in a recent prospective study by Taillefer et al.[20] In this study 115 women with known coronary anatomy underwent separate exercise testing with Tc-99m sestamibi gated SPECT imaging and thallium-201 imaging. The specificity improved from 67% with thallium to 92% with gated SPECT imaging ($P < .01$) (Fig 4).

Another benefit of gated SPECT imaging is a reduction of equivocal interpretation of perfusion imaging results. The clinical application of this decision process was shown by DePuey et al[21] and Smanio et al.[22] Both articles showed less equivocal interpretations using both perfusion and function data in comparison with perfusion data alone. A more recent article by Choi et al,[23] evaluated 365 patients and reported that in those with equivocal images, there was an 86.8% improvement from the addition of tomographic images, projection images, and gated cine images.

One problem that continues to challenge the cardiovascular nuclear medicine physician is the assessment of wall motion in an area that is severely hypoperfused. In this case the count rate is inadequate for visualizing the region well. Thus the ability to accurately interpret ventricular function as well as ejection fraction is compromised. Recently Nichols et al[24] have described an image enhancement technique that may assist in the visualization of the underperfused wall. They have also validated this technique, finding that it compares well with echocardiography.[25]

NEWER USES OF GATED SPECT IMAGING

Myocardial Viability

An area of myocardium is said to be viable if its perfusion and/or function improve after revascularization. Although viability applies equally to normally functioning myocardium and myocardium with subnormal function caused by lack of perfusion, the main concern of physicians is in patients

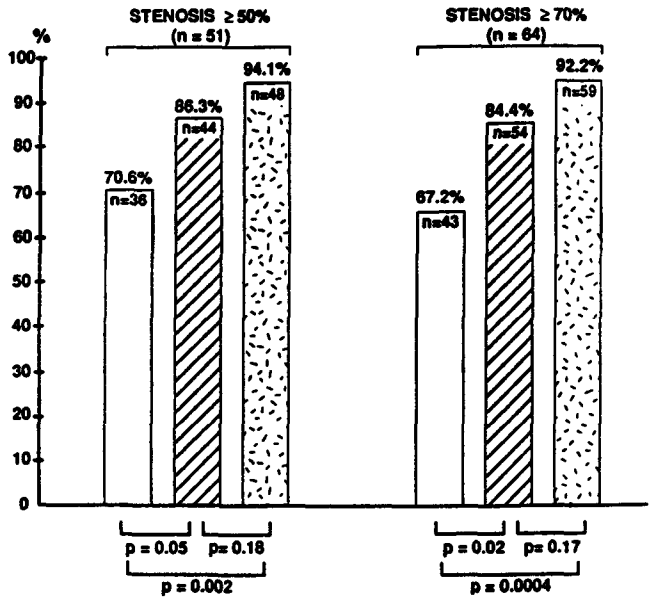

Fig 4. Specificity of Tl-201 (*open bars*), Tc-99m sestamibi perfusion (*striped bars*) and Tc-99m sestamibi perfusion and gated SPECT (*speckled bars*). Reprinted with permission from the American College of Cardiology (Journal of the American College of Cardiology, 1997, 26, 69-77).

with hypofunctioning myocardium and the ability to predict recovery after revascularization.

It has been assumed that because technetium-99m sestamibi does not redistribute, it was not a good agent to evaluate viability. Therefore rest-redistribution thallium or stress-redistribution thallium was considered the perfusion agent of choice for viability assessment. Chua et al[9] first reported using a dual isotope technique (rest thallium-201 and stress Tc-99m sestamibi SPECT) that gated SPECT corresponded with echocardiography in the assessment of viable myocardium. Gated SPECT corresponded with echocardiographic wall thickening and wall motion. They showed that gated SPECT added to the perfusion study when assessing viability. However, gating alone may underestimate the presence of viable myocardium, which they theorized was because of the presence of postischemic stunning and myocardial hybernation. In a more recent study, Levine et al[7] using technetium-99m sestamibi SPECT imaging found that gated SPECT was more reliable than rest-redistribution thallium-201 in the identification of viable myocardium. Levine et al[26] in a very recent article evaluated the benefit of adding functional data to the perfusion data from Tc-99m sestamibi imaging, and found that it significantly improved sensitivity ($P < .025$) and overall accuracy ($p < .05$) (Fig 5).

There are many new techniques that are being examined together with Tc-99m sestamibi gated SPECT imaging to be able to better identify hibernating myocardium. Some of these newer techniques involve the infusion of nitrates during administration of Tc-99m sestamibi and during image acquisition and the infusion of low-dose dobutamine during image acquisition. This is similar in concept to the use of low-dose dobutamine echocardiography in assessing viability. Iskandrian et al[8] have described a technique in which viability was assessed using a low- and high-dose protocol with Tc-99m gated SPECT images. Levine et al[27] used low-dose dobutamine with gated SPECT imaging to assess viability and showed that if wall motion improved with low-dose dobutamine, there was a good correlation with myocardial viability. The standard use of these techniques requires further evaluation.

Ischemic and Nonischemic Cardiomyopathy

The identification of ischemic from nonischemic etiologies of dilated cardiomyopathies is of critical clinical importance in choosing appropriate therapies. Previous noninvasive studies have shown that neither assessment with perfusion imaging nor function alone is specific enough for this determination. Thus cardiac catheterization has been considered to be the only reliable means of assessing patients with dilated cardiomyopathy.

Recent studies have shown that a combined approach of both perfusion imaging and function may be more useful. Danias et al[28] showed a much

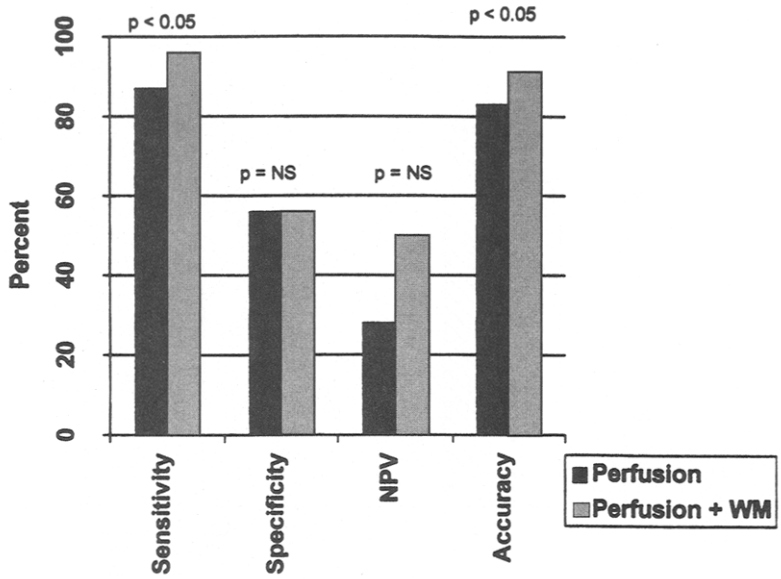

Fig 5. Comparison of perfusion alone with perfusion and wall motion. The addition of ECG gating significantly improved sensitivity, negative predictive value, odds ratio, and accuracy. Specificity and positive predictive value did not change. (Reprinted from American Journal of Cardiology, 83, Levine MG, McGill CC, Azar RR, et al, Functional assessment with electrocardiographic gated single-photon emission computed tomography improves the ability of technetium-99m sestamibi myocardial perfusion imaging to predict myocardial viability in patients undergoing revascularization, 1-5, 1999, with permission from Excerpta Medica Inc.)

lower summed stress, rest, and reversibility score in the nonischemic cardiomyopathy group, and a markedly decreased variability in wall motion abnormality, which could be used to differentiate the two types of cardiomyopathy (Fig 6). More research in this area is needed to confirm this interesting observation.

Prognosis

The evaluation of residual LV function after acute myocardial infarction is one of the most important prognostic indicators of mortality. This is illustrated in Figure 7, which is from the Multicenter Post Infarction Research Group Study.[29] Thus LV function as evaluated by gated SPECT imaging should be a significant predictor of cardiac risk.

Hachamovitch et al[30] in a recent study reported on the ability of functional measurements to independently aid in the risk stratification of patients into those at high and low risk for events. Similarly Travin et al[31] reported in a large cohort of 560 patients that a gated SPECT score greater than 10 was the best predictor of any event (odds ratio = 2.7).

Gated Thallium-201 Images

Although gated SPECT imaging with thallium-201 has been validated, several limitations exist.

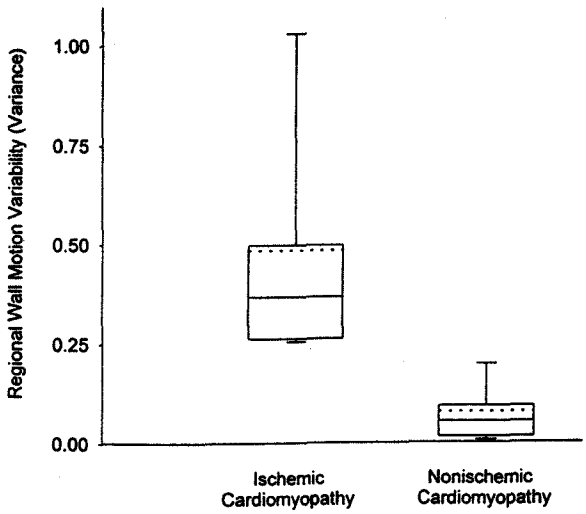

Fig 6. Individual patient wall motion variance among vascular territories, for ischemic and nonischemic cardiomyopathy groups. The horizontal *solid lines* inside the boxes represent the median values. The *dotted lines* represent the mean group values. The *upper* and *lower box* borders indicate the 75th and 25th percentiles, respectively. The *whisker caps* represent the 95th and 5th percentiles. (Reprinted from the American Journal of Cardiology, 82, Danias PG, Ahlberg AW, Clark III BA, et al, Combined assessment of myocardial perfusion and left ventricular function with exercise technetium-99m sestamibi gated single-photon emission computed tomography can differentiate between ischemic and nonischemic dilated cardiomyopathy, 1253-1258, 1998, with permission from Excerpta Medica Inc.)

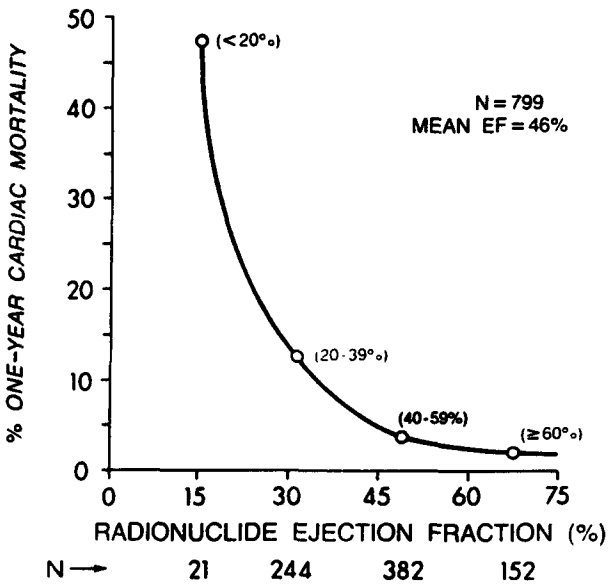

Fig 7. Cardiac mortality rate in four categories of radionuclide ejection fraction (EF) determined before discharge. *N* denotes the number of patients in the total population and in each category. (Reprinted with permission from The Multicenter Post-Infarction Research Group. N Eng J Med 309:331-6, 1983 [Copyright ©1983 Massachusetts Medical Society. All rights reserved.].)

Generally count density is uniformly lower than with technetium in any individual patient. This results in an inability to visualize and evaluate the right ventricle. As a result, valuable information is lost, including possible etiology of symptoms or distinguishing ischemic from nonischemic cardiomyopathy. In addition accurate evaluation of regional wall motion may be more difficult with thallium-201. It should be noted that validation of the method primarily has been with global ejection fraction, rather than regional wall motion. Because determination of the etiology of a fixed defect (attenuation versus CAD) is made with regional assessment, this may be a serious limitation. To date no studies exist regarding the use of gated SPECT in improving specificity of thallium-201 imaging. As the body size increases, the count density with thallium-201 becomes limited. In such patients, attenuation artifact determination as well as accurate ejection fraction measurement is more important.

Germano et al[6] compared gated thallium-201 with technetium-99m sestamibi gating and found a very good correlation between the two techniques. Similarly Maunoury et al,[32] in a study involving 104 patients, found that Tl-201 could be gated and provided excellent correlation with gated SPECT using Tc-99m sestamibi images. However others have found it difficult to reproduce the same quality of images with thallium-201 that are produced with technetium-99m gated SPECT. Ferrand et al[33] highlighted a problem with thallium SPECT ejection fraction calculation caused by the low signal-to-noise ratio. They concluded that particularly in patients with low EFs, there may be large errors.

Gated SPECT imaging has resulted in a significant advance in the use of perfusion imaging. It has resulted in an increase in particular of the specificity, and therefore more definitive reporting on perfusion studies. The clinician is able to have both a perfusion and a functional image with one study.

REFERENCES

1. Sporn V, Perez Balino N, Holman BL, et al: Simultaneous measurement of ventricular function and myocardial perfusion using the technetium isonitriles. Clin Nucl Med 13:77-81, 1988

2. DePuey EG, Nichols K, Dobrinsky C: Left ventricular ejection fraction assessed from gated technetium-99m sestamibi SPECT. J Nucl Med 34:1871-1876, 1993

3. Germano G, Hosen K, Kavanagh PB, et al: Automatic quantification of ejection fraction from gated myocardial perfusion SPECT. J Nucl Med 36:2138-2147, 1995

4. Nichols K, DePuey EG, Rozanski A: Automation of gated tomographic left ventricular ejection fraction. J Nucl Cardiol 3:475-482, 1996

5. Johnson LL, Verdesca SA, Aude WY, et al: Postischemic stunning can affect left ventricular ejection fraction and regional wall motion on post-stress gated sestamibi tomograms. J Am Coll Cardiol 30:1641-1648, 1997

6. Javaid A, Kong DE, Borges-Neto S: Demonstration of stress induced LV "stunning" using same day rest and stress gated perfusion SPECT imaging. Circulation 98:I587(3094), 1998

7. Levine MG, McGill CC, White MP, et al: Myocardial viability: a prospective comparison of technetium 99m sestamibi gated SPECT vs. rest redistribution thallium-201 myocardial perfusion imaging. Circulation 96:2475, 1997

8. Iskandrian AE, Acio E: Methodology of a novel myocardial viability protocol. J Nucl Cardiol 5:206-209, 1998

9. Chua T, Kiat H, Germano G, et al: Gated technetium-99m sestamibi for simultaneous assessment of stress myocardial perfusion, post-exercise regional ventricular function and myocardial viability: correlation with echocardiography and rest thallium-201 scintigraphy. J Am Coll Cardiol 23:1107-1114, 1994

10. Germano G, Erel J, Lewin H, et al: Automatic quatitation of regional myocardial wall motion and thickening from gated technetium-99m sestamibi myocardial perfusion single-photon emission computed tomography. J Am Coll Cardiol 30:1360-1367, 1997

11. Cwajd E, Cwajd J, He ZX, et al: Reproducibility of gated SPECT for the assessment of regional left ventricular wall motion. Circulation 98:I587(3093), 1998

12. Berman DS, Germano G: Evaluation of ventricular ejection fraction, wall motion, wall thickening and other parameters with gated myocardial perfusion single-photon emission computed tomography. J Nucl Cardiol 4:S169-171, 1997

13. Piriz JM, Kiernan FJ, Eldin A, et al: Correlation of left ventricular ejection fraction by gated SPECT Tc-99m sestamibi imaging with contrast ventriculography at subsequent cardiac catheterization. J Nucl Med 37:105P, 1996

14. Nichols K, Tamis J, DePuey G, et al: Relationship of gated SPECT ventricular function parameters to angiographic measurements. J Nucl Cardiol 5:295-303, 1998

15. Williams KA, Taillon LA: Left ventricular function in patients with coronary artery disease assessed by gated tomographic myocardial perfusion images. J Am Coll Cardiol 27:173-181, 1996

16. Jamil G, Ahlberg AW, Danias PG, et al: Visualized wall motion assessment correlates with quantitative ejection fraction using Tc-99m sestamibi ECG gated SPECT imaging in patients with dilated cardiomyopathy. J Am Coll Cardiol 31:440A, 1998

17. Everaert H, Bossuyt A, Franken PR: Left ventricular ejection fraction and volumes from gated single photon emission tomographicmyocardial perfusion images: comparison between two algorithms working in three dimensional space. J Nucl Cardiol 4:472-476, 1997

18. Iskandrian AE, Germano G, VanDecker W, et al: Validation of left ventricular volume measurements by gated SPECT Tc-99m labeled sestamibi imaging. J Nucl Cardiol 5:574-578, 1998

19. Germano G, Kavanagh PB, Kavanagh JT, et al: Repeatability of automatic left ventricular cavity volume measurements from myocardial perfusion SPECT. J Nucl Cardiol 5:447-483, 1998

20. Taillefer R, DePuey EG, Udelson JE, et al: Comparative diagnostic accuracy of Tl-201 and Tc-99m sestamibi SPECT imaging (perfusion and ECG gated SPECT) in detecting coronary artery disease in women. J Am Coll Cardiol 29:69-77, 1997

21. DePuey EG, Rozanski A: Using gated technetium 99m sestamibi SPECT to characterize fixed myocardial defects as infarct or artifact. J Nucl Med 36:952-955, 1995

22. Smanio EPS, Watson DD, Segalla DL, et al: Value of gating of technetium-99m sestamibi single photon emission computed tomographic imaging. J Am Coll Cardiol 30:1687-1692, 1997

23. Choi JY, Lee KH, Kim SJ, et al: Gating provides improve accuracy for differentiating artifacts from true lesions in equivocal fixed defects on technetium 99m tetrofosmin perfusion SPECT. J Nucl Cardiol 5:395-401, 1998

24. Nichols K, DePuey EG, Rozanski A, et al: Image enhancement of severely hypoperfused myocardia for computation of tomographic ejection fraction. J Nucl Med 38:1411-1417, 1997

25. Nichols K, DePuey EG, Krasnow N, et al: Reliability of enhanced gated SPECT in assessing wall motion of severely hypoperfused myocardium: echocardiographic evaluation. J Nucl Cardiol 5:387-394, 1998

26. Levine MG, McGill CC, Ahlberg AW, et al: Functional assessment with electrocardiographic gated single-photon emission computed tomography improves the ability of technetium-99m sestamibi myocardial perfusion imaging to predict myocardial viability in patients undergoing revascularization. Am J Cardiol 83:1-5, 1999

27. Levine MG, McGill CC, Azar RR, et al: Low dose dobutamine ECG gated SPECT myocardial perfusion imaging with technetium-99m sestamibi predicts myocardial viability: a prospective study. J Am Coll Cardiol 31:44A, 1998

28. Danias PG, Ahlberg AW, Clark III BA, et al: Combined assessment of myocardial perfusion and left ventricular function with exercise technetium-99m sestamibi gated single-photon emission computed tomography can differentiate between ischemic and nonischemic dilated cardiomyopathy. Am J Cardiol 82:1253-1258, 1998

29. The Multicenter Postinfarction Research Group: risk stratification and survival after myocardial infarction. N Engl J Med 309:331-336, 1983

30. Hachamovitch R, Berman DS, Levin H, et al: Exercise or adenosine sestamibi combined perfusion-function protocols: prediction of cardiac death and risk stratification. J Nucl Med 38:40P, 1997

31. Travin MI, Murthy DR, Campanella MW, et al: The prognostic value of gated SPECT in patients with ischemia on stress myocardial perfusion imaging. Circulation 98:I588(3096), 1998

32. Maunoury C, Chen CC, Chua KB, et al: Quantification of left ventricular function with thallium-201 and technetium-99m sestamibi myocardial gated SPECT. J Nucl Med 38:958-961, 1997

33. Ferrand SK, Smith MF, Carson JM, et al: Variability in SPECT thallium ejection fraction estimates. Circulation 98: I587(3092), 1998